UNIVERSITAT DE
BARCELONA

Tumor secretome-mediated pro-tumoral microenvironment in diffuse intrinsic pontine glioma

Mercè Baulenas Farrés

University of Barcelona

Faculty of Medicine

Doctorate program: Biomedicine

Research line: Molecular and cellular biology of cancer

Tumor secretome-mediated pro-tumoral microenvironment in diffuse intrinsic pontine glioma

Pediatric Cancer Program
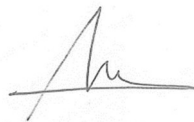
Institut de Recerca Sant Joan de Déu

&
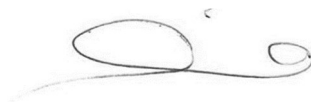
Department of Pediatric Oncology

SJD Pediatric Cancer Center Barcelona

PhD candidate: Mercè Baulenas Farrés

Thesis director: Dr. Angel Montero Carcaboso

Thesis tutor: Dra. Teresa Ribalta Farrés

Dr. Angel Montero Carcaboso, director of the thesis entitled *Tumor secretome-mediated pro-tumoral microenvironment in diffuse intrinsic pontine glioma* completed by the PhD candidate Mercè Baulenas Farrés, endorses the originality of the research work included in this thesis.

A la gent que estimo, que no és poca.

What you do makes a difference, and you have to decide what kind of difference you want to make.

Jane Goodall

AKNOLEDGEMENTS

El meu viatge en la investigació del DIPG a Sant Joan de Déu va començar l'estiu de 2013, durant el treball de recerca de batxillerat. Va ser en aquell moment que vaig descobrir el món de la recerca i aquesta malaltia tan devastadora. Avui, 11 anys més tard, tanco una etapa en la que han participat desenes de persones que m'han ajudat a arribar on sóc i, sense les quals, aquesta tesis no hagués estat possible.

Quiero empezar por agradecer a mi director de tesis, el Dr. Ángel Montero Carcaboso, el voto de confianza que dió a la Mercè de 16 años y por seguir haciéndolo hasta el día de hoy; por contribuir a que tenga una mente mucho más crítica y por enseñarme a desconfiar de lo que, a priori, parece la respuesta más obvia.

Segueixo pels que m'han acompanyat tots aquests anys al laboratori. Gràcies a la Dra. Sonia Paco per ensenyar-me tant els primers anys, així com per confiar-me i traspassar-me plenament el seu projecte a posteriori. Gràcies a l'equip de diagnòstic molecular (Óscar, Isa, Ana i Mònica) per ser-hi sempre que he necessitat consell, fora i dins del laboratori. Gràcies Mònica per ser una incondicional des dels inicis, pels cafès, la paciència a l'estabulari i per totes les abraçades en els moment més oportuns. Ana, has sido un pilar fundamental los últimos años, dentro y fuera del trabajo, siempre que lo he necesitado (y cuando no, también). Marta, mai podré agrair-t'ho tot prou. Gràcies per ser-hi sempre, entendre'm, ajudar-me, escoltar-me i aconsellar-me. Quan sigui gran vull assemblar-me a tu. Gracias Esteliña por ser un ejemplo de perseverancia, por tener siempre buenas palabras, y por ser un apoyo y ayuda constantes. Gracias,

Rosario, por ser la mejor post-doc y jefecita del mundo mundial, por acompañarnos, ayudarnos, aguantarnos y cuidarnos todo este tiempo. Gràcies Clàudia per les incomptables hores d'estabulari i per fer-me riure en els moments més insospitats possibles; ets la millor (i visca la Catalunya interior! ;)). Víctor, qui ens hagués dit que estaríem on som avui sent persones tan oposades (però tan semblants alhora)... Gràcies per aguantar bronques, fer-me riure i escoltar-me sempre que ho he necessitat. Leire, l'altra meitat del team DIPG. Gràcies per haver sigut la millor companya d'aventures en aquest camí, sovint difícil i frustrant (la Rita, l'Aleix i el Chanquete estarien orgullosos de nosaltres, segur! ;)). Chao Liang, you are one of the nicest people I have had the pleasure to meet lately. Thank you for making us laugh through everything! Gràcies Ana J, Núria i Yas, també, per formar part d'aquesta tragicomèdia tan surrealista. Pablo, mi galeguiño. Gracias por las risas infinitas y por tus abrazos curativos (escasos, pero increiblemente perfectos). Gràcies Carlitis per arribar i completar el puzzle de "Las reinas de las basuras" que no sabíem que necessitavem. Mari, la otra mitad de Uganda, tan opuestas y complementarias a la vez, desde el primer día. No sabria decirte qué porcentaje te pertenece de esta tesis, pero te aseguro que es muy alto, altísimo. Jamás te podré agradecer lo suficiente todos estos años ni olvidaré nada de lo que hemos vivido juntas. A la resta de gent del lab: noies d'hemato (Helena, Clara, Mercè i Alba, heu tardat a pujar de les catacumbes, però ha valgut tantíssim la pena...), Sole (eres la mejor, et trobem MOLT a faltar), grup AA (Àlex i Valentín, tan de bo haver compartit molt més temps), Carlos (eres un broncas, pero me has dado momentazos increibles todo este tiempo), Jara, Xènia, Sara P, Sara S, Sílvia, gent que ja no hi és... gràcies per haver-hi sigut tots aquests anys!

Passo ara a tota aquella gent que hi ha sigut totes les altres hores, sovint rebent, per part meva, menys amor i carinyo del que mereixien i que espero poder compensar algun dia. Gràcies, Anna, Guiu i Àlex, el Can Pixa original. No podria haver demanat millors companys de pis i de vida que vosaltres. I a en Mateu, l'última adició a aquesta bogeria de casa. Carla (MVP de la vida sempre), Mònica (nextlevel per sempre), Peix, Clàudia i Martí, Mireia i Helen, gràcies per tot i més, per ser increïbles. A la resta de Barri del Mig (Ferri, Laura, Gerard, Nil i Marina), gràcies per intentar solucionar el món tots plegats un cop per setmana; al vostre costat tot sembla una mica més possible. Als iogus (Joan, Maria, Enric, Xuma, Clàudia, Martina, Berta, Erola...) gràcies per fer més surrealista i divertit qualsevol moment. Marta, Laura, Alba, Èric, Meri, Laia, Marina i Montse, gràcies per ser tan a prop meu des de ja fa molts anys tot i, sovint, estar separats per molts quilòmetres. Cris, gràcies per confiar en mi molt més que jo mateixa i per tota la resta. Carla, gràcies per seguir-hi sent, 27 anys després, igual o més que mai.

Gràcies a la meva família per fer que em senti plena sempre. I sobretot, gràcies als meus pares, Ramon i Eulàlia, per ser-hi; acompanyant-me quan ha calgut, aconsellant-me quan ho he necessitat, frenant-me quan he perdut el control i, sobretot, animant-me incansablement per donar-ho tot de mi. Avui no seria aquí presentant la tesis si no fos per vosaltres, en una grandíssima part. Sou exemple de treball, constància, esforç i amor incodndicional. Em sento molt afortunada de tenir-vos i mai us ho podré agrair prou.

Finalment, m'agradaria dedicar aquesta tesis a totes les petites i petits valents que han lluitat, lluiten o lluitaran contra el càncer, així com a les seves famílies. Sou el motor que ens empeny cada dia a voler ser millors per intentar donar-vos

les respostes que mereixeu, tan aviat com sigui possible. Perquè us ho devem.

Gràcies de tot cor.

TABLE OF CONTENTS

FIGURES AND TABLES

Figures

Tables

INTRODUCTION

1. Pediatric cancer

According to World Health Organization (WHO), 400,000 children and adolescents of 0-19 years old are diagnosed of cancer every year, compared to approximately 18 million adult diagnoses, worldwide. Although the survival rate of children with cancer has increased to almost over 80% in the last decades, cancer remains the leading cause of disease-related death in children under 15 years old[1,2].

Growth and development is a physiological process which, from a pluripotential and undifferentiated cell, makes possible the differentiation, maturation, organization, and function of tissues, organs, and apparatuses that, as a whole, make up the human body[3]. Genomic technology advances over the last decade allowed for a better understanding of the genetics of cancers, finding key sporadic somatic mutations a cell may suffer which can lead to malignant cells potentially causing a tumor, and discovering germline inherited mutations present in the genome from birth that may predispose an individual to cancer. Childhood cancers have not generally been associated to genetic predisposition, with only approximately 10% of them harboring a germline mutation in an oncogene[2]. Most adult cancers are caused by the exposure to environmental factors, which induce de-novo mutations in somatic cells of the already fully developed tissues. In contrast, pediatric cancer develops in apparent absence of environmental factors, tends to originate from stem and progenitor cells, have low mutational burden, and present more oncogenic fusion genes and a greater epigenetic dysregulation. Recently, thanks to the deep DNA sequencing, several genes have been associated with a high risk of childhood cancer. Germline variants in

these genes have been identified in approximately 10% of cases, many being de novo[4].

2. Pediatric-type diffuse high-grade gliomas and diffuse midline gliomas

Central nervous system (CNS) tumors are the most common developmental solid malignant neoplasms (**Figure 1**). Gliomas in particular represent the most prevailing subgroup, corresponding to a 52% and 31% of total cases of CNS cancers in children (0-14) and adolescents and young adults (15-19), respectively[5]. Moreover, these cancers represent the leading cause of childhood deceases due to cancer, accounting for 30% of deaths.
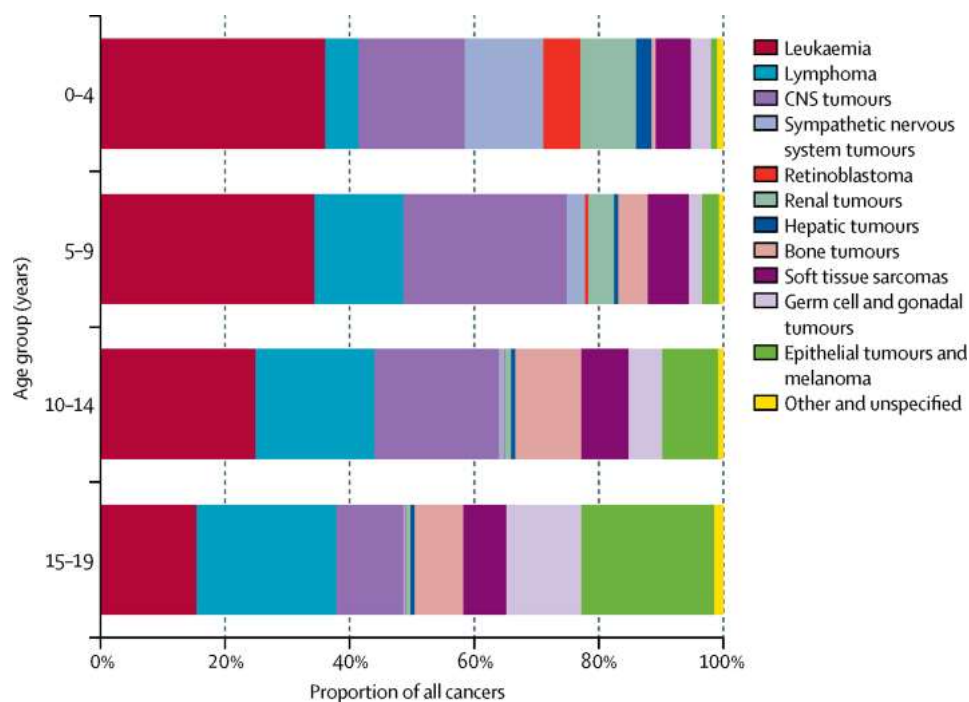
Figure 1. Proportional distribution of cancer type by age group. Proportional distribution of cancer type by age group. CNS tumors represent the second most common cancer type in children and young adults. Reproduced from *Steliarova-Foucher et al. 2017*[6].

Pediatric-type diffuse high-grade gliomas (pHGG) are the most lethal and aggressive pediatric brain tumors and, for many years, they have been grouped and studied from the same perspective as their adult analogues, despite various differences have been stablished between them[7]. However, the identification in 2012 of unique genetic aberrations in pHGG allowed the distinction of different entities and their consequent reclassification in different subgroups, based on histopathological and molecular characteristics[8] (**Table 1**).

Table 1. Clinical and molecular characteristics of the four pHGG subtypes according to the WHO CNS5 classification. Adapted from and *Gianno et al. 2022*[9].

WHO CNS5 diffuse pHGG subtypes	Location	Molecular characteristics
Diffuse midline glioma H3 K27-altered	Thalamus, brainstem	Mutation K27M in H3F3A or HIST1H3B, EZHIP overexpression
Diffuse hemispheric glioma H3 G34-mutant	Cerebral hemispheres	Mutation G34R/V in H3F3A
Diffuse pediatric-type high-grade glioma, H3-wildtype and IDH-wildtype	Supratentorial, brainstem, cerebellum	Lack of IDH1/IDH2/H3 mutations, MYCN/RTK1/RTK2 amplifications
Infant-type hemispheric glioma	Cerebral hemispheres	Fusion genes ALK, ROS1, NTRK1/2/3 or MET

Around 80% of diffuse midline gliomas H3 K27-altered (DMG) are expansive lesions in the pons, also known as Diffuse Intrinsic Pontine Glioma (DIPG)[8], which account for 10-20% of pediatric brain tumors. DIPG is the leading cause of death of brain cancer in the pediatric age with a survival rate of 0%[10]. Only 10% of patients survive for more than two years from diagnosis; in all other cases, life expectancy does not exceed 16 months[11]. Primarily occurring in children, DMG

infiltrates midline brain structures, and it is considered the most aggressive pediatric cancer. The median age at which DMG is diagnosed is 6-7 years old, and it is rarely identified in adult patients[12]. Diagnosis is based on clinical presentation (ataxia, diplopy, nystagmus, hemiparesis, equilibrium problems and difficulty controlling movement and body position), MRI findings and molecular studies. Surgical resection remains an unsuitable option for patients due to tumor location and diffuse behavior[10]. However, the use of stereotactic catheters as relatively common technique in CNS surgeries has allowed obtaining precious biopsy samples, widely contributing to the understanding of the unique biology of this disease[13,14].

2.1. Genomic Landscape

Genome-wide sequencing of tumors allowed the identification of the driver mutations in histone 3 (H3) in diffuse pHGG, which are not found in adult high-grade gliomas and evidence a unique molecular signature[15]. Post-translational histone modifications represent the dysregulation of key mechanisms responsible for the control of gene transcription and, consequently, the control of gene expression, stem-signature maintenance and cell differentiation processes[16,17]. H3 mutations can occur in two different residues and allow the classification of diffuse pHGG into different subgroups with distinct molecular signatures, biology, anatomical location and behavior[18]. G34R/V mutation, characteristic of hemispheric gliomas of adolescents and young adults, results in the substitution of a glycine (G) in position 34 for arginine (R) or valine (V)[15] (**Figure 2A and B**). H3K27M mutations, on the other hand, are characteristic of DMGs and result in the substitution of a lysine (K) for a methionine (M) at position 27[15] (**Figure 2A and B**). *H3F3A* (H3.3K27M) and *HIST1H3B* (H3.1K27M) represent two hotspot

mutations for this subclassification. Both histone isoforms, H3.3K27M and H3.1K27M, are synthesized during the cell cycle and have the functions of replacing histones in disrupted nucleosomes and packaging newly replicated DNA in the S phase, respectively. *HIST1H3B* mutant DMG represents a smaller subgroup (20-25%) of mostly female younger patients (4-5 years) with a longer survival time (15 months) and is located exclusively in the pons. *H3F3A* mutated tumors represent a larger group of patients in which the tumor can be originated in a wider set of anatomical structures, such as the pons and the whole midline[19,20]. H3-wild type tumors can be originated in either the cortex, the midline or the pons, and are associated with longer survival rates and mostly affect male patients[20,21].

Besides H3 post-translational modifications, several recurrent mutations can be detected in pHGG, affecting several regulatory pathways of the cell. Clonal missense *ACVR1* mutations have been found exclusively in around 30% of DMGs and are strongly associated with younger patients, longer survival time and *HIST1H3B, PIK3CA or PIK3R1* mutations[22,23]. Moreover, PI3K/AKT/mTOR signaling pathway, which regulates cell growth and metabolism, has been shown to be aberrantly active in 70% of DIPGs[18], affecting the viability and proliferation of the tumor cells. Focal amplifications in platelet-derived growth factor receptor A (*PDGFRA,* associated to *H3F3A[21]*), *CDK4/6* and Cyclin D genes (*CCND1*), together with the reduction of p16 (*CDKN2A*, endogenous *CDK4/6* inhibitor) are described in about 30% of the patients[24]. All types of pHGG present other highly prevalent somatic nucleotide mutations (SNVs) such as the ones affecting *TP53* (detected in >70% of DIPG patients, associated to *H3F3A[21]*), which result in p53

the reduction or loss and the consequent alteration of cell cycle of the malignant cells[25] **(Figure 2C)**.
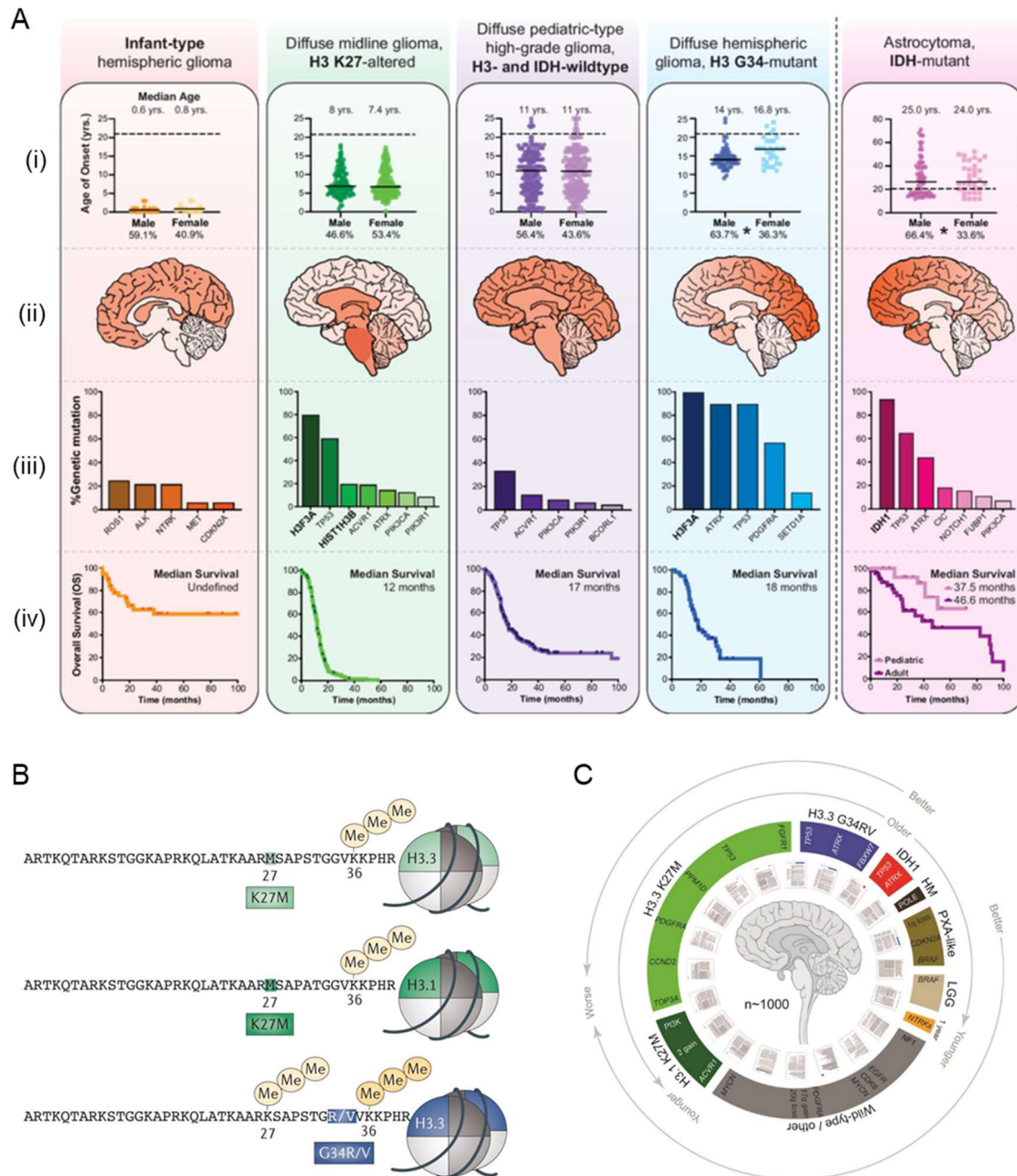
Figure 2. Molecular subgroups of diffuse pediatric high-grade gliomas. (A) (i) Age of onset in years across pediatric high-grade glioma subgroups with the median age for each sex denoted above the graph and the percentage of patients of each sex denoted below the graph. (ii) Illustration of common tumor locations (in shades of red) within each subgroup. The darker color represents a higher incidence for the associated subgroup. (iii) Graphical representation of the most common non-synonymous genetic mutations associated with each tumor subgroup, excluding amplifications and losses. (iv) Kaplan–Meier curves portraying overall survival rates

across subgroups with the median survival indicated in months in the top right corner of each graph. Reproduced from *Ocasio, 2023*[26]. (B) Specific recurrent mutations in the genes encoding the histone variants H3.3 and H3.1 which result in a global reduction of H3K27me3, leading to derepression of targets of the polycomb repressive complex 2 (PRC2). Adapted from *Jones and Baker, 2014*[15]. (C) Most common SNVs in pHGG and its association to H3 mutational state, age and prognosis. Reproduced from *Mackay et al. 2017*[21].

2.2. Diagnosis

2.2.1. Clinical presentation

Due to the infiltrated anatomical structures, DMG patients present a wide variety of neurological symptomatology that evolve towards the irreversible deterioration of their physical condition. The brainstem is the structure that connects the brain with the cerebellum and the spinal cord. This structure includes critical white and grey matter areas. The grey matter includes many important brainstem nuclei from where axons originate and connect the brain and the rest of the CNS, conforming the white matter[27]. Axons from the extracranial CNS also travel to the brainstem. The brainstem is composed of three structures: midbrain, pons and medulla oblongata (**Figure 3**). The midbrain is involved in visual reflexes and eye movement coordination, auditory processing, movement associated to basal ganglia, reward pathways and pain suppression[28-30]. The pons assists in the movement coordination and help in the breathing modulation[31]. The anterior portion of the medulla oblongata contains the pyramids, which englobe the majority of the motor fibers of the contralateral side of the body and connect the nervous system with the muscular system[27]. Due to the tumor infiltration in these structures, over 50% of the patients present a combination of cranial nerve palsies (facial asymmetry and diplopia), long tract signs, ataxia and dysmetria. Less than 10% of the patients present hydrocephalus at the time of the diagnosis,

but this symptom is highly common in patients reaching advanced states of the disease. Because DIPG progresses rapidly, children typically manifest symptoms for only one month or less before coming to clinical attention[12].
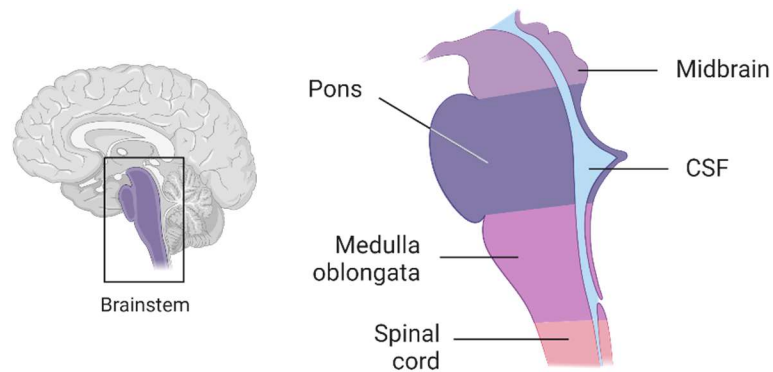
Figure 3. Brainstem anatomical structure.

2.2.2. Imaging

DMG diagnosis has been classically based on clinical presentation and neuroimaging, such as magnetic resonance imaging (MRI), which provides limited information regarding prognosis and tumor biology. Due to the infiltrative biology of the lesion, DMGs are T1-hypointense with ill-defined margins and are hyperintense in T2-weighted images. The tumor core is found centered in the pons and typically engulfs the basilar artery[32] (**Figure 4**). In more advanced states of the disease, tumor dissemination appears in the white matter tracts to the cerebellum and the rest of brainstem. Tumor necrosis is detected in approximately half of the tumors and hemorrhagic processes in about the 30%. Gadolinium largely exceeds the penetration cut-off of the blood brain barrier (BBB) with limited contrast enhancement in DIPG, suggesting a largely intact BBB. Localized areas of relative diffusion restriction are also present in most tumors. Metastasis in other CNS structures or peripheral nervous system is rarely

observed although leptomeningeal spread accounts for up to a 20% in DMG diagnosis[33]. Although MRI allows the visualization of the therapeutic effect of radiotherapy (early cystic or necrotic changes), no correlation between histological grade and response to treatment has been described in DMG.
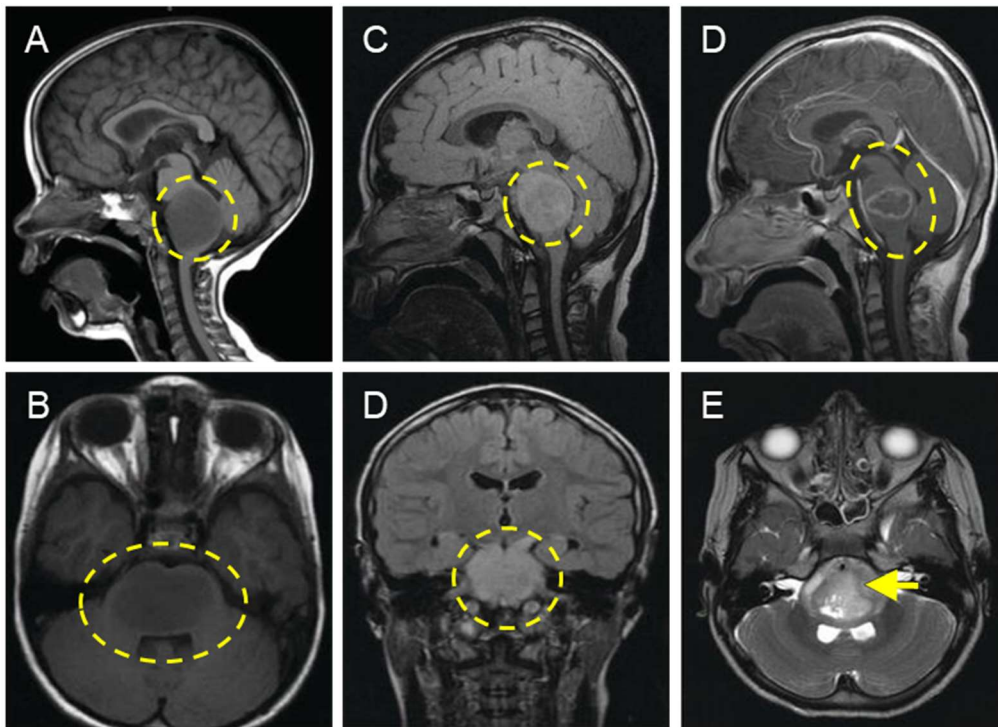
Figure 4. Classical MRI appearance of a DMG-infiltrated brain. (A) Sagittal and (B) axial T1-weighted pre-contrast MRI images showing an expansive, poorly marginated and hypointense lesion in the pons. (C) Sagital and (D) coronal images of a T2-weighted/FLAIR where the tumor presents an hyperintense signal. (E) Minimal post-gadolinium enhancment. (F) Basilar artery engulfment by the tumor (yellow arrow). Adapted from *Valvi and Gottardo, 2018*[32].

2.2.3. Anatomic pathology

For initial studies, DMG tissue was obtained from autopsies[34]. From 15 years ago, biopsy became a standardized practice by a wide group of neurosurgical teams around the world[14,35]. They demonstrated that stereotactic biopsy is a safe technique for the patients, with minimal or non-post-surgical complications. Solving the bottleneck of the access to tumor samples made molecular studies

increase exponentially thereafter. In parallel, tumor histology and tissue staining procedures complemented imaging diagnosis[34].

Until 2019, when the World Health Organization (WHO) reclassified brain tumors according to their molecular characteristics, DMGs were histologically classified as high-grade astrocytomas, WHO grades II-IV, with increased mitotic activity and microvascular proliferation. Immunochemistry addressed the presence of H3K27M and MYC mutations and other markers such as GFAP, ATRX, p53 and ki-67[12,34].

2.2.4. Liquid biopsy

Molecular diagnosis of cancer is usually performed in tissue fragments obtained from the primary tumor or metastasis. Thus, obtaining the samples requires surgical intervention, which could be hindered by the patient clinical state and tumor location. There is also a limit for the number of interventions that can be performed during the clinical evolution of the disease, complicating its monitoring. Besides, conventional tissue biopsies may not represent tumor biology due to intra-tumoral and spatial heterogeneity of the lesion. To complement or to address the limitations of tissue biopsies, liquid biopsies, also known as fluid biopsy (i.e., sampling and analyzing non-solid tissue), provide new tools to detect, quantify and monitor cancer and other diseases in a non-invasive way[36]. Liquid biopsy facilitates the repetitive sampling through time and a consequent dynamic follow-up of tumor evolution. Moreover, liquid biopsy usually represents tumor heterogeneity. There are many circulating components susceptible of being detected in body fluids. Nowadays, circulating tumor cells (CTCs), tumor-educated platelets (TEPs), exosomes, circulating cell free DNA (cctDNA), miRNA

or even tumor-secreted cytokines can be quantified in blood, cerebrospinal fluid (CSF) or even urine.

Currently, liquid biopsy is used in pHGG as a complementary diagnosis tool. The detection of cctDNA in CSF obtained by a lumbar puncture from patients has enabled the precise classification of the tumors into the different molecular subgroups[37]. Droplet digital polymerase chain reaction (ddPCR) is a recently developed technology that is able to quantify very low circulating levels of nucleic acids[38] such as DNA sequences containing the pathognomonic histone mutations of DMG in their *H3F3A* or *HIST1H3B K27M* variants[39,40]. These molecular studies could make feasible a longitudinal tumor monitoring, but they are still not fully implemented in the clinical practice.

In this thesis, I obtained liquid biopsies from patients with DIPG and I used them to address the overexpression and secretion of immunosuppressive cytokines by the tumor cells. Specifically, the samples I handled were CSF and serum.

2.3. Treatment

2.3.1. Standard of care

The standard of care treatment is local radiotherapy, which provides a temporal symptom relief to approximately 70% of the patients, being considered palliative. In fact, for decades, the survival of patients with DMGs located in the pons (i.e., DIPG) has not improved significantly. Currently, the standard of care protocol for newly diagnosed patients is focal fractioned (1.8-2 Gy) radiotherapy to a total daily dose of 54-60 Gy, 5 days per week, for 6 weeks[41,42] and glucocorticoids are adjuvantly administrated to control the radiation-associated inflammation. This confers the patients a 3-4 month survival benefit. After the short period in which

the radiotherapy seems to control tumor growth, within a median of 6 months symptomatology reappears in most children and radiological progression evidences tumor growth[43]. Importantly, although the treatment starts right after diagnosis, there is no correlation between the start of the treatment from the diagnosis and overall survival (OS) of the patients[44].

The most challenging barrier for DMG treatment is its anatomical location and infiltrative nature. Surgical resection is not a viable option as resection of the CNS structures infiltrated by the tumor, such as brainstem, thalamus or cerebellum, control vital functions, which are already deteriorated by the disease and are responsible for the clinical status of the patients. Although many chemotherapeutic regimens have been evaluated for DMG, none of them has showed efficacy improving the OS of patients. For instance, a study applying pre-irradiation followed by a combination chemotherapy regimen and re-irradiation, showed modest improvements in the patient quality of life but did not increase long-term survival[45]. Although temozolomide administration was promising due to its evident effectivity in adult glioblastoma patients[46], DMG patients do not obtain benefit from this drug. Due to the increasing molecular knowledge of DMG, new molecular-targeted strategies have arisen, administrated with or without adjuvant radiotherapy. Single-agent therapy with the PDGFR inhibitor imatinib did not improve prognosis, nor did dasatinib[47]. As EGFR is highly expressed in a subgroup of patients, single-agent EGFR-inhibitors (nimotuzumab, erlotinib or gefitinib), have also been tested, with positive results regarding increased survival only in a small subset of participants[48]. Targeting angiogenic factors such as VEGFR with inhibitors including bevacizumab or vandetanib also opened a new therapeutic vision that has also resulted not sufficiently effective[48,49]. Other

trials have used PARP1 inhibitors (olaparib, niraparib, veliparib), CDK4/CDK6 inhibitors (PD-0332991) and WEE1 kinase inhibitor (MK1775), all of them without sufficient evident of activity against the tumor growth[12].

2.3.2. New treatment strategies

Most pharmacological treatments, even though they might show promising in vitro efficacy, result inefficient in patients with DMG, due to the impossibility to cross the blood brain barrier (BBB) and reach the tumor[48]. Different strategies are being tested to overcome the integrity of BBB in DMG, but they are not completely developed yet. Increasing drug permeability by transiently disrupting the BBB structure using controlled low dosages of radiotherapy[50] or permeability-increasing agents as mannitol or morphine may help the distribution of chemotherapeutic drugs in the brainstem[51,52], but the clinical efficacy of these approaches is not sufficiently demonstrated. Local drug delivery, such as convection enhanced delivery, enables the presence the drug at high concentrations in the tumor-invaded structures[53,54], but it is a difficult technique to implement, and it comes with incomplete anticancer activity, as well. The use of nanoparticles loading the active principle might play a roles in the future, to improve delivery and effectivity in difficult-to-reach tumors[55].

Immunotherapy is the most arising field for cancer treatment, stimulating the action of the immune system of the patient to specifically recognize tumor markers and eliminate the malignant cells (**see section 3.1.2.**). The use of CAR-T therapy anti-GD2 and anti-B7-H3 in DMG have shown promising results in pre-clinical trials and have moved into clinical trials[56-59].

Recently, the study of DMG epigenetics have suggested its role in the tumorigenic process. The use of panobinostat and GSK-4 (targeting histone demethylase and deacetylase and JMJD3 respectively) showed promising preclinical results and moved into clinical trials, as well as tazemetostat against EZH2. Other molecules explored targeting DMG epigenetics are bromodomain protein inhibitors (JQ1) and CDK7 inhibitors (THZ1)[12].

In this thesis, we evaluated a therapeutic strategy using an FDA-approved drug, primarily targeting the receptor of the overexpressed cytokines secreted by DIPG cells.

2.4. Cell of origin hypothesis

DMG in its most frequent version, DIPG, is usually diagnosed in a very specific timeframe during the first decade of life. This suggests there is a time window in which the progenitor cells differentiation become affected and, consequently, the development of the midbrain structures results aberrant, giving rise to the tumor. Various hypotheses have been developed regarding the cell of origin of DIPG, but none of them has clarified completely the mechanisms by which the tumorigenic process occurs.

The biggest expansion of the human pons occurs during the first 7 months after birth, when neural progenitor cells (NPC) exponentially proliferate[60]. Monje et al. proposed the idea of a second wave of NPC proliferation in the ventral pons and medulla in childhood, coinciding with the peak of incidence of DIPG[61]. Proliferating cells in the developing human pons express NPC markers, including Sox2, nestin, vimentin, Olig2, and glial fibrillary acidic protein. Olig2 is found overexpressed in 80% of DIPGs, and has been associated with mitosis and

aggressiveness[62]. Posterior studies from Filbin et al. and Liu et al. reaffirmed this idea and found that DMG H3 K27-altered tumors are composed by a minority of more differentiated malignant cells and a majority of cells similar to oligodendrocyte precursors (OPC-like) which are characterized by a highly proliferative rate, polycomb repressive complex 2 (PRC2) suppression and partly sustained by PDGFR-α signaling[63,64].

3. Microenvironment

The National Cancer Institute (NIH) defines the term microenvironment as all the cells, molecules and structures that surround and support other cells and tissues in a particular organ. All these components have a key influence on the resident cell populations and the immunomodulation process. Due to its function and capacities, the immune response in the CNS requires a tight control and regulation to prevent an undesired and potentially pathological inflammation process. This translates into the establishment of an immunoprivileged microenvironment due to both passive physical barriers (BBB) and active processes that control immune response[65].**Tumor microenvironment**

The tumor microenvironment (TME) is characterized by the interaction of the tumor cells with the environment that surrounds them with the objective to create a favorable niche for its growth and expansion[66]. It includes stromal cells, extracellular matrix (ECM), adipocytes, mesenchymal stem cells, blood vessels, macrophages, lymphocytes, cytokines, exosomes and metabolites, which create a structure from which the tumor acquires the nutrients, oxygen and the immune-escaping mechanisms[67].

From the immunological state of the tumor microenviroment, cancers can be classified into two basic immune profiles that in lay language are known as "hot"

and "cold"[68] (**Figure 5**). Hot or immune-inflamed tumors are characterized by the presence of inflammatory cells in the tumor parenchyma such as tumor-infiltrating lymphocytes (TILs), accompanied by monocytic and myeloid cells, cancer-associated fibroblasts (CAFs) and inflammatory cytokines. Hot cancers are potentially responsive to anti-PD-L1/PD-1 immunotherapies. Cold tumors, on the other hand, can be classified into two subtypes: "immune-excluded" and "immune-dessert". The immune-excluded phenotype presents a variable number of immune cells in its niche. However, they do not penetrate the tumor, present an exhausted phenotype and are found surrounding tumor cell nests. Their clinical response to anti-PD-L1/PD-1 therapies is uncommon, because inflammatory cells, although becoming activated, are unable to invade the tumor and kill the malignant cells. The immune-dessert phenotype is characterized by the absence of inflammatory lymphocytes in the stroma or in the tumor parenchyma. Myeloid cells are usually absent or very sparse. The presence of tumor-associated macrophages (TAMs) with anti-inflammatory capacities, T regulatory lymphocytes and anti-inflammatory cytokines also contributes to the establishment of this immune-dessert phenotype. They do not respond to immunotherapy[69,70].

Converting cold tumors into hot ones might promote the natural action of the immune system against tumor growth[71].
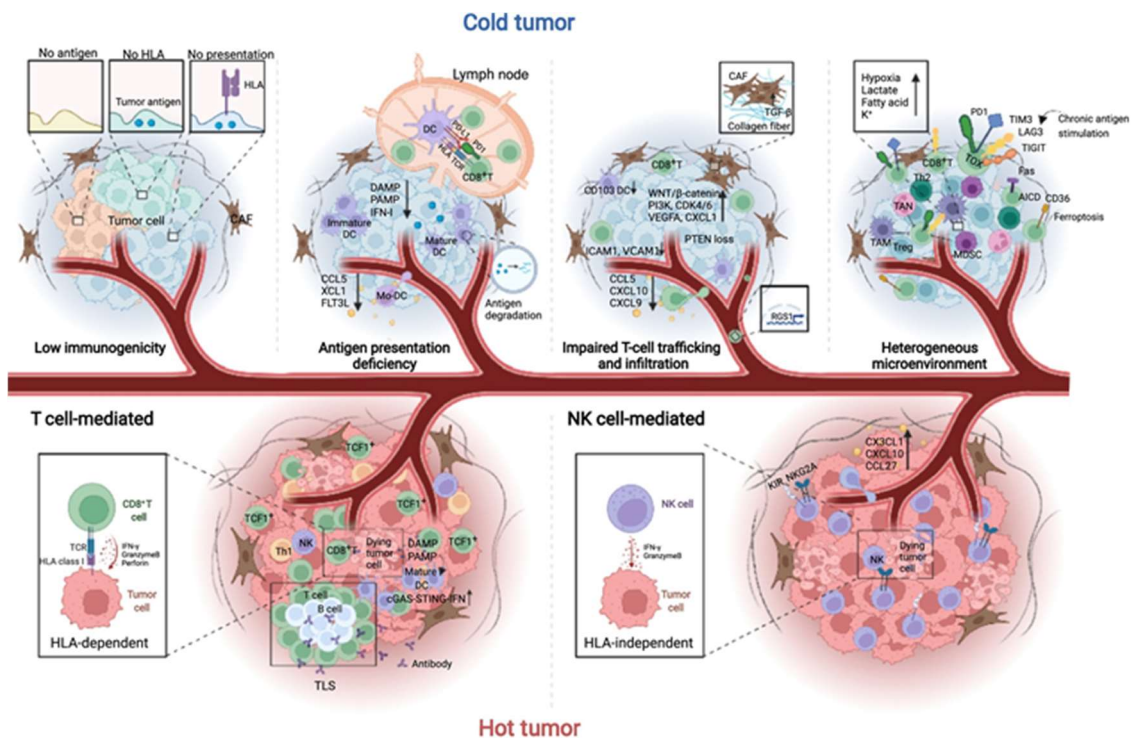
Figure 5. Tumor microenvironment characteristics. Adapted from *Zhang et al. 2022*[70].

Previous works on DMG microenvironment reported this tumor is non-inflammatory[72,73]. Lin et al. described a lower lymphocyte infiltration (predominantly CD8+) in DMG (2%) compared to adult glioblastoma multiforme (GBM; 7-50%)[73], which was later confirmed in other studies[72]. Besides, lymphocyte infiltration does not correlate with the mutational load or survival in DMG[43]. It has also been observed a general suppression of the natural killer (NK) cell population[74] that contributes to the definition of this tumor as immunosuppressed. However, the sparse immune infiltrate in the tumor tissue of DMG patients and the type of cytokine signaling observed in preliminary works suggest that this tumor may not be as immunosuppressed as it had been previously described, and some authors, such as the Seattle (USA) group, postulate that DMG might still respond well to strategies activating the immune

response, such as CAR-T cells, dendritic cell/NK cells vaccines or genetically engineered macrophages[75]. Lieberman et al. supported such proposal in their finding that DMG has fewer number of TILs[73] and fewer counts of microglia or tumor associated macrophages (TAMs) than adult glioblastoma[72]. They hypothesized that immune surveillance is low in DMG and thus immunotherapies that recruit immune cells to these tumors could be successful treatments. However, we and others believe that the activation state of the microglia (brain-resident macrophages or TAMs) of DMG has not been completely (or appropriately) studied, contributing to some missing gaps in the immune biology of the tumor[43], causing discrepancies regarding its immune-related classification. In fact, our preliminary findings in biopsies and autopsies and, most importantly, in non-tumor controls located in the brainstem, showed a high number of M2-like active microglia in DIPG, which did not fit in well with the Lieberman postulates. Also, it remains unknown which molecules or mechanisms are responsible for the acquisition of such putative TAM-mediated immune deprivation. In this thesis, we aimed to shed light on the process by which DMG escapes the immune response, with special focus on the cancer secretome leading to the immunosuppressed phenotype of non-cancer cells in the TME.

3.1.1. Tumor-infiltrating immune cells

TILs are the lymphocytes that surround and infiltrate the tumor, and play a key role in the tumor biology and response to treatment in cancer. Among TILs, CD8+ cytotoxic T cells have been considered the most important anti-tumor effector cells, being supported with the presence of CD4+ T helper cells[76]. B cells, on the other hand, mediate the humoral anti-tumor immunity[77]. Therefore, lymphocyte infiltration in tumors has been related to favorable prognosis in some cancers,

and they have been used as immunotherapeutic agents (CAR-T). In contrast, the creation of an immunosuppressed microenvironment can prevent these cells from fighting tumor growth[78]. A minor subset of CD4+ T cells called regulatory T cells (Treg) also play a major role in immunomodulation in the tumor microenvironment, and have been related both to cancer-associated inflammation and highly-suppressive functions[79]. This duality in they function may be the explanation of why Treg are associated with a poor prognosis in some cancers and with a good outcome in other neoplasias[80].

In addition to TILs, tumors are also infiltrated by macrophages. TAMs originate from monocytic precursors in the bone marrow (blood)[81] or yolk sac progenitors (tissue-resident macrophages)[82] and represent key regulators of the immunity-cancer duality. Contrarily to TILs, the presence of TAMs is often associated to poor prognosis[83]. Through years, macrophage populations have been classified into different subtypes depending on their functions (**Figure 6**). The exposure of M0-inactive macrophage to environmental stimulation enables their transcriptomic reprograming into two differentiated and active states: the classically activated M1-like (pro-inflammatory), and the alternatively activated M2-like (anti-inflammatory). M1-like macrophage polarization is promoted by classical pro-inflammatory signals such as lipopolysaccharide (LPS), interferon gamma (IFN-γ) or tumor necrosis factor alpha (TNF-α)[84]. M1-like macrophages present anti-tumor activities through inflammatory cytokine secretion, antigen presentation and tissue damage[85]. On the other hand, M2-like polarization of TAMs is induced by anti-inflammatory cytokines such as transforming growth factor beta (TGF-β) and interleukins-4, 10 and 13 (IL-4/10/13). M2-like macrophages promote the creation of an immunosuppressive microenvironment

in the tumor by producing and secreting anti-inflammatory factors, pro-angiogenic molecules and proteases necessary for tumor invasion[85-87].
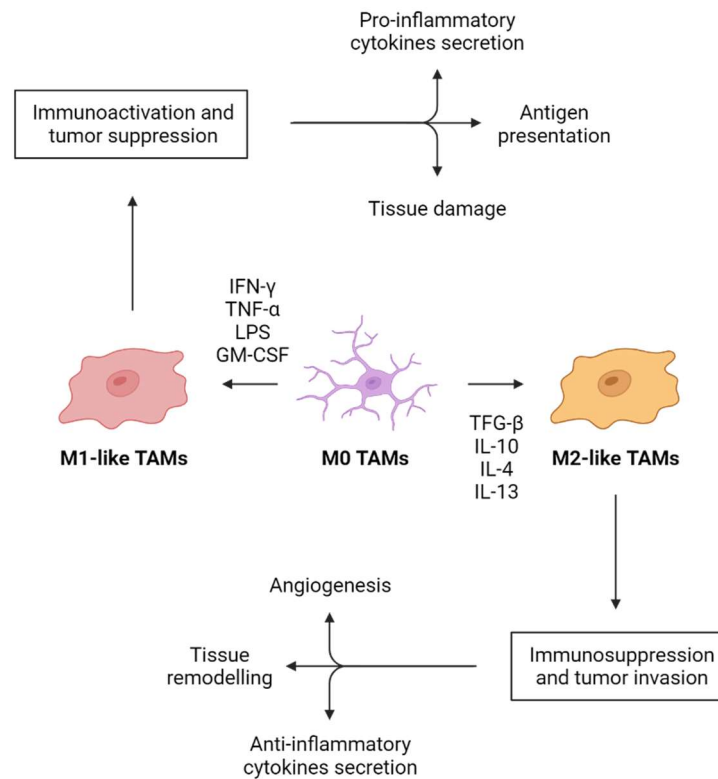
Figure 6. Macrophage polarization and specific functions of M1-like and M2-like TAMs. M0 (inactive) TAMs polarize into M1-like and M2-like active phenotypes upon pro-innflammatory (anti-tumoral) and anti-inflammatory (pro-tumoral) stimulation.

3.1.2. Immune checkpoints

Immune checkpoints are membrane molecules that inhibit immune responses against the healthy tissues of the body (**Figure 7**). However, the activation of these pathways in cancer suppresses the function of immune cells against cancer cells, enabling malignant cells to evade the immune response and promoting tumor growth[88]. Therefore, overexpression of immune checkpoints has been used as a predictive biomarker for malignancy and cancer progression, as well as immunotherapy response capacity[89].

The B7 family consists of structurally related, cell-surface protein ligands, which bind to receptors on lymphocytes that regulate immune responses. The seven known members of the B7 family include B7.1, B7.2, ICOS-L, PD-L1, PD-L2, B7-H3, and B7-H4[90].

PD-L1 (programmed death-ligand 1), also referred to as CD274 or B7-H1, is one of the most studied immune checkpoints. It is often correlated with bad prognosis in various cancers[91] due to its capacity to promote T cell exhaustion when interacting with its receptor programmed death-1 (PD-1 or CD279), which is mainly expressed in T cells, especially in tumor-associated T cells[92]. PD-L1 overexpression in cancers represents the possibility to use immune checkpoint inhibitors to suppress its activity and promote inflammation processes in the tumor[93]. PD-L2 (programmed death-ligand 2) or CD273 is also a ligand for PD-1. Their interaction also reduces the T cell receptor (TCR)-mediated proliferation and consequent cytokine production by CD4$^+$ T cells[94].

CTLA-4, also known as CD152, is another important stimulatory receptor for the regulation of T cell activation, constitutively expressed in the surface of tumor cells[95]. This molecule, homologous to CD28, binds with high affinity to CD80 and CD86 (B7.1 and B7.2, respectively) and, through not fully elucidated molecular events, transmits inhibitory signals to T cells[96,97]. CTLA-4 is also found in T regs, and contributes to their inhibitory function. Other studies propose the functionality of this molecule by the modulation of T cell motility and signaling through PI3K pathway[98].

B7-H3, also known as CD276, is found overexpressed in many cancers and was described as a co-stimulatory protein for T cell activation, increasing the

proliferation of both CD4^{+} and CD8^{+} T cells. Therefore, the expression of this molecule was initially associated to anti-tumoral functions[99]. In 2003, Suh et al. described for the first time the immunosuppressive capacity of B7-H3 through the inhibition of CD4^{+} and CD8^{+} T cells in cancer and inflammatory diseases such as rheumatoid arthritis[100]. For instance, its overexpression in oral squamous cell carcinoma was associated with poor prognosis, tumor cell proliferation, advanced clinical stage, and worse patient survival[101]. A potential cooperative role between B7-H3 and T regs has been identified in non-small cell lung carcinoma[102] and the expression of B7-H3 in cancer cells has been associated to IL-10 secretion in breast cancer[103]. It is also responsible for the regulation of cancer-associated pathways, such as PI3K/Akt/mTOR and JAK/STAT as well as angiogenesis[99]. The receptor of B7-H3 is still unknown.
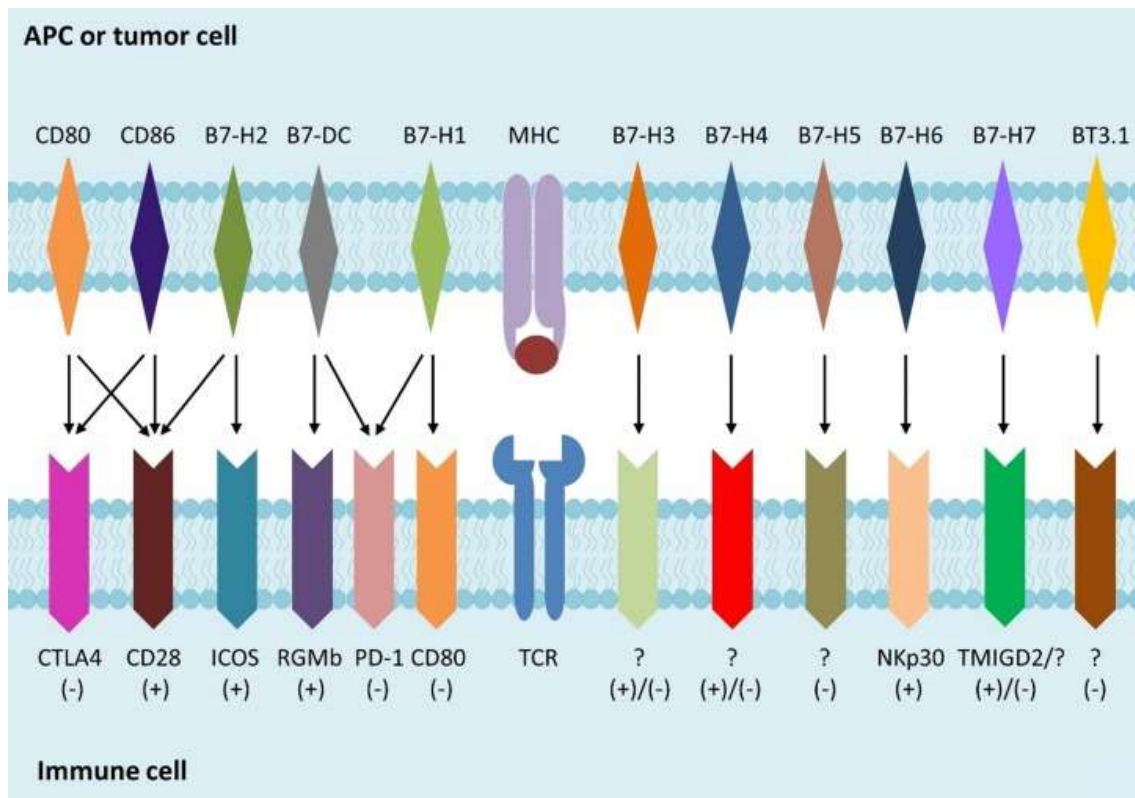
Figure 7. Immune checkpoints. The interaction of B7 family members and their receptors directs and/or regulates the response of T cells in the inflammation process. Reproduced from *Yang et al. 2020*[99].

At least eight anti-PD-L1 and anti-PD-1 monoclonal antibody-based treatments in total are approved against several cancers, some of them proving superior efficacy than standard of care regimens (**Table 2**). At least two monoclonal antibodies against CTLA-4 have been approved and are used in clinic (data consulted on the official FDA website, *https://www.fda.gov/drugs/development-approval-process-drugs*). Ipilimumab was the first anti-CTLA-4 immunotherapeutic agent approved by the FDA in 2011 for melanoma, and is also indicated for renal cell carcinoma, dMMR colorectal cancer, hepatocellular carcinoma, non-small cell lung carcinoma and malignant pleural mesothelioma, in combination with nivolumab. Another anti-CTLA-4, tremelimumab (FDA-approved on 2022), in combination with durvalumab (anti-PD-L1) is indicated for

the treatment of metastatic non-small cell carcinoma. Regarding anti-B7-H3 therapeutic strategies, several of them have been approached in pre-clinical and clinical trials. An ongoing Phase I clinical trial promoted by the Seattle group is recruiting DMG patients at any time point following completion of standard therapy (NCT04185038; partially published in Cancer Discovery in 2023[59]. This study uses a CAR-T approach focused in a locoregional adoptive therapy with autologous CD4$^+$ and CD8$^+$, which express a B7-H3-specific chimeric antigen receptor (CAR) and EGFRt. CAR-T cells are locally delivered through a catheter or Ommaya into the tumor. No results regarding the effectivity of the trial have been published yet (data consulted on the official NIH website. *https://classic.clinicaltrials.gov/).*

Table 2. FDA-approved immune checkpoint inhibitors anti PD-L1 and PD-1.

Drug	Target	FDA approval[1]	Approved indications[1]
Nivolumab	PD-1	2014	Metastatic melanoma, metastatic non-small cell lung carcinoma, malignant pleural mesothelioma, advanced renal cell carcinoma, classical Hodgkin lymphoma, squamous cell carcinoma, urothelial carcinoma, colorectal cancer, hepatocellular carcinoma, esophageal cancer, gastric cancer, gastroesophageal junction cancer, esophageal adenocarcinoma
Pembrolizumab	PD-1	2014	Advanced melanoma, non-small cell lung carcinoma, non-squamous NSCLC, classical Hodgkin lymphoma, urothelial carcinoma, neck squamous cell carcinoma, renal cell carcinoma
Atezolizumab	PD-L1	2016	Urothelial carcinoma, non-small cell lung cancer, triple-negative breast cancer, small cell lung cancer
Avelumab	PD-L1	2017	Urothelial carcinoma, renal cell carcinoma
Durvalumab	PD-L1	2017	Urothelial carcinoma, non-small cell lung cancer, small cell lung cancer, biliary tract cancer
Cemiplimab	PD-1	2018	Cutaneous squamous cell carcinoma, basal cell carcinoma, non-small cell lung carcinoma
Dostarlimab	PD-1	2021	dMMR endometrial cancer
Retifanlimab	PD-1	2023	Merkel cell carcinoma

[1] Data consulted on the official FDA website (*https://www.fda.gov/drugs/development-approval-process-drugs*).

3.1.3. The blood-brain barrier

Blood vessels are essential to deliver oxygen and nutrients to the tissue, remove waste products from the organs, transport hormones among tissues and mediate the immune response. Comprised by capillaries, arteries, veins and venules, each segment has specific characteristics that enable them to carry out distinct functions[104]. There are three main capillary classes, which differ in their structure and permeability: (i) continuous nonfenestrated (lungs and skin), (ii) continuous fenestrated vessels (intestine), and (iii) discontinuous (liver)[105]

The CNS is highly vascularized because access to oxygen and nutrients is essential for its correct function. The vasculature network in the CNS is highly specialized and presents specific and different characteristics compared to vessels in the rest of the organism. CNS vessels are classified as a continuous non-fenestrated subtype, with specialized properties responsible for a high regulation of the movement of molecules, ions and cells between the CNS and blood, necessary for the maintenance of the fragile homeostasis of the brain[106]. The BBB is the term describing the unique properties of the CNS vascular network that allow, in physiologic conditions, a proper neuronal function and the protection of the CNS from toxins, inflammation, infection and other diseases[104].

Blood vessels are basically conformed by two cell types (**Figure 8**) namely endothelial cells and mural cells. Endothelial cells are responsible for the formation of the vessel walls. At the CNS, they are held together by tight junctions, which regulate the exchange of molecules and cells between the brain and blood by limiting the paracellular flux of solutes[107]. Moreover, in the CNS, there is a very low rate of transcellular vesicle transportation[108]. Such limited movement of molecules at the BBB confers the capacity of controlling the

transportation trough two main types of transporters. First, efflux transporters transport lipophilic molecules toward the blood. Second, highly specialized nutrient transporters facilitate the transport of specific nutrients into the CNS and the removal of waste products from the CNS to the blood[104]. The BBB is also characterized by an extremely low expression of leukocyte adhesion molecules (LAMs) in comparison with blood vessels in other organs[109]. This translates in a very low number of immune cells inside the CNS, limiting the inflammatory response, which would be highly harmful for the organ.

Supporting and surrounding the endothelial wall, we can find mural cells, which include vascular smooth muscle cells and pericytes. The vascular smooth muscle is responsible for the contraction of blood vessels, necessary for regulating blood vessel tone, blood pressure and blood flow[110]. Pericytes patchedly cover the endothelial cells and are embedded in the basement membrane (BM), an extracellular matrix on which epithelial and endothelial cells grow. In the CNS, pericytes are derived from the neural crest and have the abilities of controlling the diameter of the capillaries, regulate angiogenesis, deposition of the extracellular matrix, wound healing, immune cell infiltration, regulation of blood flow and regulation of the BBB during development[104]. Some studies also report multipotent properties of this cell type[111]. Adjacent to the vascular compartment, the endfeet of astrocytes are in contact with the vascular tube, providing a cellular link between neuronal activity and blood vessels. This enables astrocytes to deliver signals that regulate blood flow in response to neuronal activity[112].
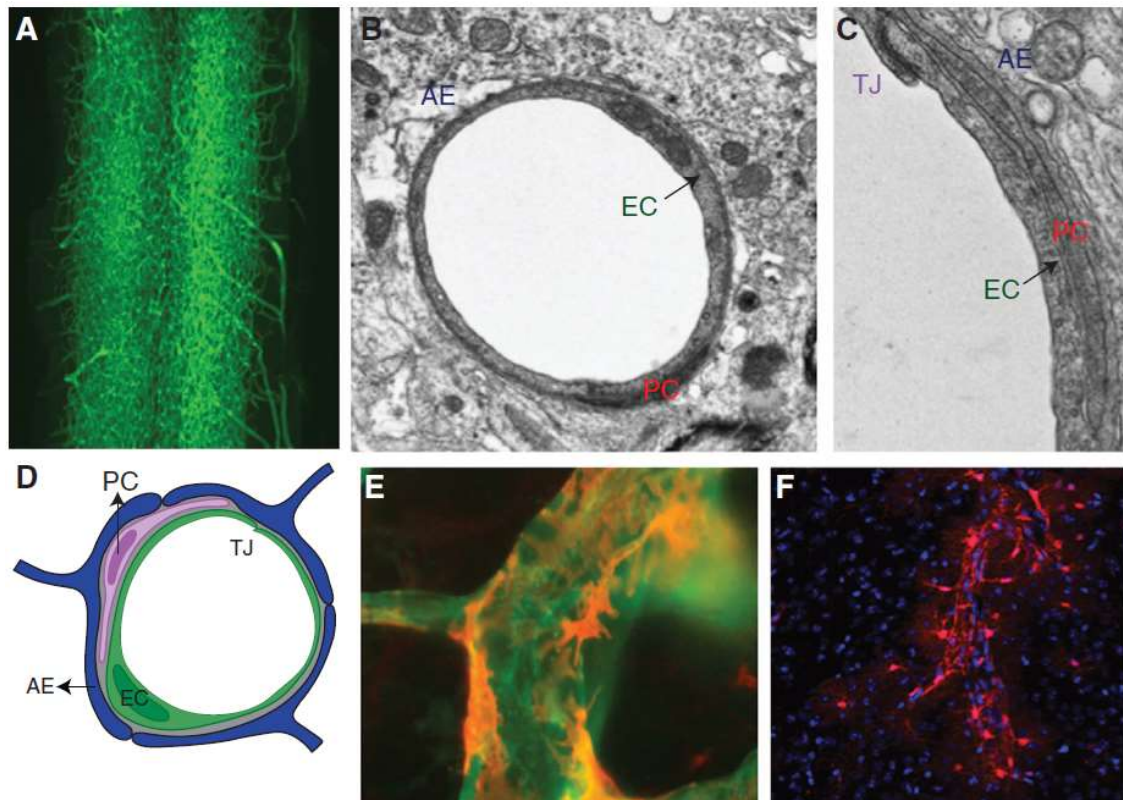
Figure 8. Components of the BBB. (A) Vascular cast of a spinal. (B) Electron micrograph of a cross section of a CNS vessel. Endothelial cells (EC), pericytes (PC) and astrocytes (AE). (C) Magnified electron micrograph a CNS vessel. Tight junctions (TJ) and astrocyte endfeet (AE). (D) Schematic representation of the cell types within the neurovascular unit. (E) Immunofluorescence micrograph depicting relationship of PCs (red) with ECs (green). (F) Micrograph depicting relationship of astrocytes (red) with blood vessels (unstained). Reproduced from *Daneman et al. 2015*[104].

Tumors also use blood vessels to obtain nutrients, paracrine signals and oxygen, necessary for their growth. They either use the pre-existing vasculature, or they induce angiogenic processes de novo. Endothelial cells are usually found in a quiescent state, but they can be induced to form new vascular structures by pro-angiogenic factors secreted principally by tumor cells, such as vascular endothelial growth factor (VEGF) (**Figure 9**). These newly formed blood vessels are also necessary for tumor cell migration to healthy tissue structures and the consequent tumor expansion.

In the presence of pro-angiogenic signals secreted in the microenvironment, the newly formed vascular networks have less ability to mature, which translates into heterogeneous diameter of the blood vessels and a chaotic blood flow through these malformed tubes[113]. Endothelial junctions are often disrupted in the tumor vasculature, leading to enhanced permeability. Moreover, pericytes can be partially detached from endothelial cells in tumor vessels, and an uneven basal lamina distribution is observed, which is compatible with an increased vessel fragility and risks of hemorrhage[114].
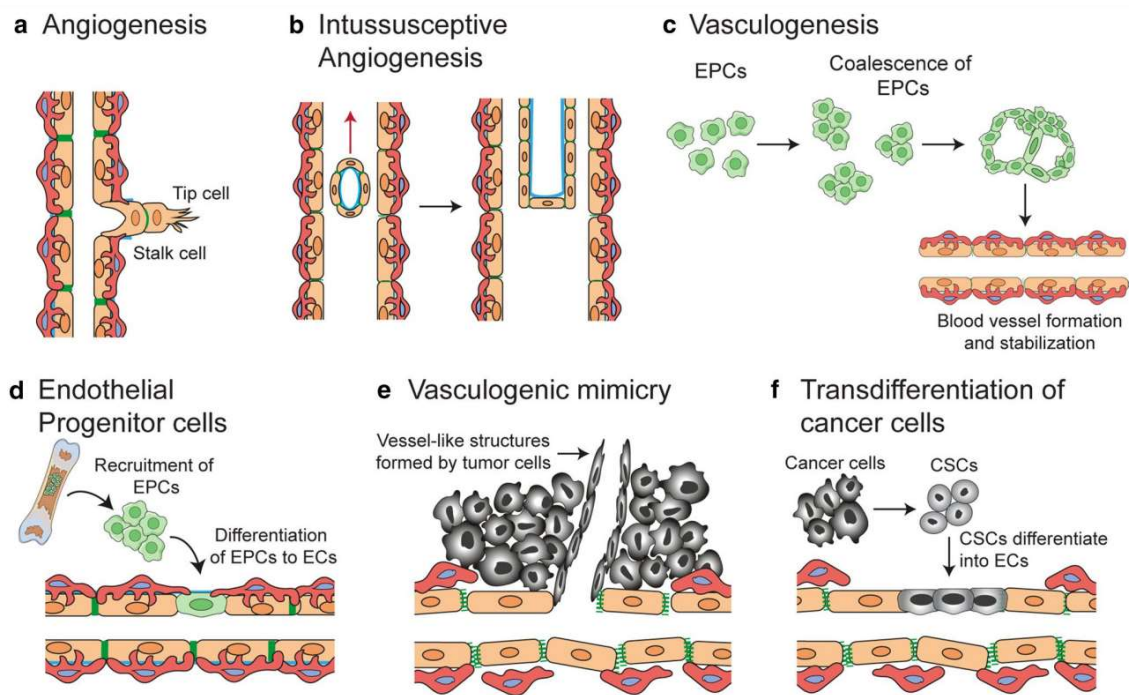
Figure 9. Mechanisms of blood vessel formation. (A) Sprouting angiogenesis, (B) intussusceptive angiogenesis, (C) vasculogenesis, (D) recruitment of endothelial progenitor cells: vessel formation in tumors by recruitment of circulating endothelial progenitor cells, (E) Vascular mimicry, and (F) trans-differentiation of cancer stem cells to endothelial cells. Adapted from *Lugano et al. 2019*[72].

Consequently, in many neurological diseases, including several adult brain tumors, the stability of the BBB becomes compromised[106,115]. However, in the

context of DMG, this structure remains intact, and its restrictive nature becomes a problematic physical barrier for drug delivery and other therapeutic options[43]. Moreover, besides using the preexisting vasculature, tumor cells orchestrate the secretion of angiogenic growth factors such as VEGF and the activation of signaling pathways to promote the creation of new aberrant blood vessels, which empower tumor growth, metastasis and expansion due to the increase of oxygen and nutrient provision[114].

The possibility of using an anti-angiogenic therapy in cancer was first proposed in 1971 by Judah Folkman[116] with the objective to reduce the oxygen and nutrients supply to the tumor and, consequently, diminish tumor growth. Decades later, FDA approved the first VEGF-targeted therapy (bevacizumab) and a new generation of drugs was developed for the dual targeting of VEGF signaling pathway and alternative angiogenic pathways that were granting treatment resistance to the tumor[117]. Phase III clinical trials have shown diverse response patterns, and tumors have been classified as sensitive, partially sensitive and insensitive to anti-angiogenic therapies (**Table 3**). Most studies show high effectivity to inhibit newly formed vasculature but less antiangiogenic activity against previously stablished vessels.

In this thesis, I aimed to elucidate the role of the secretome DMG on the angiogenic process, both structurally and molecularly.

Table 3. Tumor response to anti-angiogenic therapy. Adapted from *Lupo et al. 2017*[118].

Tumor	Response	Reference
Breast Cancer	Partially sensitive	Fakhrejahani and Toi. 2014; Earl et al. 2015
Clear cell renal carcinoma	Sensitive	Hutson et al. 2014; Rini et al. 2014
Colorectal cancer	Partially sensitive / insensitive	Bennouna et al. 2013; Grothey et al. 2013
Gastroesophageal cancer	Partially sensitive	Fuchs et al. 2014; Wilke et al. 2014
Glioma	Partially sensitive	Gilbert et al. 2014
Hepatocellular carcinoma	Sensitive	Bruix et al. 2015; Cainap et al. 2015
Lung cancer	Partially sensitive	Garon et al. 2014; Liang et al. 2014
Neuroendocrine and thyroid cancer	Sensitive	Brose et al. 2014
Ovarian and cervical cancer	Sensitive	Pujade-Lauraine et al. 2014; Tewari et al. 2014
Pancreatic cancer	Insensitive	Kindler et al. 2010
Prostate cancer	Insensitive	Michaelson et al. 2014

3.1.4. Cytokines

Cytokines are small proteins secreted by cells to interact and communicate with other cells. The action of the cytokines may be autocrine (i.e., on the same cell secreting them), paracrine (i.e., on the cells nearby) or endocrine (i.e., in distant cells). Different cytokines can activate the same functions, and are often produced in cascade. A variety of cytokines known as chemokines induce chemotaxis and are able to activate and promote the migration of immune cells, such as lymphocytes or macrophages[119].

There are two main families of cytokines: pro-inflammatory and anti-inflammatory. Pro-inflammatory cytokines are mainly produced by activated macrophages and are involved in inflammatory reactions and pathological pain processes. Some of the classical inflammatory cytokines include interleukin-1β (IL-1β), interleukin-6 (IL-6), TNF-α and IFN-γ[119]. On the other hand, anti-inflammatory cytokines are immunoregulatory molecules that control the pro-inflammatory cytokine response. Some of the most important immunosuppressive cytokines include IL-10 and TGF-β[119].

Cancer cells can autonomously secrete or exploit immunosuppressive cytokines secreted by the host tissue to escape the immune response or promote angiogenesis and, consequently, enable tumor growth and dissemination[120]. In such environment, most tumors are classified as cold, due to the presence of anti-inflammatory cells, the absence of pro-inflammatory cells and the secretion of classical anti-inflammatory cytokine secretion[68,70,71,121]. However, no clear cytokine secretion has been identified in our disease of interest, DMG[73].

In this thesis, I aimed to identify a common pattern of secreted proteins in DMG, to help explain the immunosuppressed phenotype of this tumor.

3.1.4.1.   Osteopontin

Osteopontin is a secreted, multifunctional glycol-phosphoprotein present in pathological conditions and in some of the normal physiological processes in our body. *SPP1* gene (4q22.1) includes seven exons that go through alternative splicing, resulting in the production of different variants (osteopontin-a, -b and -c)[122]. All three variants are synthesized as 287-314 aminoacid precursor proteins, which are matured to shorter active molecules.

Osteopontin is produced by many cell types in a wide range of tissues in the body[122-125] (**Figure 10A**). It is a key mediator activities such as cell adhesion, migration, proliferation, survival, differentiation, inflammatory cell activation and immune modulation. Through its interaction with its receptors, osteopontin is implicated in bone remodeling[125], vascularization[126], diabetes and obesity[127], inflammation processes, tumorigenesis, cancer invasion and metastasis[122,128]. It is also responsible for the stimulation of the migration, polarization and accumulation of macrophages[128]. One of the main roles of osteopontin in cancer is limiting inflammation to create an immunosuppressed tumor microenvironment[129]. In fact, osteopontin is often overexpressed by cancer cells (*Figure 10***B**) and other microenvironment components and it has been associated with poor prognosis in various carcinomas, melanoma, breast cancer, acute myeloid leukemia and GBM (**Figure 10C**). This protein has also been associated with tumor advanced stages and grade, tumor burden, invasiveness and metastatic capacity[39,130-136].
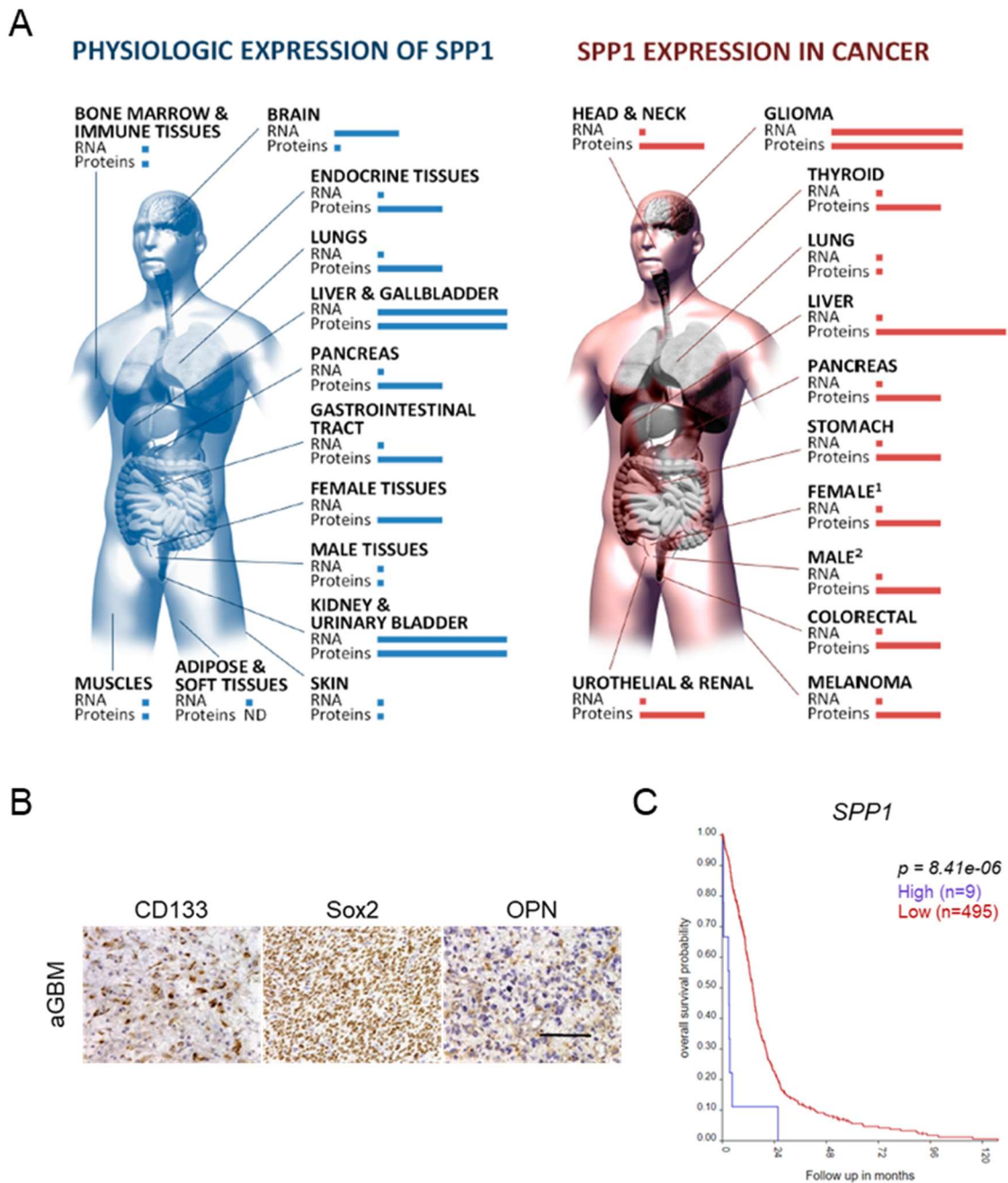
Figure 10. Osteopontin expression in cancer. (A) OPN expression in physiologic conditions and cancer. Reproduced from *Lamort et al. 2019*[137]. (B) Representative images of CD133, Sox2 and OPN in adult GBM (aGBM). Scale bar is 100 μm. Modified from *Polat et al. 2022*[138]. (C) Kaplan-Meier analysis of overall survival in aGBM for *SPP1*. Elevated expression of *SPP1* is inversely correlated with the survival of adult patients with GBM (*R2 genomics analysis and visualization platform. https://r2.amc.nl/*).

The osteopontin-associated mechanisms underlying the aggressiveness of tumors have been studied for years. Osteopontin contains a classic integrin-binding site (RGD) that binds integrins, such as integrin αvβ3. Also, the C-terminal site of osteopontin is recognized by CD44 and its variants[123]. Different enzymes, such as metalloproteinases 3 and 7 (MMP-3, MMP-7) or thrombin have the ability to cleave osteopontin, revealing an additional adhesion site which confers a higher binding efficiency to its receptors[139]. Through the interaction of osteopontin with its receptors, many cancer-related pathways are activated (**Figure 11**), leading to increased metastatic potential of the tumor cells and the secretion of pro-tumorigenic factors that interact with other tumor components. Some of the cascades that are triggered by this interaction include PI3K/Akt, JAK/STAT, Ras/Raf/MEK/ERK and NFKβ, and lead to the expression of factors and proteins involved in angiogenesis, cell migration and proliferation, inhibition of autophagy and apoptosis, and immune suppression[126,140-148].
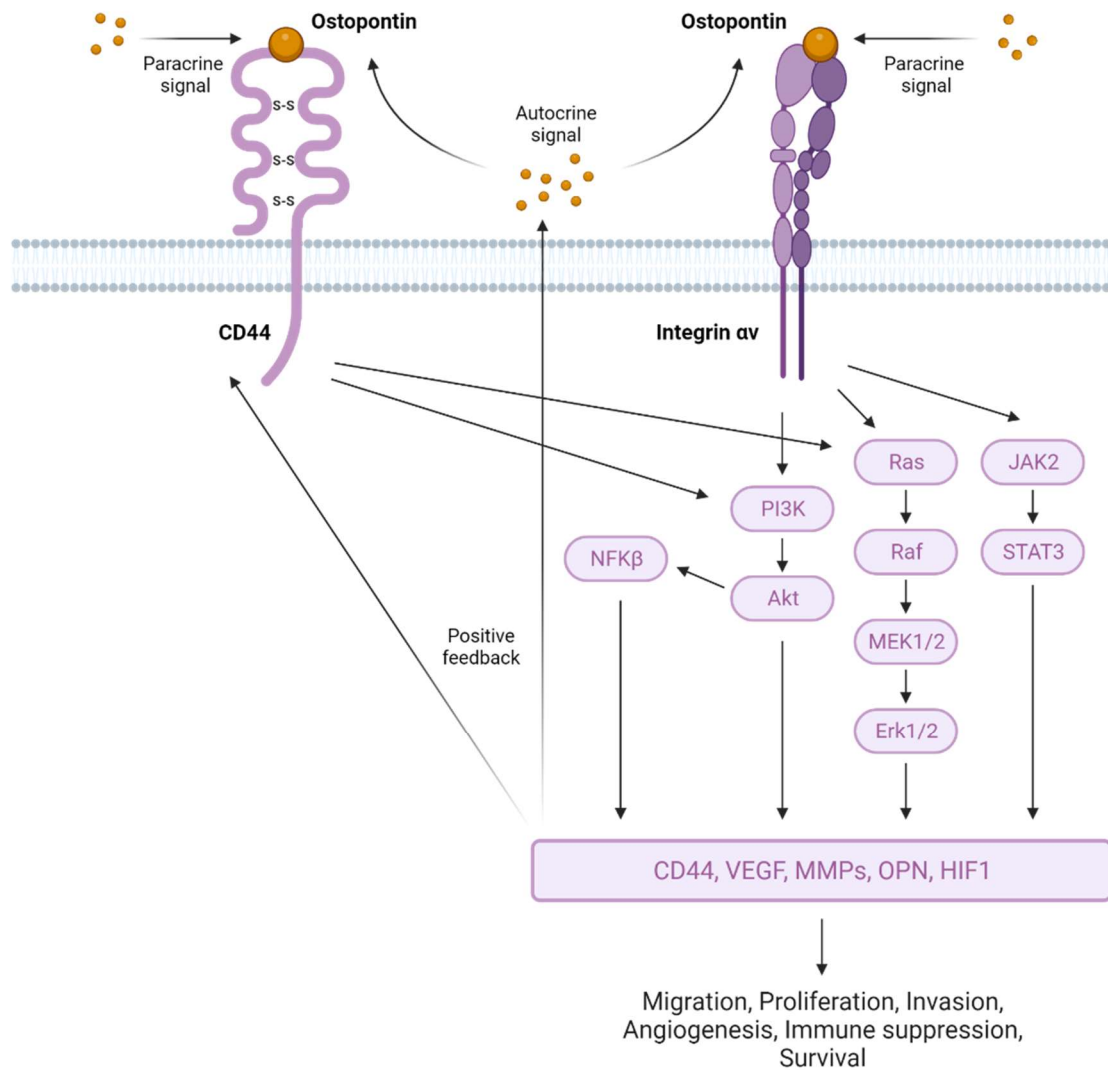
Figure 11. Osteopontin signaling cascade. Osteopontin interacts with its receptors, CD44 and integrin αvβ3, and activates various signaling pathways that lead to tumor growth. The activation of PI3K, MAPK and STAT3 induce the expression of genes related to tumor growth and metastasis (MMPs, VEGF), and leads to a positive feedback of the cascade through intrinsic osteopontin and CD44 synthesis.

In several cancers, osteopontin quantification in tumors or liquid biopsies (blood, CSF) is used as a biomarker to determine evaluate treatment response, to complement imaging diagnosis or to develop early diagnosis strategies[149-151] [57,150].

Osteopontin remains as a potential therapeutic target for cancer, and different strategies have been developed such as monoclonal antibodies, siRNAs or small molecules acting as direct or indirect inactivators of its activity[152].

In this thesis, I identified the overexpression and secretion of osteopontin in DIPG and I studied its effects on different components of the tumor microenvironment. I also quantified osteopontin in CSF and serum samples from patients.

3.1.4.2.   Chitinase 3-like 1

Chitinase 3-like 1 (CHI3L1) is a secreted, non-enzymatic glycoside hydrolase expressed in a multitude of cells, including hepatic stellate cells, endothelial cells, immune cells, astrocytes and cancer cells **(Figure 12A)**[153-158]. C*HI3L1* gene (1q31-1q32) includes ten exons and its active product is presented as a 40 kDa protein[156] with heparin, chitin, and collagen-binding properties.

CHI3L1 is expressed in physiological and pathological conditions in many tissues in the body. It has a crucial role in inflammation, oxidant-induced responses, tissue repair, apoptosis and protection against pathogens, and also in cancer and metastasis. In tumors, through its interaction with its receptors, CHI3L1 is able to reduce inflammation and promote tumorigenesis through macrophage differentiation to the M2-like type, TGF-β expression and angiogenesis[159-162]. However, many of these cascades remain unclear and raise new possible research branches.

CHI3L1 has been found overexpressed in many tumors and strongly correlates with poor prognosis, worse treatment response and advanced stages of the disease in many carcinomas, lymphomas and adult glioblastoma (**Figure 12B**)[154,163-167].
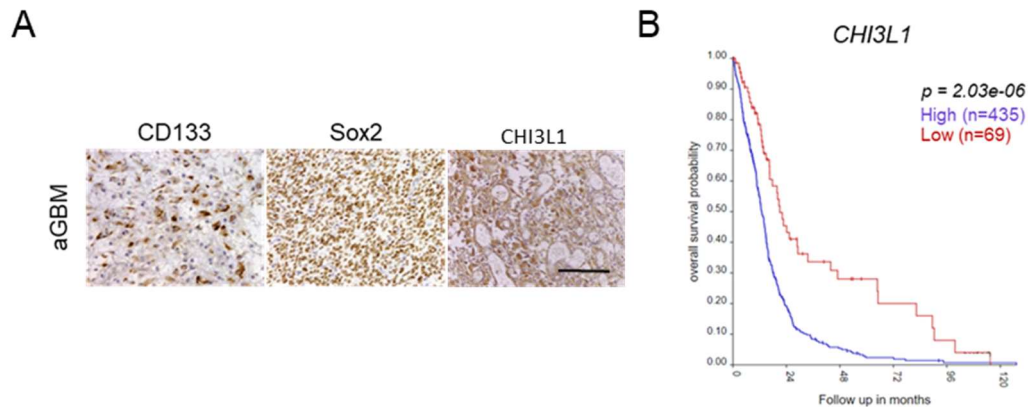
Figure 12. Chitinase 3-like 1 expression in GBM. (A) Representative images of CD133, Sox2 and CHI3L1 in adult GBM (aGBM). Scale bar is 100 µm. Modified from Polat et al. 2022 and *Nutt et al. 2005*. (B) Kaplan-Meier analysis of overall survival in aGBM for CHI3L1. Elevated expression of CHI3L1 is inversely correlated with the survival of adult patients with GBM (*R2 genomics analysis and visualization platform. https://r2.amc.nl/*).

Interacting with CD44 and its variants, integrin αvβ3 and possibly other receptors, CHI3L1 activates pathways used by the tumors to grow, such as immunosuppression or angiogenesis[168,169]. The mechanisms underlying the aggressiveness of tumors associated with CHI3L1 rely in the activation of cancer-related pathways (*Figure 12*), many of them shared with osteopontin, such as PI3K/Akt, JAK/STAT, Ras/Raf/MEK/ERK and NFKβ. These cascades lead to the expression of angiogenic factors, regulation of extracellular matrix integrity, cell migration and proliferation, and immune suppression[169,170].
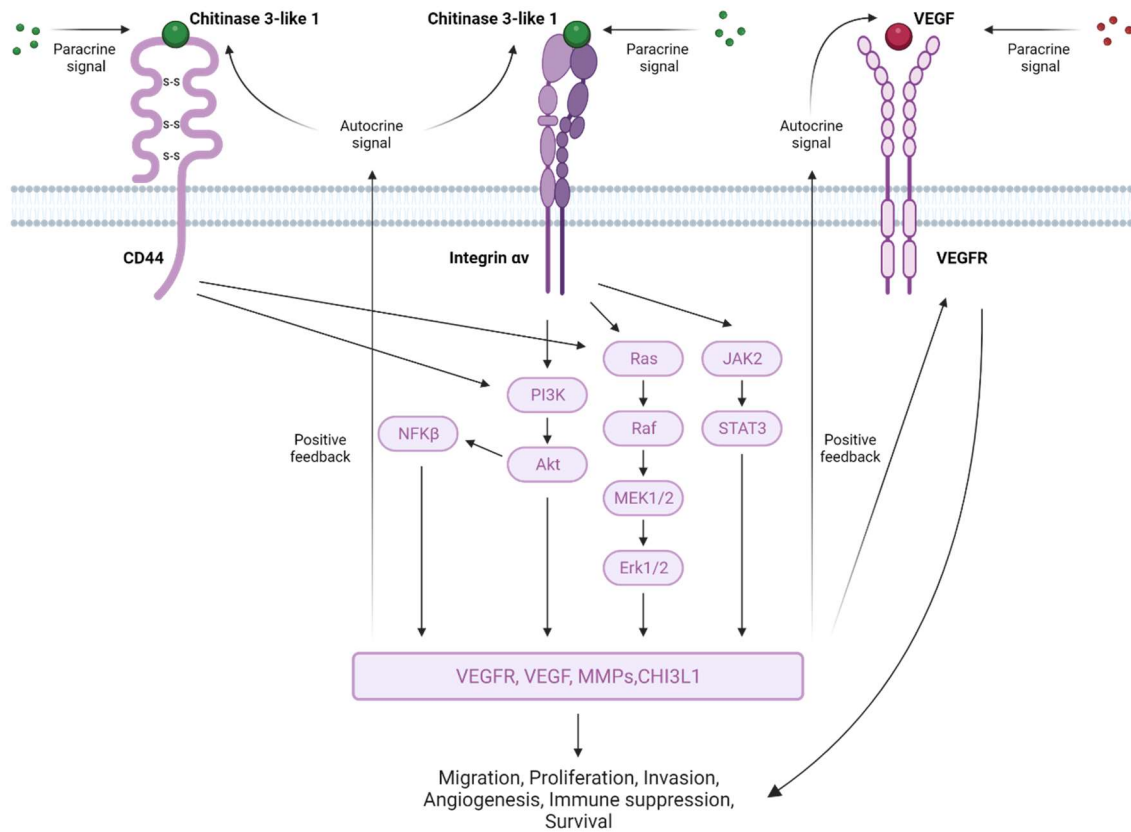
Figure 13. Chitinase 3-like 1 signaling cascade. Chitinase 3-like 1 interacts with its receptors, and activates various signaling pathways that lead to tumor growth. The activation of PI3K, MAPK and STAT3 induce the expression of genes related to tumor growth and metastasis (MMPs, VEGF and VEGFR), and leads to a positive feedback of the cascade through intrinsic CHI3L1 synthesis.

CHI3L1 analysis in blood and CSF is considered a biomarker for inflammatory diseases such as multiple sclerosis, encephalitis, traumatic brain injury or acute kidney injury[153,158,171,172]. Moreover, it is also detected in body fluids of tumor patients. Its identification in serum is used as a metastatic and prognostic marker in colorectal cancer, ovarian carcinoma and lung carcinoma[165,173,174].

In this thesis, I identified the overexpression and secretion of CHI3L1 in DIPG and I studied its effects on some of the cellular components of the microenvironment of DIPG. I also quantified CHI3L1 in CSF and serum samples from patients.

4. CD44-xCT axis

4.1. CD44

CD44 is a cell-surface class I transmembrane glycoprotein encoded by *CD44* gene, found in the short arm of the chromosome 11 (11p13) and genomically composed by 20 exons. The first five exons (1-5) together with the last five (16-20) encode for the standard form, CD44s, which is the shortest (85-95 kDa) form of the molecule and is ubiquitously expressed in all healthy tissues. CD44 is structurally organized in three regions, including the ectodomain (N-terminal, encoded by the exons 1-5), the transmembrane domain (exons 6-15) and the intracellular tail (C-terminal, encoded by the exons 16-20)[175,176]. CD44 overexpression has been previously related to cancer signatures and tumor progression[177-180]. The expression of the variant forms (CD44v) has a direct role in the tumorigenic process, being responsible for the acquisition of adaptive plasticity by cancer cells[181]. The variants of CD44 receive their nomenclature (CD44v1-v10, v1 not encoded in humans) depending on the alternative splicing site by which they incorporate the genomic exons 6-15, either singly or in combination (85-230 kDa) (**Figure 14A**). All variants are expressed in the cancer cells although one of them is always found predominant in the tumor, becoming a molecular characteristic to each one of them[11,182]. The elongation of the CD44 molecule due to the alternative splicing of the variable region of the gene, results in the incorporation of an additional membrane-proximal portion of the extracellular domain (**Figure 14B**).
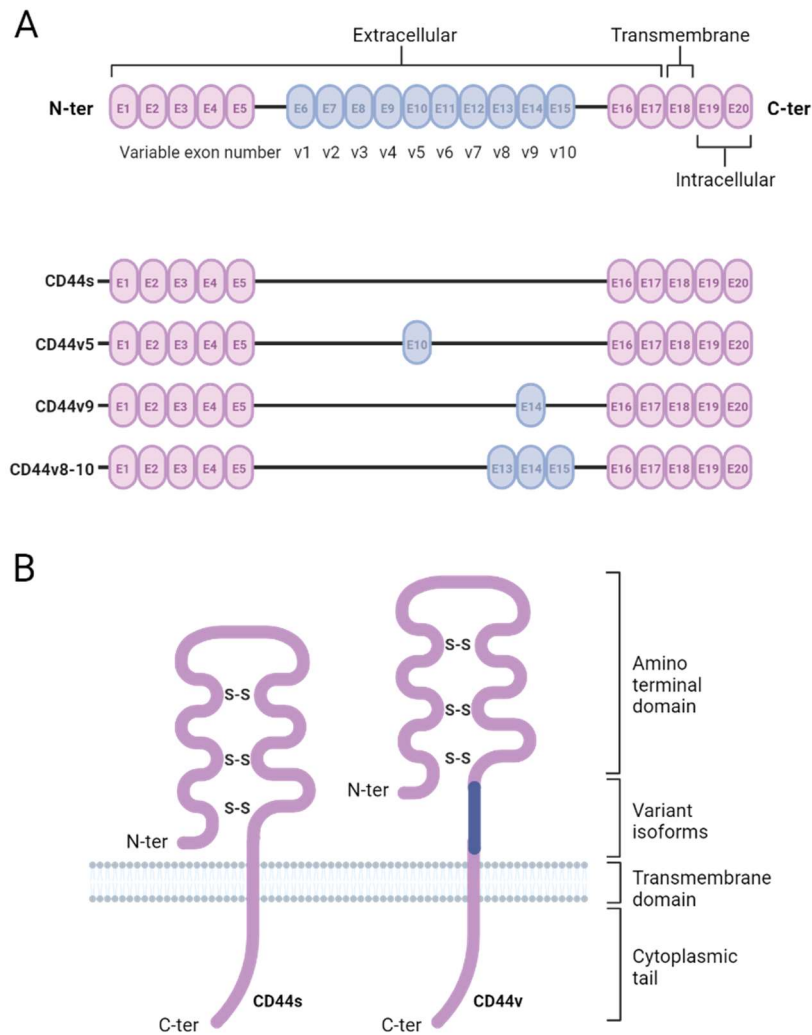
Figure 14. Structure of CD44 gene and protein. (A) CD44 consists of several exons. Some of them are constant and present in every CD44 mRNA and protein (pink), and others are variant exons (blue) which are incorporated in CD44 splicing variants (CD44v) found in cancer. (B) CD44 protein structure. The CD44 receptor is composed of an extracellular domain; a domain close to the transmembrane region where the variant exon products insert; a transmembrane region and an intracellular cytoplasmic domain.

CD44 is overexpressed in various types of cancers. Hyaluronic acid (HA), one of the main components of the ECM, is the principal ligand of CD44, but it also binds to other ECM and ECM-unrelated components[176], such as osteopontin[183]. Osteopontin increases cell surface expression of both CD44s and CD44v through positive feedback (**Figure 15**). The osteopontin-CD44 interaction promotes

tumorigenicity, especially through CD44v, and confers a stemness signature in tumor cells[177,183-185].

The expression of CD44 is regulated by a variety of molecules, such as cytokines, transcription factors, microRNAs and post-translational modifications. Its pro-tumoral effects are based in the stimulation of signaling cascades related with proliferation, apoptosis, EMT process, drug resistance, angiogenesis and the activation of transcription factors[175]. PI3K/Akt cascade activates through phosphorylation, increasing apoptosis by blocking p53 genomic survival response. MAPK/ERK signaling through Ras activation promotes cell proliferation[186]. Moreover, the ECM degradation, necessary for cell migration, is increased by MMP2[187] and MMP9[188] expression. CD44 expression has also been recently associated to the regulation of immune checkpoint in some cancers, being involved in M2-like macrophage polarization and infiltration to the tumor microenvironment[189]. Due to the direct relation of CD44 to cancer, various studies have proposed its potential as a therapeutic target for CD44+ tumors (**Table 4**).

In this thesis, I studied the expression of CD44s and CD44v in DIPG samples, and I identified CD44v5 as the most expressed variant in this cancer.

Table 4. **CD44-targeted therapy in some preclinical and clinical studies.** Adapted from *Xu H et al. 2020*[175].

Therapeutic agent name	Nature of the therapeutic agents	Cancer type	Effects
	CD44 blocking antibody	Lung cancer	Suppressing the proliferation of A549 cells
[111]In-cMAb U36	mAb specific to CD44v6	Head and neck squamous cell carcinoma	High tumor uptake
VFF18	mAb specific to CD44v6	Human squamous cell carcinomas	Fast tumor uptake
RG7356	Humanized mAb for CD44	Leukemia B cells	Cytotoxic effects
H4C4	Anti-CD44 mAb	Melanoma	Blocking cell aggregation and aggregate coalescence
USP22-NLs-CD44	USP22 siRNA-loaded nanoliposomes with CD44 Ab	Gastric cancer	Targeting CD44+ gastric cancer stem cells
	HA-coated cationic liposomes of cabazitaxel and silbinin	Prostate cancer	Showing proficient cytotoxicity against CD44+ cells
	HA-coated gold nanorods conjugated with pH-sensitive groups and loaded with doxorubicin	Cancer	Enhancing the killing of cancer cells and the inhibition of tumor growth
MTX-EDA-PEG-EDA-HA nanoparticles	Polyethylene glycol-HA nanoparticles conjugated with mitoxantrone	Breast cancer	Delivering toward CD44 receptor-positive MDA-MB-231 cells
GNS/siHSP72	Nanosystem containing gold nanostar/siRNA of heat shock protein 72/HA	Triple negative breast cancer	Selectively sensitizing CD44+ TNBC cells to hyperthermia
HA-IR	A phase IIa study: HA-irinotecan and carboplatin versus standard irinotecan and carboplatin	Extensive-stage small cell lung cancer	Selectively delivering anti-tumor drugs to CD44+ tumor cells with enhanced efficacy

4.2. xCT

xCT is the light-chain subunit (gene *SLC7A11*) of the x_c^-/xCT cysteine-glutamate antiporter system (**Figure 15**), a transmembrane protein responsible for the exchange of intracellular glutamate and extracellular cysteine capable of regulating the accumulation of reactive oxygen species (ROS) inside the cells. ROS accumulate as result of the action of chemotherapeutic agents and other anti-cancer approaches, by the synthesis of intracellular glutathione (GSH). The expression of xCT has been widely associated to tumor growth, progression and chemoresistance. For instance, xCT levels are causally linked with the malignancy grade of glioblastoma[190]. Inhibition of this antiporter has demonstrated antitumor effectivity in glioblastoma, melanoma and prostate cancer[191], resensitizing the tumor to classical treatments and offering an alternative to apoptosis due to the activation of ferroptosis, a programmed cell death pathway dependent on iron. xCT activity and expression has been related to the presence of CD44v in the tumor cells. The variants of CD44 are responsible for x_c^- system stabilization, which entails a higher antioxidant activity in the tumor cell[192].
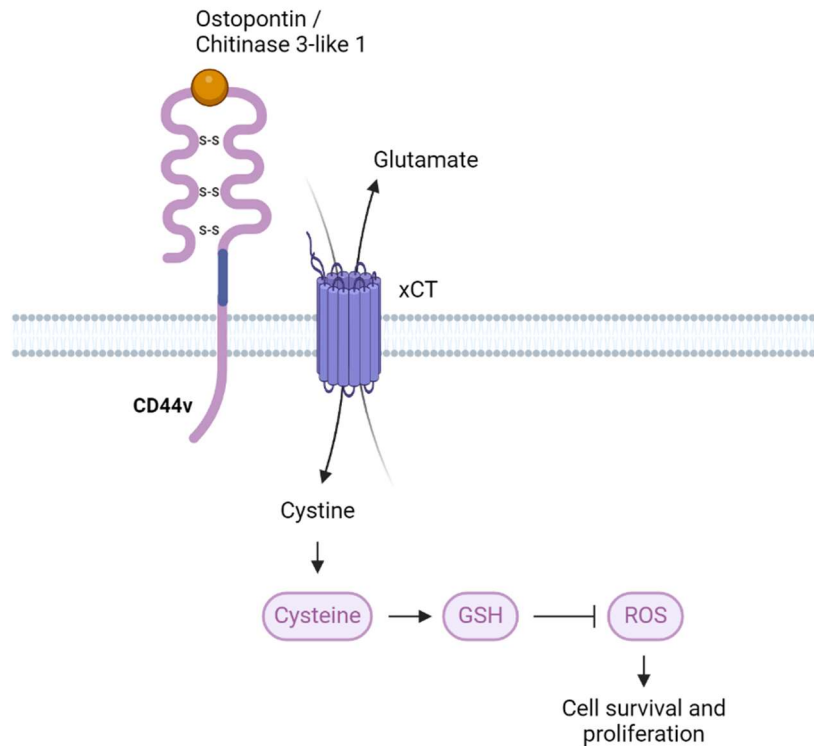
Figure 15. CD44v-xCT axis. x_c^-/xCT is a heterodimeric glutamate-cystine antiporter system that transports glutamate out of the cell in exchange for cystine. Cystine is then reduced to cysteine, which is after used for protein and glutathione (GSH) synthesis. These channels are associated to CD44v and are used by the tumor cells to reduce intracellular ROS accumulation for cell survival and proliferation.

4.3. Sorafenib

Sorafenib (BAY 43-9006, Nexavar®) is a bi-aryl urea multikinase inhibitor. It targets cell surface tyrosine kinase receptors (VEGFR, PDGFR), downstream intracellular kinases implicated in tumor cell proliferation and tumor angiogenesis[193] (B-raf, RAF, VEGF 1/2/3, FLT3, FGF) and the x_c^- system[190] (**Figure 16**). Sorafenib was first approved by the FDA and European Commission in 2007 for the treatment of hepatocellular carcinoma[131], and now is also indicated to treat renal carcinoma[78] and differentiated thyroid carcinoma[194]. Although sorafenib is usually administered as monotherapy, many studies suggest its use

as a combination with other drugs in order to reduce the doses of the multikinase ihibitor[195].

Previous studies have suggested xCT as a potential drug target for glioblastoma, which has been associated to chemotherapeutic resistance. Some studies report the selective efficacy of this drug against glioblastoma cells proliferation and survival in vitro[196,197]. Moreover, Siegelin et al. demonstrated that sorafenib suppresses tumor growth in preclinical glioblastoma mouse models, postulating its capacity to cross the blood-brain barrier, without being associated with systemic or organ toxicity[198]. Consequently, numerous clinical trials arised for the administration of this treatment alone or in combination with other chemotherapeutic agents or radiation. However, none of them demonstrated sufficient improvements in patient survival or disease progression (**Table 5**)

Table 5. Completed clinical trials for adult GBM using sorafenib. Data consulted from *https://classic.clinicaltrials.gov/*

Clinical trial ID	Phase	Conditions	Treatment
NCT00544817	Phase II	Glioblastoma Multiforme	Radiation, temozolomide, sorafenib
NCT00597493	Phase II	Recurrent Glioblastoma Multiforme	Sorafenib, temozolomide
NCT00329719	Phase I and II	Adult Glioblastoma, Adult Gliosarcoma and Recurrent Adult Brain Neoplasms	Surgery, sorafenib tosylate, temsirolimus
NCT00445588	Phase II	Adult Giant Cell Glioblastoma, Glioblastoma, Adult Gliosarcoma and Adult Recurrent Brain Tumor	Erlotinib hydrochloride and sorafenib tosylate
NCT00335764	Phase I and II	Adult Giant Cell Glioblastoma, Glioblastoma, Adult Gliosarcoma and Recurrent Adult Brain Tumor	Sorafenib tosylate, erlotinib hydrochloride, tipifarnib, temsirolimus
NCT00621686	Phase II	Brain and Central Nervous System Tumors	Sorafenib tosylate, bevacizumab
NCT01434602	Phase I and II	Brain Tumor, Glioblastoma and Anaplastic Glioma	Everolimus, sorafenib
NCT00884416	Phase I	Glioblastoma, Gliosarcoma, Anaplastic Astrocytoma, Anaplastic Oligoastrocytoma and Anaplastic Oligodendroglioma	Sorafenib
NCT00093613	Phase I	Adult Anaplastic Astrocytoma, Adult Anaplastic Oligodendroglioma, Adult Giant Cell Glioblastoma, Adult Gliosarcoma and Recurrent Adult Brain Tumor	Sorafenib tosylate
NCT01183663	Phase I	Advanced cancers	Lenalidomide, Sorafenib

In a different scenario, patients with carcinoma generally benefit from the sorafenib therapy, but several of them develop resistance due to several mechanisms[199,200]. One of the most common ones is the crosstalk involving PI3K/Akt and JAK-STAT pathways[201]. The PI3K pathway regulates survival, cell growth, differentiation, cellular metabolism, and cytoskeletal reorganization of cells in reaction to a range of signals[202]. Deregulation of this signaling cascade activates oncogenic events or inactivates tumor suppressors. The PI3K–Akt is aberrantly activated in several cancers[203]. Significantly, the overactivation of the PI3K pathway can confer chemoresistance to the treated tumors. Consequently, the inhibition of PI3K could have beneficial clinical effect to enhance other treatments. Therefore, inhibitors of PI3K and, more precisely, PI3Kα, have become an interesting new approach for the treatment of malignancies, and many of them have evolved into clinical trials or even approved for standard use in clinic[204].

In my thesis, I have evaluated the activity of sorafenib to inhibit DIPG and endothelial cells, evaluating its ability to induce ROS in cancer cells. I addressed resistance to sorafenib by targeting the PI3K pathway with a PIK3CA inhibitor.
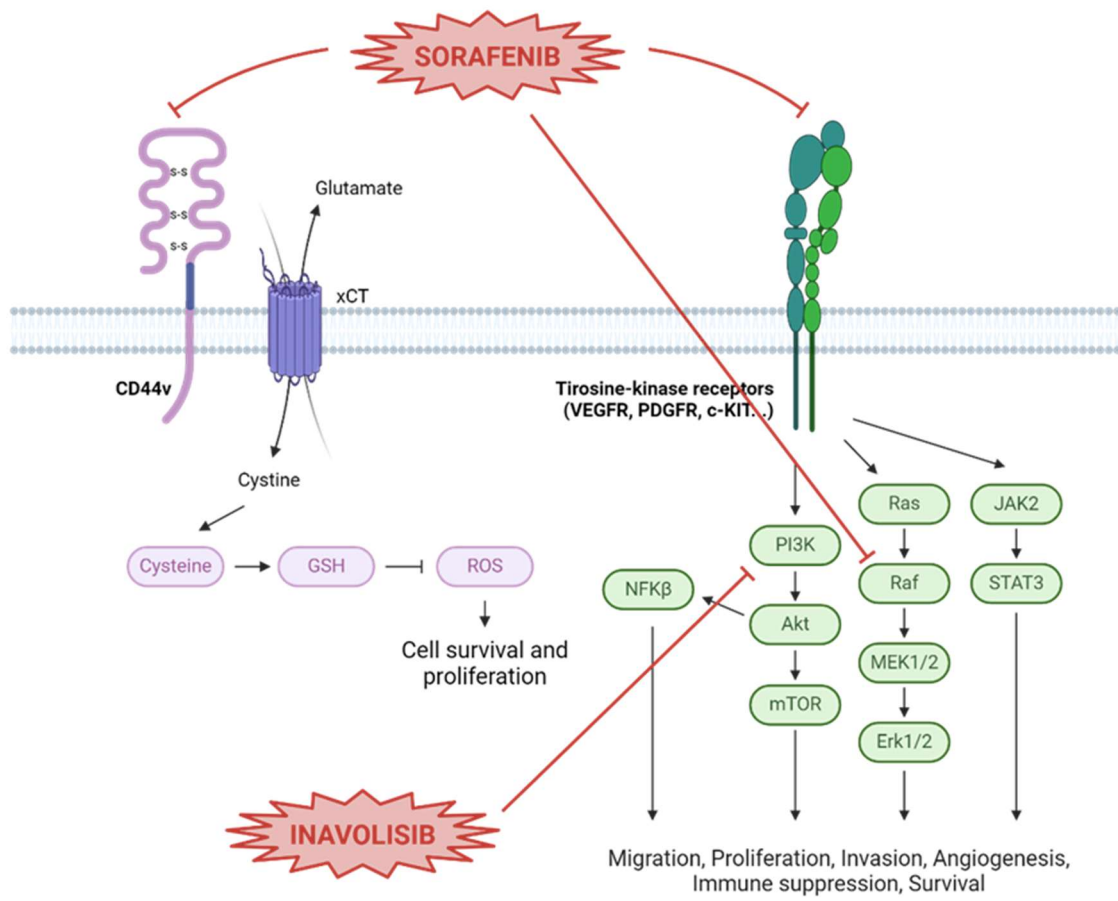
Figure 16. Sorafenib and Inavolisib inhibitory mechanisms in cancer.

HYPOTHESIS AND AIMS

The development of immunotherapy for DIPG is justified by its dismal prognosis and the need for radically new therapeutic approaches for this disease. Recent success in treating melanoma, renal cell carcinoma, non-small lung cancer or prostate cancer with immune checkpoint inhibitors[205], or treating leukemia, carcinomas, and even glioblastoma multiforme with CAR-T cells[206] has triggered interest in this approach. To optimize immunotherapy for DIPG, we must understand the immune escape mechanisms exerted by these tumors, likely through the generation of a pro-tumoral microenvironment, characterized by the presence of anti-inflammatory cytokines, immunosuppressive cells, or neovascularization. Previous work found that the microenvironment of DIPG is non-inflammatory, with a low or absent expression of immunomodulatory molecules, including immune checkpoints PD-L1 and CTLA-4[72,73]. While such findings are clear regarding the absence of inflammation, it remains unknown which molecules or mechanisms are responsible for the acquisition of immune deprivation, as no classical chemokines have been identified to date as overexpressed in this cancer[73]. A precise and in-depth analysis of the immune infiltrate of DIPG and the study of its secretome may unveil immunological mechanisms by which the tumor is able to escape and grow. Such knowledge would contribute to identify potential immune-related druggable targets, necessary for increasing the lifespan and survival of the patients.

In this thesis, I will approach (i) the characterization of DIPG immunoenvironment, (ii) the identification of potential cancer-secreted proteins responsible for the microenvironmental phenotype in the tumor, and (iii) the testing of a novel therapy targeting one of the proposed mechanisms.

Our general hypotheses are that (i) immunohistochemical markers in DIPG tissues will be consistent with immune suppression, including low counts of TILs and high counts of TAMs, consistent with a cold tumor microenvironment; (ii) primary DIPG cells in culture secrete specific cytokines, which are shared among different patients, constituting a common "DIPG secretome"; (iii) the secretome of DIPG modifies different cellular components of the microenvironment, such as mesenchymal stem cells (MSCs), endothelial cells and macrophages, favoring the establishment of a pro-tumorigenic niche; and (iv) blocking cytokine-activated pathways leads to anticancer activity in DIPG and pHGG models, in vitro and in vivo. To address our hypotheses, we set three main objectives:

I.   To characterize the immune cell infiltrate in DIPG and the immune escape mechanisms. We will quantify TIL and TAM populations in a large set of DIPG tissue samples from biopsies and necropsies of patients, and we will compare them to the counts obtained from non-tumoral brainstems. We will study the expression of the immune checkpoints PD-L1, CTLA-4 and B7-H3 by immunohistochemistry (IHC) in the same samples. We will also study the expression of these proteins in vitro, in primary cell cultures.

II. To characterize the DIPG secretome by identifying specific cytokines secreted by primary DIPG cells in culture, which are common among DIPG patients. We will analyze the expression of soluble and secreted proteins in tissue samples, in primary DIPG cultures, and in CSF and serum from patients. Then, we will expose cells of the tumor microenvironment, such as MSCs, endothelial cells and peripheral blood mononuclear cell (PBMC)-derived macrophages, to the DIPG

secretomes and to the recombinant versions of the identified cytokines, to address phenotypic changes in the cells.

III. To evaluate a new therapy for DIPG blocking the pathway activated by osteopontin and CHI3L1, two cytokines overexpressed in the secretome of the tumor. We will study whether sorafenib, an FDA-approved drug targeting one of the pathways activated by osteopontin and CHI3L1, presents anticancer activity against DIPG models. We will also assess changes on microenvironmental components after treatment.

MATERIALS AND METHODS

Cell models and samples

We obtained primary pHGG cultures from the repository at Hospital Sant Joan de Deu (HSJD, Barcelona, Spain). All of them were obtained from tumors located in the pons (i.e., DIPG) and were classified as DMG H3 K27-altered. In the text, we omit the institutional prefix HSJD of cell identification, for clarity purposes. Cells grow as tumorspheres in pHGG culture medium, which is also known as Tumor Stem Cell complete medium (TSMc). The composition of this medium is neurobasal-A (10888022) and DMEM/F-12 (11320074) (50:50 volume) supplemented with B-27 (12587010), HEPES buffer 10 mM (15630056), sodium pyruvate 1 mM (11360039), minimum essential medium (MEM) non-essential aminoacid solution 1x (11140035), L-alanyl-L-glutamine 2 mM (35050038), penicillin 100 units/mL, streptomycin 100 µg/mL and amphotericin B 0.25 µg/mL (15240062), all from Thermo Fisher Scientific (Waltham, MA, USA). Medium contains recombinant human growth factors EGF (AF-100-15) and FGF-basic (AF-100-18B) (20 ng/mL each), PDGF-AA (100-13A) and PDGF-BB (100-14B) (10 ng/mL each), from PeproTech (Cranbury, NJ, USA) and heparin 2 µg/mL (H3149-10KU, Sigma-Aldrich, Saint Louis, MO, USA). The institutional review board at HSJD approved the collection of patient samples (DIPG from biopsy or autopsy, CSF or serum), under protocol PIC-157-15 and informed consent M-1608-C. Other samples obtained under consent were from the BioBank HGUA (PT13/0010/0044), integrated in the Spanish National Biobank Network.

Adipose tissue-derived human mesenchymal stem cells (hMSC-AT, C-12977) were from PromoCell (Heidelberg, Germany), the human brain microvascular endothelial cell line hCMEC/D3 (SCC066) was from Sigma-Aldrich, human astrocytes (K1884) were from Gibco (Grand Island, NY, USA), human microglia

56

HMC3 (CRL-3304) was from ATCC (Manassas, VA, USA) and the cancer cell lines LAN-1 (neuroblastoma), A4573 (Ewing sarcoma) and RH (rhabdomiosarcoma) were from the HSJD repository.

Patient-derived xenografts (PDX) samples were obtained from subcutaneous tumors established in athymic nude mice as described in previous work[207]. PDX samples included Ewing sarcoma HSJD-ES-002, neuroblastoma HSJD-NB-007, Wilms tumor HSJD-WT-005, and pHGG HSJD-GBM-001 and HSJD-DMG-005. Orthotopic intracraneal pHGG tumor xenografts were harvested from mice bearing HSJD-GBM-001 and HSJD-DMG-005.

Immunostaining of patient samples

For 4-µm paraffin-embedded tissue sections, we incubated the samples with peroxidase blocking solution (RE7101, Leica) for 30 minutes. Then, we washed the sections and we used primary antibodies for CD3 (PA0553, ready-to-use, Leica, Wetzlar, Germany), CD8 (ab17147, 1:50, Abcam, Cambridge, UK), CD4 (NCL-L-CD4-368, 1:200, Novocastra, Newcastle upon Tyne, UK), FoxP3 (ab20034, 1:400, Abcam), CD20 (MOB004, ready-to-use, Diagnostic Biosystems, Pleasanton, CA, USA), CD45 (PA0042, ready-to-use, Leica), CD68 (MOB167, ready-to-use, Diagnostic Biosystems), Iba1 (ab178846, 1:2000, Abcam), CD163 (NCL-L-CD163, 1:400, Novocastra), PD-L1 clone SP142 (M4420, 1:60, Spring Bioscience, Pleasanton, CA, USA), PD-L2 (#82723, ready-to-use, Cell Signalling, Danvers, MA, USA), CTLA-4 (anti-CD152 clone 14D3, 14-1529, 1:100, eBioscience, San Diego, CA, USA), B7-H3 (#14058, 1:200, Cell Signalling), CD31 (ab28364, 1:100, Abcam), breast cancer resistance protein (BCRP; OACD01214, Aviva Systems Biology, San Diego, CA, USA) and CD90 (ab181469, 1:200, Abcam) Secondary antibodies and diaminobenzidine solution

for staining were those included in the Novolink system for the detection of mouse IgG, mouse IgM and rabbit IgG primary antibodies (RE7150, Leica).

For immunofluorescence, we pretreated 4-µm paraffin tissue sections with Sudan black 0.1% in 70% ethanol to remove tissue autofluorescence. After 20 min, we washed them with phosphate buffered saline (PBS) and blocked unspecific unions with 5% bovine serum albumin (BSA, A3294, Sigma-Aldrich) for 30 min. Then, we incubated the sections overnight at 4 ºC with primary antibodies diluted in blocking solution for osteopontin (ab8448, 1:400, Abcam), chitinase 3-like 1 (ab77528, 1:1000, Abcam), SOX2 (ab171380, 1:400, Abcam), B7-H3 (#14058, 1:200, Cell Signalling), CD31 (ab32457, 1:1000, Abcam), CD90 (ab181469, 1:200, Abcam), CD163, (ab182422, 1:500, Abcam), PDGFR-β (#3169, 1:100, Cell Signalling) and tri-methyl-histone H3 (Lys27) (#9733, 1:1000; Cell Signalling). The next morning, we washed with PBS and added 4′,6-diamidino-2-phenylindole (DAPI; D1306, 1:5000, Thermo Fisher Scientific) and the secondary antibodies anti-rabbit-Alexa 594, (A11012, 1:100) and anti-mouse-Alexa 488, (A32723, 1:100) from Invitrogen (Waltham, MA, USA). After 1 h in the dark, we washed the slides with PBS and mounted them with antifade mountant (P36961, Thermo Fisher Scientific). We obtained images using the Leica SP8 confocal microscope and acquired them with the Leica Application Suite software.

Morphology of the microglia in human tumor samples

To determine the activation state of the microglia in the human samples, we analyzed the morphology of Iba1^{+} cells in paraffin sections. Following a published method[208], we used FracLac plugin for ImageJ (National Institutes of Health, Bethesda, MD, USA) and calculated the parameters of area fraction of Iba1^{+} in the selected field and soma area (i.e., the total number of pixels in the cell soma,

multiplied by the pixel area of 0.013 μm^2). We selected cells randomly, no overlapping with neighboring cells and with complete nucleus and branches.

Real-time quantitative polymerase chain reaction (RT-qPCR)

We quantified mRNA expression of immune checkpoints and cytokines from brain and tumor tissue samples and primary DIPG cell cultures. We purified total RNA from cell models and tissue samples using TRIzol Reagent (15596018, Life Technologies, Carlsbad, CA, USA) following the manufacturer's instructions. We determined the quantity and quality of RNA obtained with Nanodrop 8000 spectrophotometer (Thermo Fisher Scientific). A total of 1 μg of RNA was retrotranscribed with M-MLV reverse transcriptase system (Life Technologies) to obtain cDNA. We performed RT-qPCR according to the manufacturer's protocol using Taqman Gene Expression Master Mix (4444557, Thermo Fisher Scientific) and Taqman Gene Expression Assays detailed in **Table 6**. The relative expression of the target genes was calculated using the ΔΔCt method with control *TBP*.

Table 6. Primers used for RT-qPCR assays with TaqMan probes references.

Gene symbol	Protein	TaqMan probe
CD274	PD-L1	Hs01125301_m1
CD273	PD-L2	Hs01057777_m1
CD152	CTLA-4	Hs03044418_m1
CD276	B7-H3	Hs00987207_m1
IDO1	Idoleamine 2,3-dioxygenase 1	Hs00984148_m1
IDO2	Idoleamine 2,3-dioxygenase 1	Hs01589373_m1
TDO	Tryptophan 2,3-dioxygenase	Hs00194611_m1
PTGES	Prostaglandin E synthase	Hs00610420_m1
PTGS2	Prostaglandin-endoperoxide synthase 2	Hs00153133_m1
HLA-A	Major histocompatibility complex, class I, A	Hs01058806_g1
HLA-B	Major histocompatibility complex, class I, B	Hs00818803_g1
HLA-C	Major histocompatibility complex, class I, C	Hs03044135_m1
HLA-DRA	Major histocompatibility complex, class II, DR alpha	Hs00219575_m1
HLA-DRB1	Major histocompatibility complex, class II, DR beta 1	Hs99999917_m1
B2M	Beta-2-microglobulin	Hs00984230_m1
CIITA	Class II major histocompatibility complex transactivator	Hs00172094_m1
HSPA1A	Heat shock protein family A (Hsp70) member 1A	Hs00359163_s1
HSPA4	Heat shock protein family A (Hsp70) member 4	Hs00382884_m1
HSPD1	Heat shock protein family A (Hsp60) member 1	Hs01036753_g1
HSP90AA1	Heat shock protein 90 alpha family class A member 1	Hs00743767_sH
TGFB1	Transforming growth factor beta 1	Hs00998133_m1
TGFB2	Transforming growth factor beta 2	Hs00234244_m1
TGFB3	Transforming growth factor beta 3	Hs01086000_m1
STAT3	Signal transducer and activator of transcription 3	Hs00374280_m1
CALR	Calreticulin	Hs00189032_m1
HMGB1	High mobility group box 1	Hs01923466_g1
HPRT1	Hypoxanthine phosphoribosyltansferase 1	Hs02800695_m1
SPP1	Osteopontin	Hs00959010_m1
CHI3L1	Chitinase 3-like 1	Hs01072228_m1
TBP	TATA-box binding protein	Hs00427620_m1

In brain endothelial cells, we performed RT-qPCR according to the manufacturer's protocol using Power SYBR Green PCR Master Mix Gene Expression Master Mix (4367659, Thermo Fisher Scientific) and SYBR Gene Primers for genes *FN1, NRP1* and *ABCG2* (**Table 7**). The relative expression of the target genes was calculated using the ΔΔCt method with control *GUSB* (**Table 7**). In brain endothelial cells, we analyzed gene expression of angiogenesis markers using a TaqMan™ Human Angiogenesis Array (4414071, Thermo Fisher Scientific). For microglial cells and PBMC, we addressed macrophage polarization using the GeneQuery™ Human Macrophage Polarization Markers qPCR Array Kit (GK120, ScienCell Research Laboratories, Carlsbad, CA, USA).

We quantified mRNA expression of *CD44s*, *CD44v2-v10* and *SLC7A11* from brain and tumor tissue samples and primary pHGG cell cultures. We performed RT-qPCR according to the manufacturer's protocol using Power SYBR Green PCR Master Mix Gene Expression Master Mix (4367659, Thermo Fisher Scientific) and SYBR Gene Primers for *CD44s*, *CD44v2-v10* and *SLC7A11* (**Table 7**). The relative expression of the target genes was calculated using the ΔΔCt method with control *ACTB*.

Table 7. SYBR-Green primers used for RT-qPCR assays.

Gene symbol	Protein	Fw primer (5'-3')	Rv primer (5'-3')
FN1	Fibronectin 1	ACAACACCGAGGTGACTGAGAC	ACAACACCGAGGTGACTGAGAC
NRP1	Neuropilin 1	AACAACGGCTCGGACTGGAAGA	GGTAGATCCTGATGAATCGCGTG
ABCG2	BCRP	AAAGCCACAGAGATCATAGAG	GATCTTCTTCTTCTTCTCACC
GUSB	Glucuronidase Beta	CTGTCACCAAGAGCCAGTTCCT	GGTTGAAGTCCTTCACCAGCAG
CD44s	CD44s	GGAGCAGCACTTCAGGAGGTTAC	GGAATGTGTCTTGGTCTCTGGTAGC
CD44v2	CD44v2	ATCACCGACAGCACAGACAGAAT	AACCATGAAAACCAATCCCAGG
CD44v3	CD44v3	TACGTCTTCAAATACCATCTCAGCA	AATCTTCATCATCATCAATGCCTG
CD44v4	CD44v4	AACCACACCACGGGCTTTTG	TCCTTGTGGTTGTCTGAAGTAGCA
CD44v5	CD44v5	TGCTTATGAAGGAAACTGGAAC	TGTGCTTGTAGAATGTGGGGT
CD44v6	CD44v6	CCAGGCAACTCCTAGTAGTACAACG	CGAATGGGAGTCTTCTTTGGGT
CD44v7	CD44v7	GCCTCAGCTCATACCAGCCATC	TCCTTCTTCCTGCTTGATGACCT
CD44v8	CD44v8	TGGACTCCAGTCATAGTATAACGC	GGTCCTGTCCTGTCCAAATC
CD44v9	CD44v9	AGCAGAGTAATTCTCAGAGC	TGATGTCAGAGTAGAAGTTGTT
CD44v10	CD44v10	CCTCTCATTACCCACACACG	CAGTAACTCCAAAGGACCCA
SLC7A11	xCT	TGCTGGGCTGATTTTATCTTCG	GAAAGGGCAACCATGAAGAGG
ACTB	B-ACTIN	GTGAAGGTGACAGCAGTCGGTT	GAAGTGGGGTGGCTTTTAGGAT

Induction of immune checkpoints expression in DIPG

To evaluate whether the immune checkpoint machinery could be activated by a pro-inflammatory niche, we exposed DIPG cells and human astrocytes in culture (5 x 10^5 cells per well, in 6-well plates) to 20 ng/mL interferon-γ (IFN-γ, 300-02, Peprotech) for 48 h. We analyzed by RT-qPCR *CD274* (PD-L1), *CD273* (PD-L2) and *CD276* mRNA expression of treated and untreated cells (**Table 6**).

Cytokine expression in patient tissue samples, cell culture supernatants, and patient CSF and serum

We assessed the presence of 105 human cytokines in frozen pHGG samples, brainstem control samples (non-tumoral and non-inflamed), and DIPG cell culture supernatants, using a proteome profiler array (Human XL Cytokine Array Kit, ARY022B, R&D Systems, Minneapolis, MN, USA). We homogenized tissues in lysis buffer (0.5% IGEPAL, 0.5% sodium deoxycholate, 0.1% sodium dodecyl sulfate, 50 mM Tris-HCl (pH 7.5), and 150 mM NaCl; all from Sigma) supplemented with protease inhibitor cocktail 0.4% (4693132001, Promega, Madison, WI, USA). We quantified protein concentration in homogenates or supernatants using the Bradford assay (B6916, Sigma-Aldrich). We added to the array membranes either patient tumor tissue lysates (200 µg protein in 1.5 mL of array buffer), or DIPG cell culture supernatant (300 µL). After overnight incubation at 4 °C, we added the biotinylated detection antibody cocktail and streptavidin-HRP. We acquired images using the iBrightCL1000 (Invitrogen) and quantified the intensity of the spots with QuickSpots HLIimage++ software (Ideal Eyes System, Bountiful, Utah, USA). Exposure time was 5 min for supernatant samples and 15 min for tissue samples. In each array membrane, we subtracted the signal of the negative control spots to each of the individual signals obtained from each

protein spot. Then, we normalized the signal value of each of the spots to the mean signal value of the positive controls, which we considered 100% signal. We compared the cytokine expression between control brainstem tissue and tumor samples and we identified the significantly overexpressed cytokines in tumor lysates using a parametric multiple t test.

To quantify selected proteins in tissue samples, DIPG cell supernatants, CSF and serum, we used ELISA kits for osteopontin (DOST00) and chitinase-3-like protein 1 (DC3L10) (both from R&D Systems). We read the plates using an Infinite 200 PRO TECAN microplate reader (Tecan Trading, Männedorf, Switzerland) set at 450 nm, with a wavelength correction set at 540 nm.

We validated the protein expression in tissue samples by immunoblotting of osteopontin and CHI3L1 using GAPDH as loading control. We blocked membranes for 1 h at room temperature (RT) with 5% BSA and incubated them overnight at 4 °C with the primary antibodies for osteopontin (ab8448, 1:1000, Cell Signaling, Danvers, MA), CHI3L1 (ab77528, 1:1000, Abcam) and GAPDH (MAB374, 1:50000, Merck Millipore, MA, USA). The following day, we incubated the membranes with the secondary fluorescent antibody (C80626-08, Li-Cor Biosciences, Lincoln, Nebraska, USA) for 1 h, in the dark. We detected the signal using the Li-Cor Odyssey® CLx Imaging System (C81205-05, Li-Cor Biosciences). We quantified the density of the bands using ImageJ.

Tumor secretome-induced pericyte-like differentiation of human mesenchymal stem cells (hMSC)

To address whether the DIPG secretome induced phenotypic changes of hMSC towards B7-H3-expressing pericytes frequently found in the aberrant blood vessels of DIPG, we incubated hMSC-AT with DIPG-conditioned culture medium

supernatants for 7 days. We cultured 10^5 hMSC-AT cells in 3 mL of hMSC culture medium (C-28009, PromoCell) in T25 flasks. The next day, we treated flasks with 3 mL of either hMSC culture medium, pericyte culture medium (P60121, Innoprot, Spain), pHGG medium, DIPG supernatants (DIPG-007, -012 and -021), human astrocytes supernatant, neuroblastoma cell (LAN-1) supernatant, Ewing sarcoma cell (A4573) supernatant, and cytokines dissolved in pHGG medium, including 50 nM human recombinant osteopontin (1433-OP, R&D Systems), or 50 nM human recombinant chitinase 3-like protein 1 (2599-CH-050, R&D Systems). We renewed the culture media every 72 h. After 7 days, we trypsinized and homogenized hMSC-AT cells in RIPA buffer (10 mM Tris-HCl pH 8.0, 1 mM EDTA, 1% Triton X-100, 140mM NaCl; all from Sigma-Aldrich) supplemented with a protease inhibitor cocktail (4693132001, Promega). We determined protein concentrations with the Bradford protein assay and performed immunoblotting of B7-H3, PD-L1, NG2 and PDGFR-β using GAPDH as loading control. We blocked membranes for 1 h at RT with 5% BSA and incubated them overnight at 4 °C with the primary antibodies for B7-H3 (#14058, 1:1000, Cell Signaling), PD-L1 (ab205921, 1:200, Abcam), NG2 (ab129051, 1:200, Abcam), PDGFR-β (#3169, 1:1000, Cell Signaling) and GAPDH (MAB374, 1:50000, Merck Millipore). The following day, we incubated the membranes with the secondary fluorescent antibody (C80626-08, Li-Cor Biosciences, Lincoln, Nebraska, USA) for 1 h, in the dark. We detected the signal using the Li-Cor Odyssey® CLx Imaging System (C81205-05, Li-Cor Biosciences). We quantified the density of the bands using ImageJ.

Tumor secretome-induced changes in the brain endothelial cell phenotype

First, we performed a microtubule formation assay of hCMEC/D3 cells exposed to DIPG supernatants. We coated 24-well cell culture plates with 100 µL of unpolymerized geltrex (12760021, Thermo Fisher Scientific) and incubated at 37 °C for 30–45 minutes. We plated 10^5 hCMEC/D3 cells in 300 µL of either endothelial cell culture medium (C-22011, PromoCell), pHGG medium, DIPG supernatants (DIPG-007, -012 and -021), human astrocytes supernatant, LAN-1 supernatant, A4573 supernatant, and cytokines (50 nM of recombinant osteopontin or chitinase 3-like 1) dissolved in endothelial cell culture medium. We used endothelial cell culture medium as negative control. After 18 h incubation, we took photographs with an inverted photomicroscope at 10x. We analyzed four randomly selected fields from each condition to assess tube formation with the Angiogenesis Analyzer plugin for ImageJ. To determine the complexity of the vascular structures formed in vitro, we measured the total length of the vascular network (in mm), as the addition of the lengths of segments, isolated elements and branches in the analyzed area. We also counted the number of junctions of the new network, adding the total number of vertices formed by the vascular branches.

Second, we studied phenotype changes in co-cultured mesenchymal cells and brain endothelial cells changed in the presence of DIPG secretomes. We performed a microtubule formation assay of hCMEC/D3 cells co-cultured with hMSC-AT cells exposed to conditioned media. We coated 8-well glass chamber slides with 30 µL of unpolymerized geltrex and incubated at 37 °C for 30–45 minutes. We plated 6×10^4 hCMEC/D3 and 1.2×10^4 hMSC-AT cells in 300 µL of either endothelial cell culture medium, mesenchymal medium, pericyte medium,

pHGG medium, DIPG supernatants (DIPG-007, -012 and -021), human astrocytes supernatant, LAN-1 supernatant, A4573 supernatant, and cytokines (50 nM of recombinant osteopontin or chitinase 3-like 1) dissolved in endothelial cell culture medium. After 18 h incubation, we assessed tube formation.

Cell immunofluorescence

For hMSC-AT cells, we cultured them in 8-well glass chamber slides (PEZGS0816, Merck Millipore). After treatments with conditioned media for 7 days, we fixed the cells with 4% PFA for 30 min, followed by 0.1% Tween 20-PBS permeabilization for 30 min. Then we used 5% BSA as a blocking solution for 1 h. We added primary antibodies for NG2 (ab12905, 1:200, Abcam) and CD90 (ab181469, 1:200, Abcam), kept at 4ºC overnight.

For cultures of geltrex-embedded human endothelial cells and their co-cultures with hMSC-AT cells, we used 8-well glass chamber slides and treated them with conditioned media for 18 h. Then, we fixed the gels with 80% methanol and 20% DMSO for 30 min at RT. We rehydrated with 50% methanol and 50% PBS for 1 h at RT. Finally, we added 20% methanol and 80% PBS followed by a permeabilization process with 0.1% Tween 20-PBS at RT for 1 h. Then, we added blocking solution (10% FBS, 5% BSA in PBS) for 2-4 h. We washed with 0.1% Tween 20-Tris Buffered Serum (TBS-T) for 1 h and added the primary antibody diluted in blocking solution at 4 ºC overnight. Antibodies were endothelial marker CD31 (ab32457, 1:200, Abcam), pericyte marker NG2 (ab129051, 1:200, Abcam) and blood-brain barrier marker BCRP (ab3380, 1:200, Abcam).

For cultures of pHGG tumorspheres and RH cells (used as negative control) we embedded them in OCT embedding matrix and posteriorly sliced them into 4-µm sections. First we fixed the cells with 4% PFA for 30 min, followed by 0.1% Tween

20-PBS permeabilization for 30 min. Then we used 5% BSA as a blocking solution for 1 h. We incubated the primary antibodies for osteopontin (ab8448, 1:200, Cell Signaling), chitinase 3-like 1(ab77528, 1:200, Abcam) or xCT (B300-318, 1:200, Novus Biologicals, Littleton, Ontario, Canada).

For all the above-mentioned preparations, we used the secondary antibodies anti-mouse-Alexa-488 (A32723, 1:1000, Invitrogen), anti-rabbit-Alexa-594 (A21207, 1:1000, Invitrogen) or anti-rabbit-Alexa-488 (A11034, 1:1000, Invitrogen) for 1 h. Finally, we added DAPI (1:5000, 1 min) and mounted the preparations using Vectashield Antifade Mountant (NC9532821, Fisher Scientific). We obtained images with the Leica Thunder Imager Live cell and 3D Assay software.

Tumor secretome-induced changes in the macrophage phenotype

To address whether the DIPG secretome induced polarization of the tumor microglia towards the M2-like phenotype, we exposed macrophage cultures to cell culture-conditioned medium. First, we isolated PBMC from blood buffy coats by density gradient centrifugation gradient separation using Histopaque®-1077 (10771, Sigma-Aldrich). We then cultured cells in macrophage medium (X-VIVO 15, Lonza, Basel, Switzerland) supplemented with 2% human serum, in T75 cell culture flasks for 2 h. To select the adherent macrophages we removed the medium with the non-adherent cells and added fresh macrophage medium supplemented with 2% human serum and 10 ng/mL M-CSF (300-25, Peprotech, Rocky Hill, NJ, USA). We considered macrophage cultures were established after 3 days at 37 ºC in a 5% CO_2.

We plated 2×10^6 macrophages per well in 6-well plates, in a total of 2 mL. The next day, we exposed them to experimental conditions including an M1 cocktail

composed by 20 ng/mL IFN-γ, 20 ng/mL tumor necrosis factor-α (TNF-α, 300-01A) and 100 ng/mL lipopolysaccharide (LPS, L2630, Sigma-Aldrich) to obtain a control of M1-like polarized cells, and an M2 cocktail consisting of 10 ng/mL transforming growth factor-β (TGF-β, 100-21) and 10 ng/mL interleukin 10 (IL-10, 200-10), all from PeproTech. Other experimental conditions included pHGG medium, DIPG supernatant (DIPG-007), and 50 nM recombinant osteopontin dissolved in pHGG medium. We incubated the macrophages for 24 h and then harvested and incubated them with anti-CD11b-Alexa647 (557686, BD Pharmingen, San Diego, CA, USA), anti-CD80-PE (ab69778, Abcam), anti-CD163-FITC (563697, BD Pharmingen) and DAPI for 20 min at 4 ºC in the dark, washed twice and analyzed using a BD FacsCanto™ II Cytometer (BD biosciences, Franklin Lakes, NJ, USA). We selected CD11b$^+$ living cells (macrophages) and analyzed them using Infinicyt™ software (Cytognos, Santa Marta de Tormes, Spain). We repeated the experiment seven times, with macrophage cultures from seven different patients. To mitigate the variability in the basal levels of macrophage polarization, we expressed the results as the ratio of CD163$^+$ cells (M2-like) to CD80$^+$cells (M1-like).

To address whether DIPG cells modify the migration and invasion of macrophages, we performed a transwell assay using DIPG supernatant and osteopontin as chemoattractants. We plated 2.5 x 10^4 macrophages per well in 200 µL of macrophage medium in the upper chamber of the transwells (CLS3422-48EA, Merck Millipore), previously coated with geltrex, and fetal bovine serum (FBS)-free macrophage medium in the inferior chamber. After 24 h, we filled the lower chamber with either 200 µL of either 10% FBS (12389802, Thermo Fisher Scientific) dissolved in pHGG medium (positive control), 0.1% BSA dissolved in

pHGG medium (negative control), or the experimental conditions including DIPG supernatant (DIPG-007), or 50 nM recombinant osteopontin dissolved in pHGG medium. We also included one experimental control of pHGG medium.

After incubation for 72 h at 37 ºC and 5% CO2, we removed the cells on the upper surface of the membrane with a dry cotton swab, fixed the cells attached to the bottom with 4% paraformaldehyde and stained them with 1% crystal violet (548-62-9, Sigma-Aldrich) for 30–60 min. We obtained photographs at 20x using an inverted microscope and counted the cells of randomly selected fields (12 from each condition).

Expression of CD44 and xCT in DIPG

We studied the expression of CD44 and xCT in tissue samples and pHGG cell models by immunoblotting. We blocked membranes for 1 h at RT with 5% BSA and incubated them overnight at 4 °C with the primary antibodies for CD44 (MA4405, Invitrogene, Waltham, MA, USA), xCT (B300-318, Novus Biologicals) and GAPDH (MAB374, Merck Millipore). The following day, we incubated the membranes with the secondary fluorescent antibody (C80626-08, Li-Cor Biosciences, Lincoln, Nebraska, USA) for 1 h, in the dark. We detected the signal using the Li-Cor Odyssey® CLx Imaging System (C81205-05, Li-Cor Biosciences). We quantified the density of the bands using ImageJ.

We confirmed the expression of CD44 in cell models by flow cytometry. We washed cells (DIPG-007/008/011/012/013/014/018 and GBM-001) twice with PBS and we posteriorly fixed them with 70º ethanol for, at least, 2 h. We repeated the PBS washes and we stained the cells for 30 min at 4°C with mouse anti-CD44 (MA5-13890, Thermo Fisher). We then added the secondary anti-mouse-alexa 488 (A32723, Invitrogene) and anti-CD133-PE (120-000-425, Miltenyi Biotec,

Germany) for 30 min. We finally added DAPI and analyzed the samples using a NovoCyte Flow Cytometer.

Cell viability and proliferation assays

We tested sorafenib antiproliferative activity in pHGG cells (DIPG-007, GBM-001, DMG-001) and hCMEC/D3 in vitro. We plated 3000 cells into 96-well plates in TSMc. After 24 h, we treated them with sorafenib at concentrations ranging 40 to 6.1×10^{-4} µM. After 48 h, 72 h and 7 days, we analyzed cell viability using the colorimetric-based assay CellTiter 96 (Promega), in which viable cells reduce th tetrazolium compound [3-(4,5-dimethylthiazol-2-yl)-5-(3-carboxymethoxyphenyl)-2-(4-sulfophenyl)–2H-tetrazolium], inner salt (MTS) into soluble and colored formazan. The color change was determined using Infinite® 200 PRO TECAN. We also tested the antiproliferative activity of inavolisib (HY-101562, MedChem Express, Monmouth Junction, NJ, USA) in vitro in DIPG-007 and GBM-001. We plated 3000 cells/well in 96-well plates (3000 cells/well) and after 24 h we added inavolisib at concentrations ranging 25 to 6.4×10^{-5} nM. Cell viability was determined as above after 48 h, 72 h and 7 days.

ROS accumulation

We measured cellular ROS using a detection assay kit (Abcam, Cambridge, MA, USA), following the manufacturer instructions. We added 2′,7′-dichlorofluorescein diacetate (DCFDA), a fluorogenic dye that measures intracellular ROS activity, to pHGG cells (DIPG-007 and GBM-001) growing in 96-well plates with or without sorafenib 3 µM. We detected the fluorescence from the DCF with Infinite® 200 PRO TECAN microplate reader with maximum excitation and emission spectra of 495 nm and 529 nm, respectively.

We also carried out immunoblots on pHGG cells (DIPG-007, DMG-005 and GBM-001) treated with sorafenib and inavolisib. We incubated the membranes with the primary antibodies for PI3K$^{p110\alpha}$ (#4249), P-Akt^{Ser473} (#9271S), Akt (#9272S), P-S6$^{Ser235/236}$ (#2211), S6 (#2217S), CDK4 (#12790), Cyclin D1 (#2978) and Cas3 (#9664S), all diluted at 1:1000, and all purchased from Cell Signaling.

Sorafenib effects on tumor cell invasion and migration capacity

Tumor cell invasion capacity was determined by the analysis of metalloproteinases 9 (MMP-9) and 2 (MMP-2). We studied their expression by immunoblotting in pHGG cells (DIPG-007, DMG-005 and GBM-001) treated with sorafenib 3 μM for 24 h. We incubated the membranes with the primary antibodies for MMP-2 (#13132, Cell Signaling), MMP-9 (#13667, Cell Signaling) and GAPDH (MAB374, Merck Millipore). We also evaluated MMP-2 and MMP-9 activity by gelatin zymography in pHGG cells treated with sorafenib 3 μM for 24 h. The conditioned media were collected and centrifuged to remove cellular debris. Equal amounts of protein were deposited on 0.1 % gelatin 8 % SDS-PAGE under non-reducing conditions. Gels were stained with Coomassie brilliant blue and posteriorly destained. Areas of gelatinolytic activity were detected as clear bands against a blue background. A parallel SDS-PAGE without gelatin was loaded with the same amount of sample and run under the same experimental condition, to be used as internal loading control.

We determined the effect of sorafenib on the migration of cancer cells with a scratch wound assay. Cells (DIPG-007, DMG-005 and GBM-001) were cultured with pHGG medium without growth factors and with 10% FBS in 24-well plates pre-coated with poli-D-lysine (16021412, Fisher, USA) until they reached 90% of confluence. Posteriorly, each monolayer was artificially wounded by creating a

scratch with a 200 μL plastic pipette tip. We removed debris with PBS and posteriorly added the cell culture supernatants (DIPG-007, GBM-001 and DMG-005) with or without sorafenib 3 μM. Cells were cultured for 24 h and images of scratch wounds were captured using an inverted microscope at 0, 4, 8 and 24 h after wounding. The wound closure areas were measured with ImageJ.

Sorafenib effects on angiogenesis

We performed a microtubule formation assay of hCMEC/D3 cells exposed to pHGG cell supernatants and treated with sorafenib. We coated 24-well cell culture plates with 100 μL of unpolymerized geltrex (12760021, Thermo Fisher Scientific) and incubated at 37 °C for 30–45 minutes. We plated 10^5 hCMEC/D3 cells in 300 μL of either endothelial cell culture medium (C-22011, PromoCell), pHGG medium, pHGG supernatants (DIPG-007, DMG-005 and GBM-001) and the same pHGG supernatants supplemented with sorafenib 3 μM. We used endothelial cell culture medium as negative control. After 18 h incubation, we took photographs with an inverted photomicroscope at 10x. We analyzed four randomly selected fields from each condition to assess tube formation with the Angiogenesis Analyzer plugin for ImageJ.

Sorafenib activity in orthotopic pHGG xenografts

Mouse experiments were approved by the Animal Experimental Ethics Committee at the University of Barcelona and carried out in accordance with institutional and European guidelines (EU Directive 2010/63/EU) and the "Animal Research: Reporting of In Vivo Experiments" (ARRIVE) guidelines. Briefly, DIPG-007 and GBM-001 cells ($5×10^5$) were inoculated into the fourth ventricle of 4-6-week-old athymic nude mice using a dull 33-gauge needle. We started oral

gavage treatments (60 mg/kg sorafenib for 21 days, 5 on-2 off, morning and afternoon) 11 days post-inoculation in GBM-001-bearing mice model and at day 25 in DIPG-007 mice. A 15 day-break followed the first treatment cycle, which was complemented by a second 21-day cycle. Mice were monitored for local clinical signs (ataxia, weight loss and general condition) and tumor growth. We obtained samples from mice at the end of treatment. All remaining mice achieved the endpoint, defined as more than 25% weight loss or acute neurological symptomatology.

To objectively determine the tumor infiltration in the orthotopic models, que performed immunohistochemistry in 4-µm paraffin-embedded brain sections. we incubated the samples with peroxidase blocking solution (RE7101, Leica) for 30 min. Then, we washed the sections and stained with primary antibodies for CD31 (ab28364, 1:100, Abcam), anti-nuclei (MAB4383, 1:200, Merck Millipore) and hematoxylin-eosin. Secondary antibodies and diaminobenzidine solution for staining were those included in the Novolink system for the detection of mouse IgG, mouse IgM and rabbit IgG primary antibodies (RE7150, Leica).

Statistical analysis

We used GraphPad Prism 10 software for the statistical analysis (GraphPad, La Jolla, CA, USA). For the comparison of cytokine expression in tumors and controls of the proteome array we used the parametric t test corrected for multiple comparisons with the Holm-Sidak method. To compare numerical data between two different groups we used the Mann-Whitney test, and for more than two groups we used Kruskal-Wallis test, both non-paired, non-parametric tests. For the comparison of more than two groups that follow a normal distribution and

have similar SD, non-paired, we have applied the ANOVA test. For all analyses,

we considered $P < 0.05$ was a statistically significant difference.

RESULTS

Comparative infiltration of tumor-infiltrating lymphocytes (TILs) and tumor-associated macrophages (TAMs) in DIPG and non-tumor brainstem samples

We obtained paraffin-embedded samples from 24 patients with pHGG, all DIPG, and five brainstem samples from five patients who died of causes other than brain cancer (**Table 8**). Tumor samples corresponded to seven biopsies at initial diagnosis and 17 necropsies (**Table 8**). From the 24 patients with DIPG, 21 had tumors classified as DMG H3 K27-altered. We performed molecular profiling of H3 mutations in 14 of such DIPG, being four H3.1 K27M-mutant and 10 H3.3 K27M-mutant. In the seven DIPG samples without molecular confirmation, we found immunohistochemistry features suggestive of K27M histone mutations. Of the remaining three DIPG, two were classified as diffuse pHGG, H3-wildtype and IDH-wildtype, and one was radiologically classified as a DIPG but the mutational status was not assessed (**Table 8**).

Table 8. Human tissue samples included in the study

Sample type	Code	Sex	Tumor location	Tumor histology	WHO Classification	Histone Mutation
Brainstem controls	HSJD-CNS-001	M	-	-	Cardiac arrest	H3K27- WT
	HSJD-CNS-002	M	-	-	Steinert syndrome	H3K27- WT
	HSJD-CNS-003	M	-	-	Fetal death	H3K27- WT
	HSJD-CNS-004	F	-	-	Tetralogy of Fallot	H3K27- WT
	HSJD-CNS-005	F	-	-	-	H3K27- WT
Tumor biopsies	HSJD-DIPG-021	F	Pons	Anaplastic astrocytoma	DMG, H3 K27-altered	H3K27M
	HSJD-DIPG-023	F	Pons	Glioblastoma multiforme	DMG, H3 K27-altered	H3K27M
	HSJD-DIPG-018	F	Pons	Anaplastic astrocytoma	DMG, H3 K27-altered	H3.1K27M
	HSJD-DIPG-019	M	Pons	Anaplastic astrocytoma	DMG, H3 K27-altered	H3.3K27M
	HSJD-DIPG-022	M	Pons	Glioblastoma multiforme	H3-wildtype and IDH-wildtype	H3K27- WT
	HSJD-DIPG-038	F	Pons	Glioblastoma multiforme	DMG, H3 K27-altered	H3K27M
	HSJD-DIPG-040	F	Pons	Anaplastic astrocytoma	DMG, H3 K27-altered	H3K27M
Tumor necropsies	HSJD-DIPG-002	F	Pons	Anaplastic astrocytoma	DMG, H3 K27-altered	H3.3K27M
	HSJD-DIPG-018	F	Pons	Anaplastic astrocytoma	DMG, H3 K27-altered	H3.1K27M
	HSJD-DIPG-004	F	Pons	Glioblastoma multiforme	DMG, H3 K27-altered	H3.1K27M
	HSJD-DIPG-014	F	Pons	Glioblastoma multiforme	DMG, H3 K27-altered	H3.3K27M
	HSJD-DIPG-015	M	Pons	Glioblastoma multiforme	DMG, H3 K27-altered	H3.3K27M
	HSJD-DIPG-036	F	Pons	Anaplastic astrocytoma	DMG, H3 K27-altered	H3.3K27M

HSJD-DIPG-001	F	Pons	Glioblastoma multiforme	DMG, H3 K27-altered	H3.3K27M
HSJD-DIPG-008	M	Pons	Glioblastoma multiforme	DMG, H3 K27-altered	H3.3K27M
HSJD-DIPG-003	M	Pons	Glioblastoma multiforme	DMG, H3 K27-altered	H3.3K27M
HSJD-DIPG-010	F	Pons	Glioblastoma multiforme	DMG, H3 K27-altered	H3.3K27M
HSJD-DIPG-022	M	Pons	Anaplastic astrocytoma	H3-wildtype and IDH-wildtype	H3K27- WT
HSJD-DIPG-016	F	Pons	Glioblastoma multiforme	DMG, H3K27-altered	H3.1K27M
HSJD-DIPG-005	F	Pons	Glioblastoma multiforme	DMG, H3K27-altered	H3K27M
HSJD-DIPG-009	F	Pons	Anaplastic astrocytoma	DMG, H3K27-altered	H3K27M
HSJD-DIPG-039	M	Pons	Anaplastic astrocytoma	-	-
HSJD-DIPG-006	F	Pons	Anaplastic astrocytoma	DMG, H3K27-altered	H3K27M
HSJD-DIPG-007	M	Pons	Glioblastoma multiforme	DMG,H3 K27-altered	H3.3K27M
HSJD-DIPG-037	F	Pons	Glioblastoma multiforme	DMG, H3 K27-altered	H3K27M
HSJD-DIPG-023	F	Pons	Glioblastoma multiforme	DMG, H3 K27-altered	H3K27M
HSJD-DIPG-021	F	Pons	Glioblastoma multiforme	DMG, H3 K27-altered	H3K27M
HSJD-DIPG-038	F	Pons	Glioblastoma multiforme	DMG, H3 K27-altered	H3K27M

For analysis, we grouped separately tumor biopsies and necropsies. We immunostained seven consecutive paraffin slides of each patient sample, one for each marker (**Figure 17**). Staining of immune cells with the marker CD45 was profuse in all samples, including nontumor controls, in the range 32-757 cells/mm^2 (**Figure 17**). The density of the T lymphocyte population (CD3$^+$ cells) was low in the control brainstem samples, in the range 3-14 cells/mm^2, and slightly higher in DIPG biopsies (1-52 cells/mm^2) and necropsies (1-212 cells/mm^2) (**Figure 17**). T helper (CD4$^+$) cells were almost undetectable (1-2 cells/mm^2) in control nontumor samples, while they were significantly more abundant in DIPG biopsies (0-18 cells/mm^2) and necropsies (1-174 cells/mm^2) (**Figure 17**). Among CD4$^+$ cells, Tregs (FoxP3$^+$) were not detectable in control brainstem samples, while they were significantly more abundant (0-10 cells/mm^2) in the cancer biopsies (**Figure 17**). The density of cytotoxic T cells (CD8$^+$) and B cells (CD20$^+$) was not significantly different between tumor and control samples (**Figure 17**).
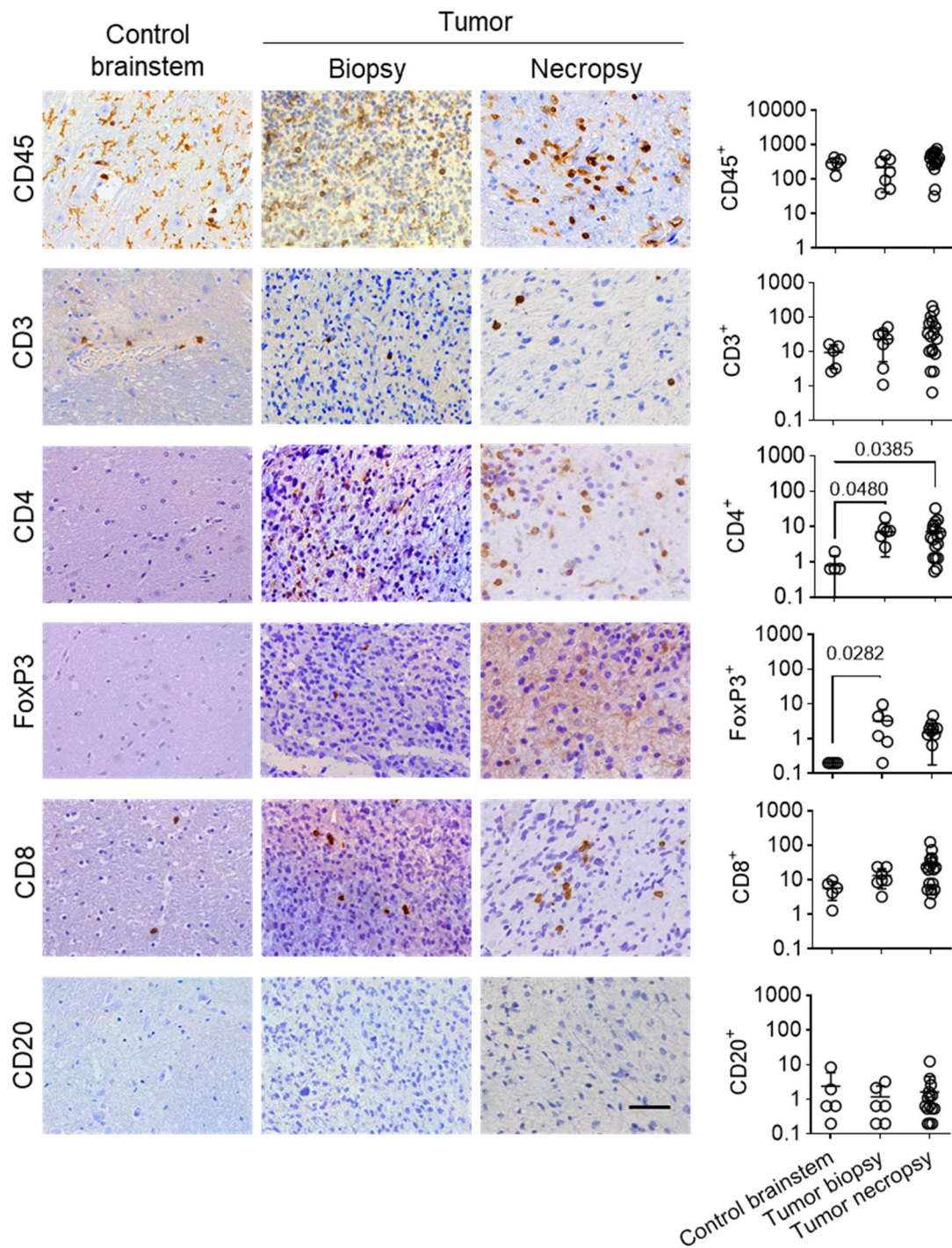
Figure 17. Quantification of TILs in DIPG and control brainstem. Representative images (left) and quantification (right) of CD45, CD3, CD4, FoxP3, CD8 and CD20 stainings in control brainstem (n = 5), DIPG biopsies (n = 7) and DIPG necropsies (n = 17). Units of the y axis are cells/mm^2. Scale bar is 40 µm.

There were two patterns of CD45 staining, CD45^{high}, corresponding to round lymphocytes, and CD45^{low}, corresponding to microglia/macrophages. CD45^{low}

cells were the most abundant and presented a more ramified shape in the control brainstem than in tumors (**Figure 18A**). CD68$^+$ macrophages infiltrated all samples (**Figure 18B**). CD68$^+$ cells were significantly more abundant in the tumor necropsies (2-578 cells/mm^2), compared to control brainstem samples (0-50 cells/mm^2) (**Figure 18B**). Iba1$^+$ microglial cells were equally abundant in control brainstem (173-404 cells/mm^2), biopsies (6-400 cells/mm^2) and necropsies (210-785 cells/mm^2) (**Figure 18B**). In tumors, Iba1$^+$ cells were bushy and round, in contrast to the ramified morphology observed in healthy brainstem (**Figure 18B**). Iba1$^+$ cells in tumors showed higher area fraction and soma area than in healthy brainstems (**Figure 18C**). The finding of CD163$^+$ M2-like TAMs in DIPG was very significant. They were abundant in tumor samples, in the range 104-1074 cells/mm^2 in necropsies and 117-509 cells/mm^2 in biopsies, and rare in brainstem controls, in the range 16-54 cells/mm^2 (**Figure 18B**).
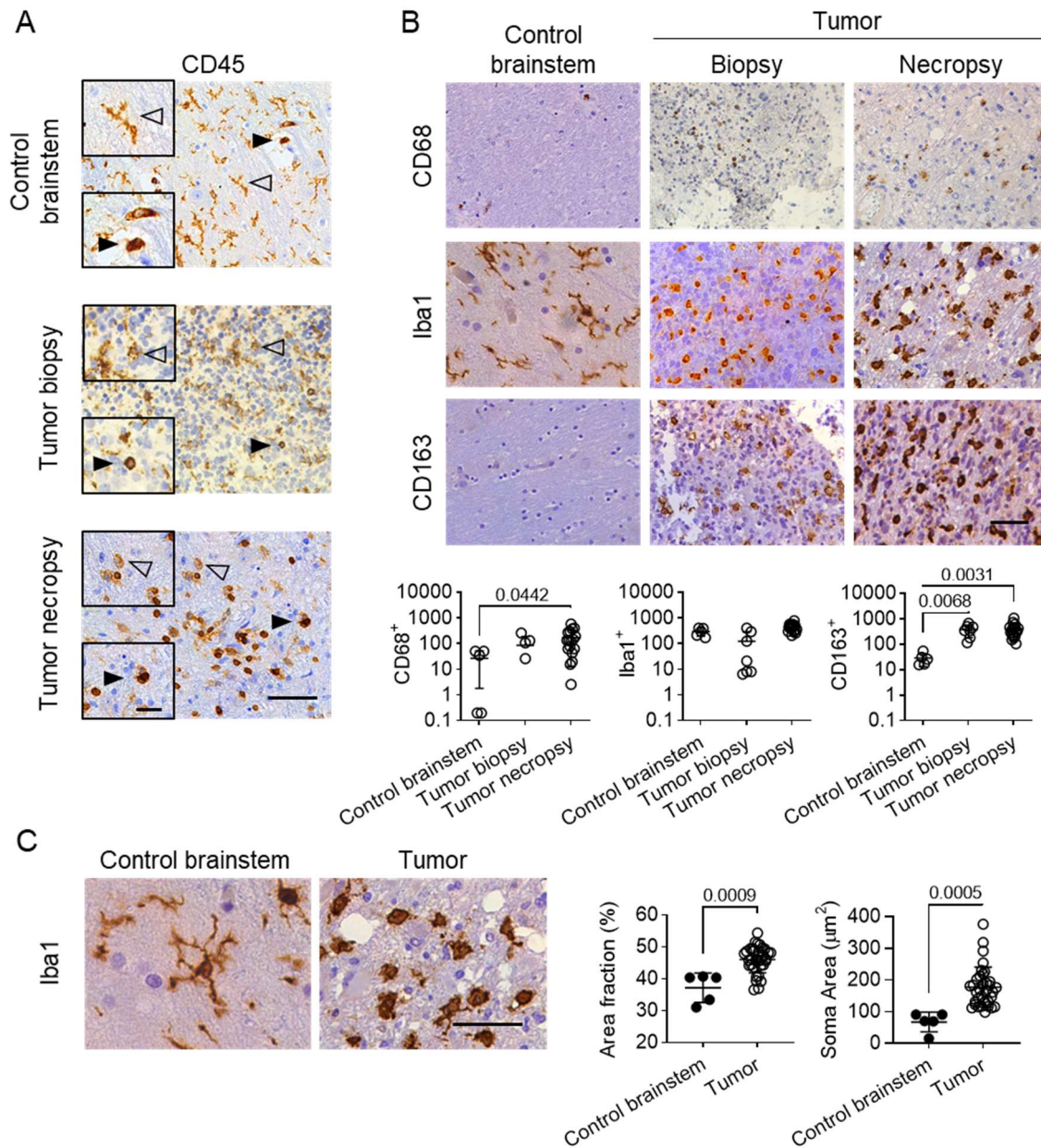
Figure 18. Quantification of TAMs in DIPG and control brainstem. (A) Staining of CD45 in representative samples of the study (control brainstem, tumor biopsy and tumor necropsy). Black arrows (▶) indicate CD45^{high} staining, corresponding to round lymphocytes. Empty arrows (▷) indicate CD45^{low} staining, corresponding to ramified microglia/macrophages. Scale bars are 40 μm (20 μm in the zoomed pictures). (B) Representative images (left) and quantification (right) of CD68, Iba1 and CD163 stainings in control brainstem (n = 5), DIPG biopsies (n = 7) and DIPG necropsies (n = 17). Units of the y axis are cells/mm^2. (C) Representative images (left) and morphology analysis (right) of Iba1 in control brainstem (n = 5) and DIPG samples (n = 33). All images were obtained at a 20x objective magnification. The scale bar is 40 μm. Dots in the graphics (panels A, C and D) are data from individual patient samples (one dot per sample). Samples from panels A and C in which the count was 0 are represented as 0.2 in the logarithmic scale.

Expression of immune checkpoints and immune scape mechanisms in DIPG

Using RT-qPCR in tissue from 4 control brainstem and 12 tumor samples, we found that gene *CD276* (B7-H3) was significantly overexpressed in tumors, compared to brainstem controls, while *CD274* (PD-L1), *CD273* (PD-L2) and *CD152* (CTLA-4) were not (**Figure 19A**). We assessed mRNA expression of enzymes involved in the catabolism of tryptophan into kynurenine, which are involved in the induction of an immune tolerant microenvironment in gliomas[209]. Tryptophan-2,3-dioxygenase 1 (*TDO*) was similar in control and tumor samples, while we did not detect indoleamine 2,3-dioxygenase 1 (*IDO1*) or indoleamine 2,3-dioxygenase 2 (*IDO2*) genes (**Figure 19B**). Regarding cyclooxygenase-2 prostaglandin E2 pathway-related genes (Prostaglandin E Synthase and Prostaglandin E Synthase 2; *PTGES* and *PTGES2*), also associated with immunosuppression in glioma[210], we did not detect changes in DIPG patients (**Figure 19C**). There were no significant differences for the expression of HLA class I and II molecules (except in *HLA-DRA*) (**Figure 19D**) and TGF-β isoforms (**Figure 19E**), previously described mechanisms used by glioma cells to escape the immune system[211,212]. Heat shock proteins (HSP) were increased in DIPG samples, although only *HSPA1A* was significant (**Figure 19F**). The main role of HSP is to facilitate protein folding in physiological conditions in process of immune modulation[213] and they have been associated to the creation of a favorable microenvironment for glioblastoma invasion[214]. Other immunomodulatory molecules we analyzed due to their previous association with glioma progression were *STAT3*[215], calreticulin (*CALR*)[216], high mobility group box 1 (*HMGB1)*[217] and hypoxanthine guanine phosphoribosyltransferase 1

(*HPRT1*)[218]. We found *CALR* and *HPRT1* significantly overexpressed in DIPG samples, and no differences for the other two genes (**Figure 19G**).
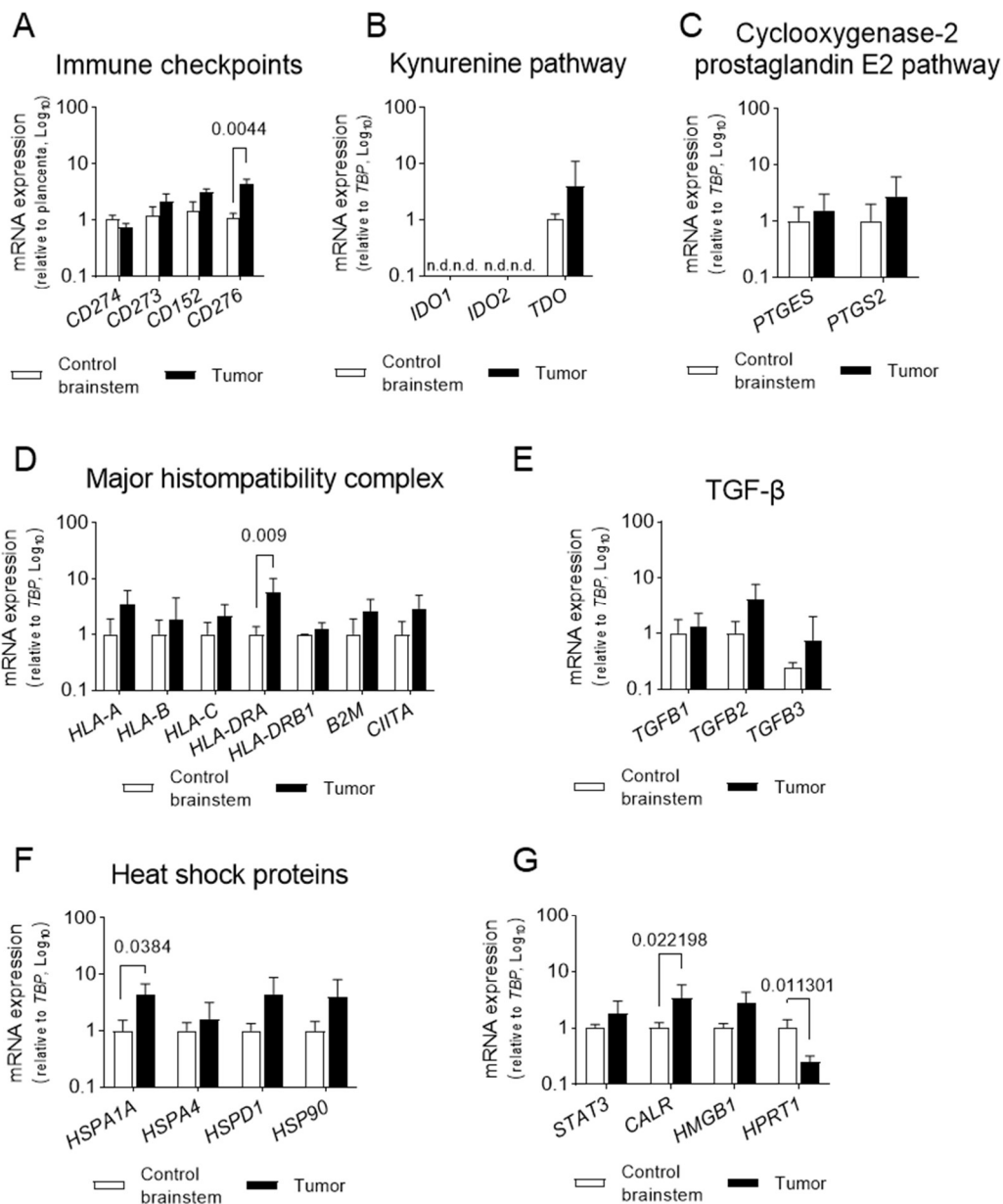
Figure 19. mRNA expression of immune escape mechanisms in DIPG. mRNA expression levels of different immune escape mechanisms in tissue from healthy brainstem (n=3) and tumor (n=11) samples. n.d.: not detected. Bars and error bars represent means and SD. (A) Expression of immune checkpoints. (B) Expression of genes associated to kynurenine pathway. (C) Expression of genes associated to cyclooxygenase-2 prostaglandin E2 pathway. (D) Expression of the gene constant region (B2M), the polymorphic regions (HLA-A/B/C) of the HLA class I and HLA class II molecules (HLA-DRA/DRB1) and the MHC-II transactivator (CIITA). (E) Expression of TGF-β isoforms. (F) Expression of heat shock proteins. (G) Expression of other immunomodulatory molecules associated with glioma progression.

In paraffin samples, we found scarce PD-L1$^+$ and CTLA-4$^+$ cells in 1 of 16 and 14 of 18 analyzed DIPG, respectively (**Figure 20A**). B7-H3 staining was positive in all (13/13) analyzed samples (**Figure 20**). None of the analyzed control brainstem samples expressed PD-L1 or B7-H3, while 60% of them (3 of 5) expressed CTLA-4 in a minority of cells (**Figure 20A**). We found three patterns of B7-H3 expression in tumors. In a third of the samples (4 of 13), B7-H3 was exclusively expressed by perivascular cells (**Figure 20B**). In another third, B7-H3 was expressed only by cancer cells (**Figure 20B**). In the remaining samples (5 of 13), B7-H3 had an intermediate expression pattern, both in cancer cells and perivascular cells (**Figure 20B**). Such perivascular cells were CD90$^+$ in DIPG, while no control brainstem was positive for CD90 (**Figure 20C** and **F**). CD90$^+$ cells were also positive for B7-H3 staining (**Figure 20**) and for pericyte markers PDGFR-β (**Figure 20E**) and NG2 (**Figure 20E** and **F**). Moreover, they were negative for the endothelial cell marker CD31, the tumor cell marker SOX2, the normal stromal cell marker H3me3 and the TAM marker CD163 **Figure 20E**).
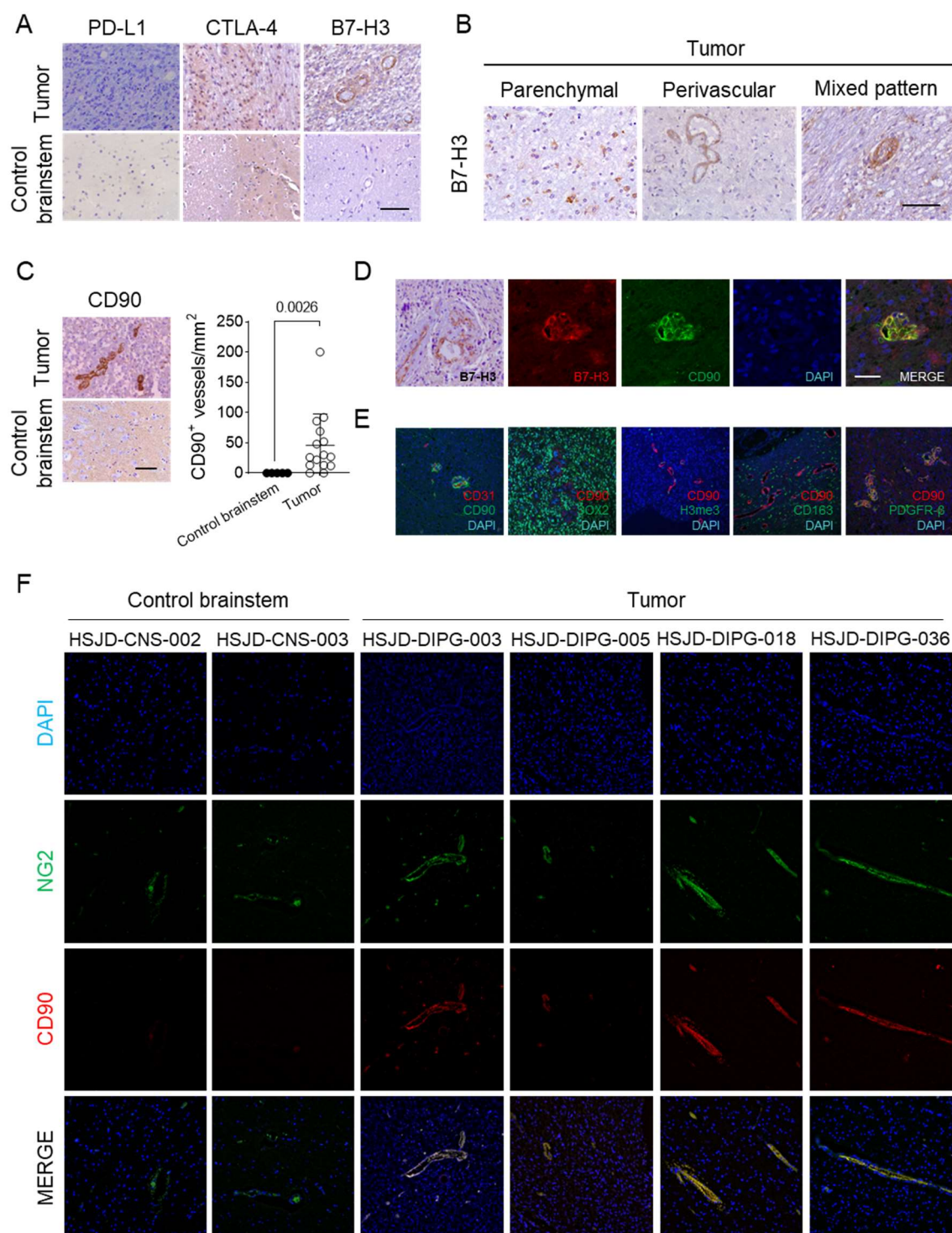
Figure 20. Protein expression of immune checkpoints in DIPG. (A) Representative images of PD-L1, CTLA-4 and B7-H3 immunostaining in control brainstem (n = 5), DIPG biopsies (n = 7) and DIPG necropsies (n = 17). Scale bar is 40 μm. (B) Representative images of B7-H3 staining for the parenchymal, perivascular and mixed patterns. Scale bar is 40 μm. (C) Representative immunohistochemistry of CD90 in control brainstem and tumor samples. The scale bar is 40 μm. Quantification of CD90⁺ blood vessels/mm² in control brainstem and tumor. (D) Immunofluorescence of B7-H3, CD90 and DAPI in a DIPG sample with perivascular expression of B7-H3. Scale bar is 40 μm. (E) Double confocal immunofluorescence of CD90/CD31,

CD90/SOX2, CD90/H3me3, CD90/CD163 and CD90/PDGFR-β in tumor tissue. Scale bar is 40 µm. (F) Double immunofluorescence images of NG2/CD90 with DAPI in control brainstem (n = 2) and tumor tissue samples (n = 4). The scale bar is 100 µm.

Following the addition of IFN-γ to primary DIPG cells in culture, the expression of genes *CD274* (PD-L1) and *CD273* (PD-L2) increased abruptly (**Figure 21**), suggesting that these immune checkpoint scape mechanisms are functional but they are likely repressed at the tumor location. In contrast, the expression of *CD276* (B7-H3) did not change upon exposure to IFN-γ (**Figure 21**).
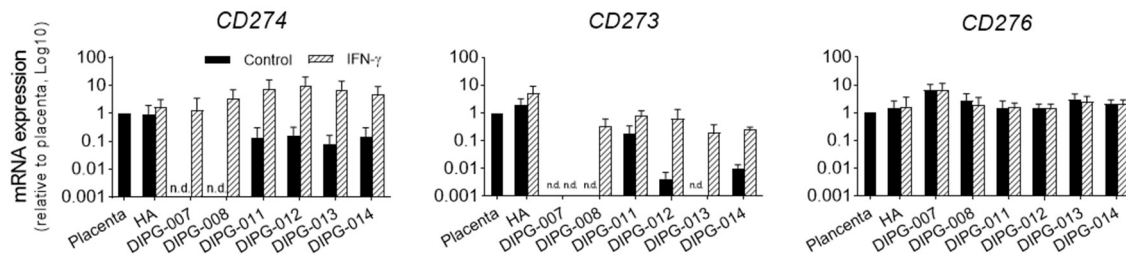
Figure 21. mRNA expression of immune checkpoints in DIPG cell models upon exposure to artificial pro-inflammatory microenvironment. mRNA expression of *CD274*, *CD273* and *CD276* after exposure to 10 ng/mL IFN$^\gamma$ for 48 h.

DIPG secretome

To identify tumor-associated proteins involved in the protumoral immune microenvironment of DIPG, we analyzed 105 cytokines in homogenized brainstem samples obtained from necropsies of 14 patients with DIPG and four patients without brain tumors (**Figure 22A**). Clinical information of the samples is in **Table 8**. We found the cytokines chitinase 3-like protein 1 (CHI3L1) and osteopontin significantly enriched in DIPG, compared to control brainstem samples (**Figure 22**). We did not detect expression of classical M2-like polarizers such as IL-10 or IL-4, proangiogenic factors such as VEGF, or immunoactivators

such as IL-7, IL-9 or IFN-γ (**Figure 22A**). To test whether the identified proteins were secreted by DIPG cells in culture, we analyzed the cytokine profile of the supernatants of seven primary cell models and the human astrocyte cell line for comparison. Clinical information of the samples is found in **Table 9**. We detected CHI3L1 and osteopontin in the supernatants of five of seven DIPG models (**Figure 22B**). Osteopontin was also secreted by human astrocytes, while CHI3L1 was exclusively secreted by DIPG cells (**Figure 22B**).

Representative images of the array membranes are in **Figure 22C**.
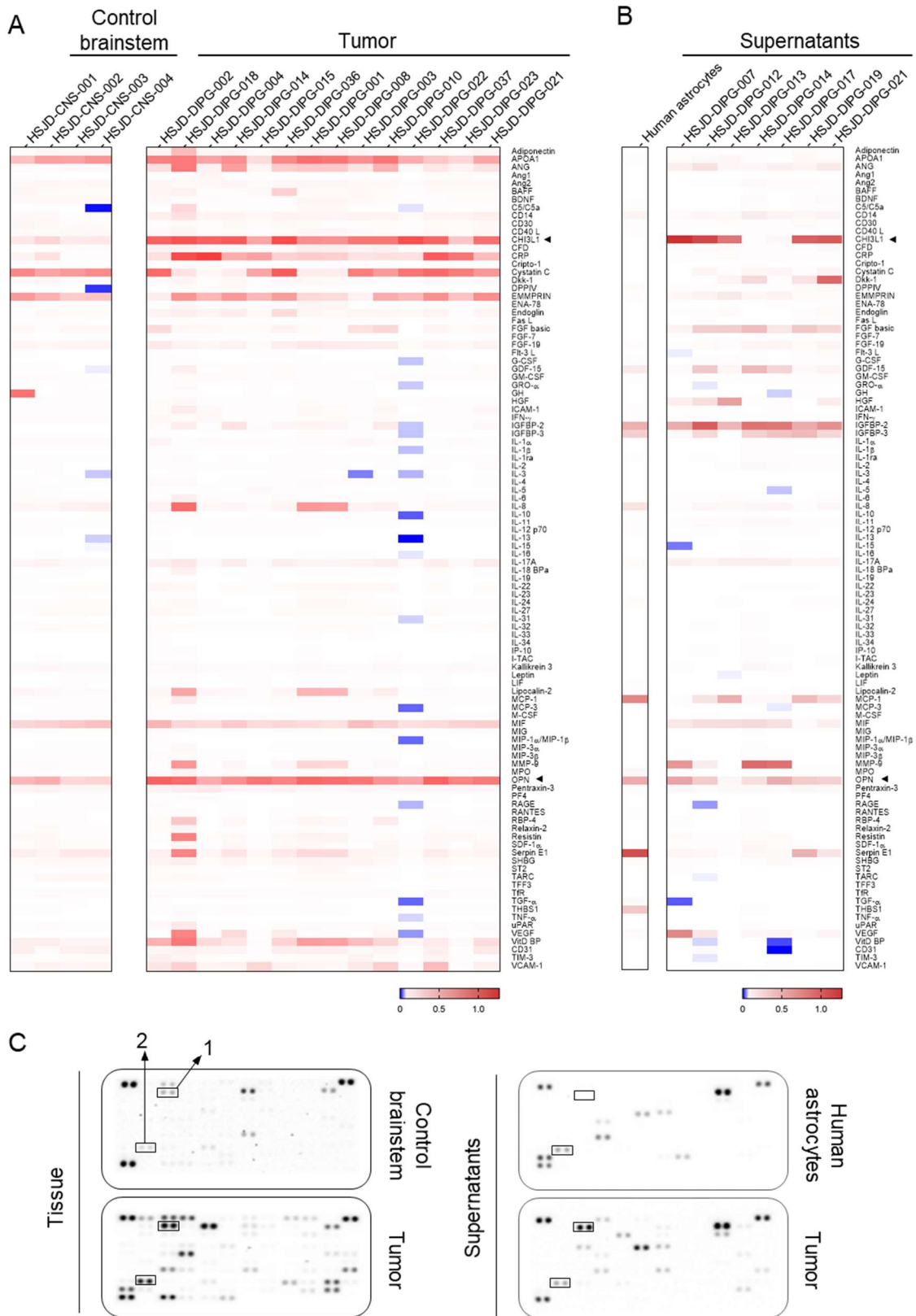
Figure 22. Analysis of the secretome of pHGG. (A) Heatmap representation of the cytokine array of the tissue homogenates of control brainstem samples and tumor samples. (B) Heatmap representation of the cytokine array of supernatants of human astrocytes and DIPG primary cells in culture. (C) Representative images of array membranes corresponding to different samples in

which the numbered spots indicate the two proteins that showed statistical differences in signal intensities among the array membranes, CHI3L1 (1) and osteopontin (2).

Table 9. Cell models included in the study.

Code	Sex	Tumor location	Tumor histology	WHO Classification	Histone Mutation
HSJD-DIPG-007	M	Pons	Glioblastoma multiforme	DMG, H3K27-altered	H3.3K27M
HSJD-DIPG-008	M	Pons	Glioblastoma multiforme	DMG, H3K27-altered	H3.3K27M
HSJD-DIPG-012	M	Pons	Anaplastic astrocytoma	DMG, H3K27-altered	H3.3K27M
HSJD-DIPG-013	F	Pons	Anaplastic astrocytoma	DMG, H3K27-altered	H3.3K27M
HSJD-DIPG-014	F	Pons	Glioblastoma multiforme	DMG, H3K27-altered	H3.3K27M
HSJD-DIPG-017	M	Pons	Anaplastic astrocytoma	DMG, H3K27-altered	H3.3K27M
HSJD-DIPG-019	M	Pons	Anaplastic astrocytoma	DMG, H3K27-altered	H3.3K27M
HSJD-DIPG-021	F	Pons	Anaplastic astrocytoma	DMG, H3K27-altered	H3.3K27M
HSJD-DMG-005	F	Pons	Anaplastic astrocytoma	DMG, H3 K27-altered	H3.3K27M
HSJD-GBM-001	F	Right frontal lobe	Glioblastoma multiforme	H3-wildtype and IDH-wildtype	H3K27-WT

Next, we quantified (ELISA) the top-2 secreted cytokines, CHI3L1 and osteopontin, in DIPG samples and cell culture supernatants (**Table 8** and **Table 9**, respectively). In frozen tissue samples, median CHI3L1 concentration was around 100 times higher in tumor samples (2266 ng/mL; range 208-6012 ng/mL; n = 10) than in controls (23.7 ng/mL; 7.7-36.8 ng/mL; n = 4) (**Figure 23A**). Osteopontin concentration in tumors (18.1 ng/mL; 3.8-44.7 ng/mL; n = 7) was

also significantly higher, around 10 times, than in the brainstem tissues (1.8 ng/mL; 0-3.3 ng/mL; n = 4) (**Figure 23A**). CHI3L1 and osteopontin concentrations correlated well with the signals obtained in the protein arrays in tissue (**Figure 23C**). In DIPG cell supernatants, CHI3L1 and osteopontin were detectable by ELISA in 100% of the cell models, in the range 0.3-1475 and 0.7-120 ng/mL, respectively (**Figure 23B**), and such levels correlated well with the signals obtained in the protein arrays in supernatants (**Figure 23D**). Protein results were also concordant with the RT-qPCR analyses of the two genes (*CHI3L1* and *SPP1*) in the patient samples (**Figure 23E**) and tumor cells (**Figure 23F**), with higher levels in the tumor samples.

Then, we analyzed the CSF of 18 pHGG patients (13 DMG H3 K27-altered and five pHGG H3-wildtype and IDH-wildtype) and 18 non-oncologic patients free of inflammation. CHI3L1 concentration was significantly higher in pHGG (92.2 ng/mL; 18-267 ng/mL) than in controls (19.6 ng/mL; 3.33-130 ng/mL) (**Figure 23G**). Osteopontin concentration was around 10 times higher in the tumor group (140 ng/mL; 11.3-299 ng/mL) compared to the controls (12.6 ng/mL; 0.8-55 ng/mL) (**Figure 23G**). Upon analysis of serum samples, the concentration of CHI3L1 was significantly higher in patients with pHGG (38.8 ng/mL; 7.1-165 ng/mL; n = 10) than in controls (12.2 ng/mL; 1.5-31.6 ng/mL; n = 9) (**Figure 23H**). Osteopontin levels in serum were similar in patients with pHGG (51 ng/mL; 25.3-111 ng/mL, n = 10) and controls (49.2 ng/mL; 12.2-106 ng/mL; n = 15) (**Figure 23H**).
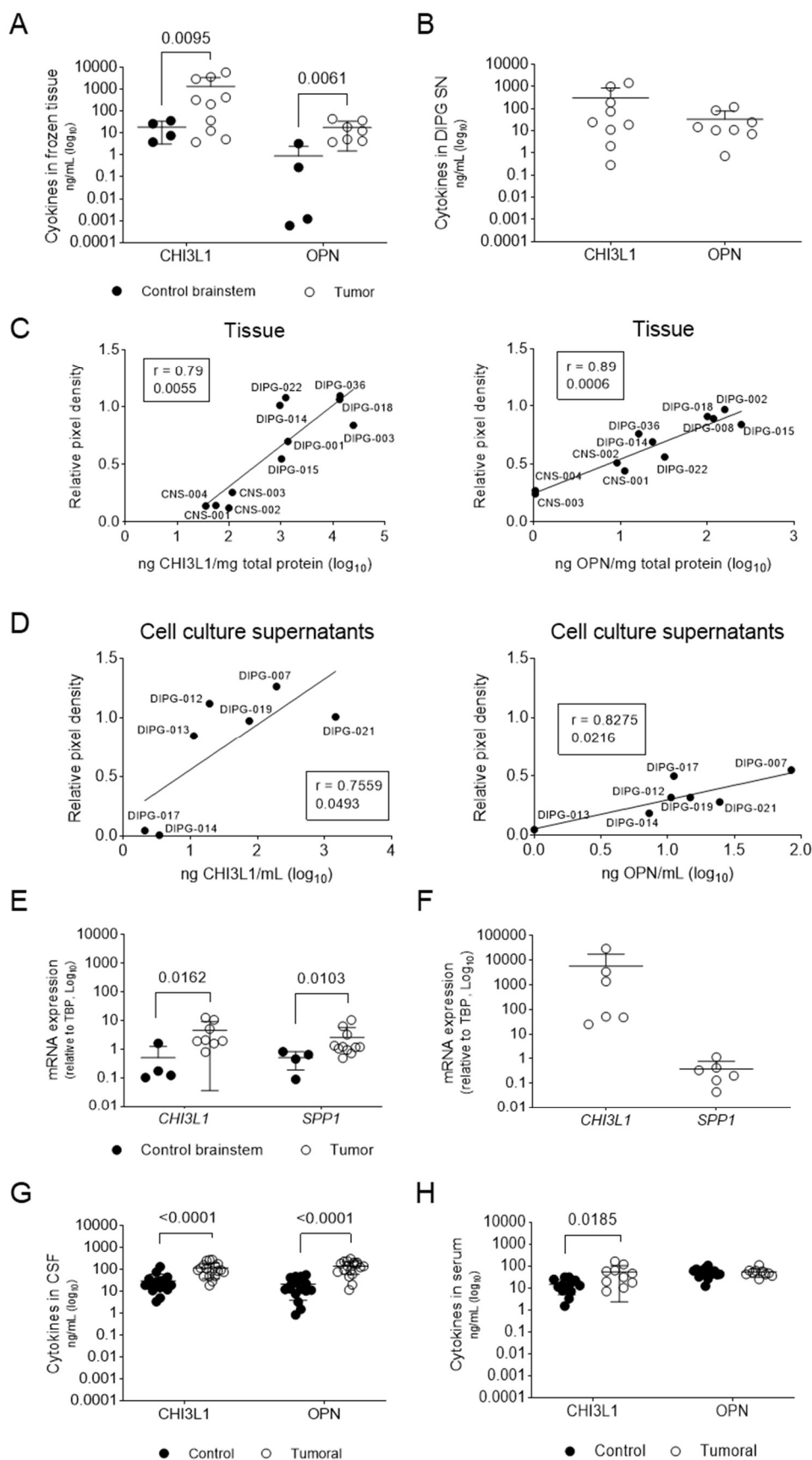
Figure 23. Analysis of CHI3L1 and OPN in DIPG samples. (A) Quantification of CHI3L1 and osteopontin in frozen tissue samples. (B) Quantification of CHI3L1 and osteopontin in pHGG

supernatants. (C) Correlation assay between the results of the cytokine array and the ELISA in tissue lysates (n=11). The line indicates the simple regression line between the two parameters. Individual data (labeled dots) are represented. (D) Correlation assay between the results of the cytokine array and the ELISA in DIPG cell supernatants (n=7). The line indicates the simple regression line between the two parameters. Individual data (labeled dots) are represented. (E) Quantification of *CHI3L1* and *SPP1* mRNA expression and in control brainstem (n = 4) and tumor tissue samples (n = 10). (F) Quantification of *CHI3L1* and *SPP1* mRNA expression in DMG cell models (n = 6). (G) Quantification of CHI3L1 and osteopontin in patient CSF samples. (H) Quantification of CHI3L1 and osteopontin in patient serum samples.

Using immunoblotting, we detected higher levels of CHI3L-1 and osteopontin (in its full-length –66 kDa - and cleaved 45 kDa form, which increases the adhesion capacity to its receptors[219]) in frozen DIPG samples, compared to brainstem controls (**Figure 24A**). We detected the expression of these proteins in the cytoplasm of DIPG cells in culture (**Figure 24**). In frozen patient samples, CHI3L1 and osteopontin immunostaining were significantly more intense in tumor samples than in control brainstem, and they were associated to cancer cells expressing SOX2 (**Figure 24C**).
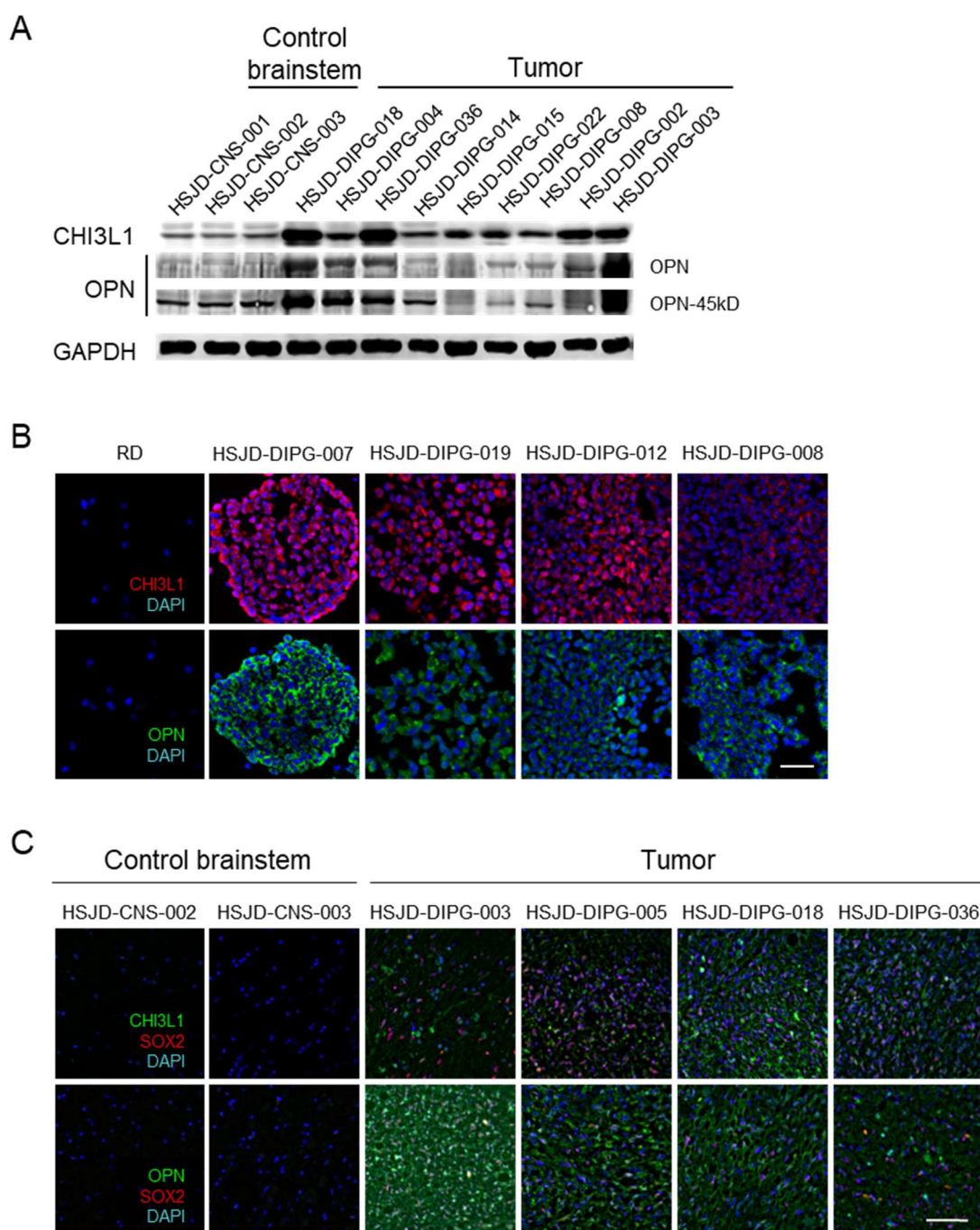
Figure 24. OPN and CHI3L1 protein expression in DIPG. (A) Immunoblotting of osteopontin and CHI3L1 with DAPI in brainstem control and tumor tissue samples. (B) Immunofluorescence images of osteopontin and CHI3L1 in RD cell line (rhabdomyosarcoma) and DIPG tumorspheres. The scale bar is 50 μm. (C) Double immunofluorescence images of CHI3L1 (green) and SOX2 (red), or OPN (green) and SOX2 (red), with DAPI (blue), in control brainstem (n = 2) and tumor tissue samples (n = 4). Areas merging green and red appear as pink in the images. The scale bar is 50 μm.

Differentiation of mesenchymal stem cells towards B7-H3-expressing pericytes in the presence of DIPG-secreted factors

Following the finding of perivascular CD90$^+$ B7-H3$^+$ cells in DIPG, we studied whether the DIPG secretome could induce a pericyte-like phenotype in CD90$^+$ cells of the mesenchymal lineage. Following the exposure of hMSC-AT cells to the supernatant of osteopontin-rich DIPG cells DIPG-007, CHI3L1-rich DIPG-021 and osteopontin, and CHI3L1-intermediate cells DIPG-012 (see individual quantifications in **Figure 25D**), we found an increase in the expression of B7-H3 for the first two conditions, but not for the third (**Figure 25A**). Exposure to recombinant proteins osteopontin and CHI3L1, and to pericyte culture medium, also increased B7-H3 (**Figure 25A**). PD-L1 expression did not change in any of the experimental conditions (**Figure 25A**). The marker NG2, associated to early-stage differentiated pericytes in the neovascularization process[220], increased sharply in the presence of DIPG cell supernatants and recombinant osteopontin and more discretely with CHI3L1 (**Figure 25A**). The marker of late-stage pericyte differentiation, PDGFRβ, appeared only following incubation in pericyte medium (**Figure 25A**). Additionally we observed that NG2 expression changes in hMSC-AT coincided with a decrease in the expression of the mesenchymal stem cell marker CD90 (**Figure 25B**). Exposure of hMSC-AT cells to supernatants of human astrocytes, LAN-1 or A4573 cells did not induce changes in B7-H3, PD-L1, NG2 and PDGFRβ (**Figure 25A, B**). Overall, our experiments show that the secretome of DIPG cells, but not other cancer cells, induce the differentiation of mesenchymal cells into a pericyte-like phenotype.
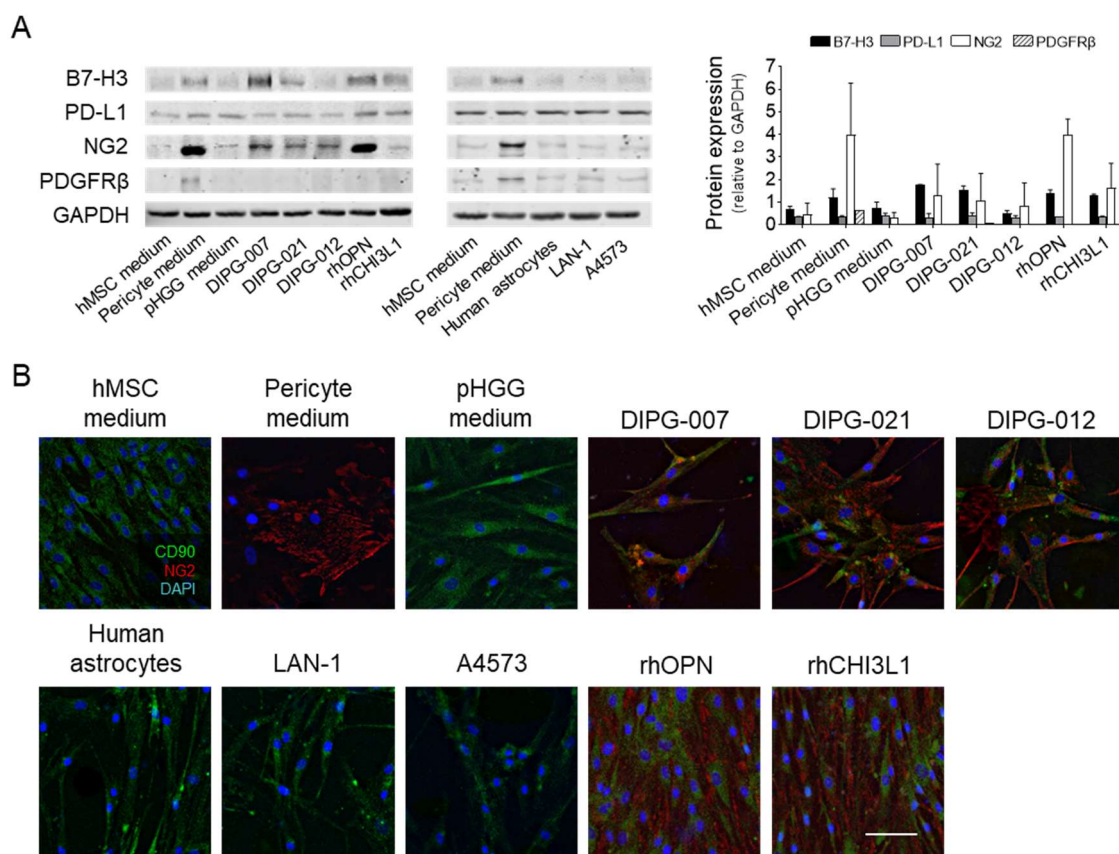
Figure 25. Effect of the DIPG secretome on pericyte differentiation. (A) Immunoblotting of B7-H3, PD-L1, NG2 and PDGFR-β in hMSC-AT exposed for 7 days to fresh culture media, DIPG-conditioned media, recombinant osteopontin (rhOPN), recombinant CHI3L1 (rhCHI3L1), human astrocytes conditioned media, LAN-1 conditioned media or A4573 conditioned media. Immunoblot quantification. Bars are means and SD of 2 independent experiments. (B) Double immunofluorescence images of CD90/NG2 with DAPI (blue) on hMSC-AT incubated with conditioned media for 7 days. The scale bar is 100 μm.

Modulation of the angiogenic process by the DIPG secretome

Endothelial hCMEC/D3 cells exposed to DIPG supernatants or culture medium supplemented with recombinant osteopontin or CHI3L1 formed tube networks of higher complexity than those formed after culturing the cells in endothelial or pHGG culture media (**Figure 26A**), or the supernatant of other cells such as human astrocytes, or other pediatric cancer cell lines (**Figure 26A**). Endothelial cell exposure to DIPG secretomes, osteopontin and CHI3L1, but not other cell

lines, induced the formation of significantly longer and more complex endothelial structures in vitro, compared to the endothelial cell culture medium alone (**Figure 26B**).
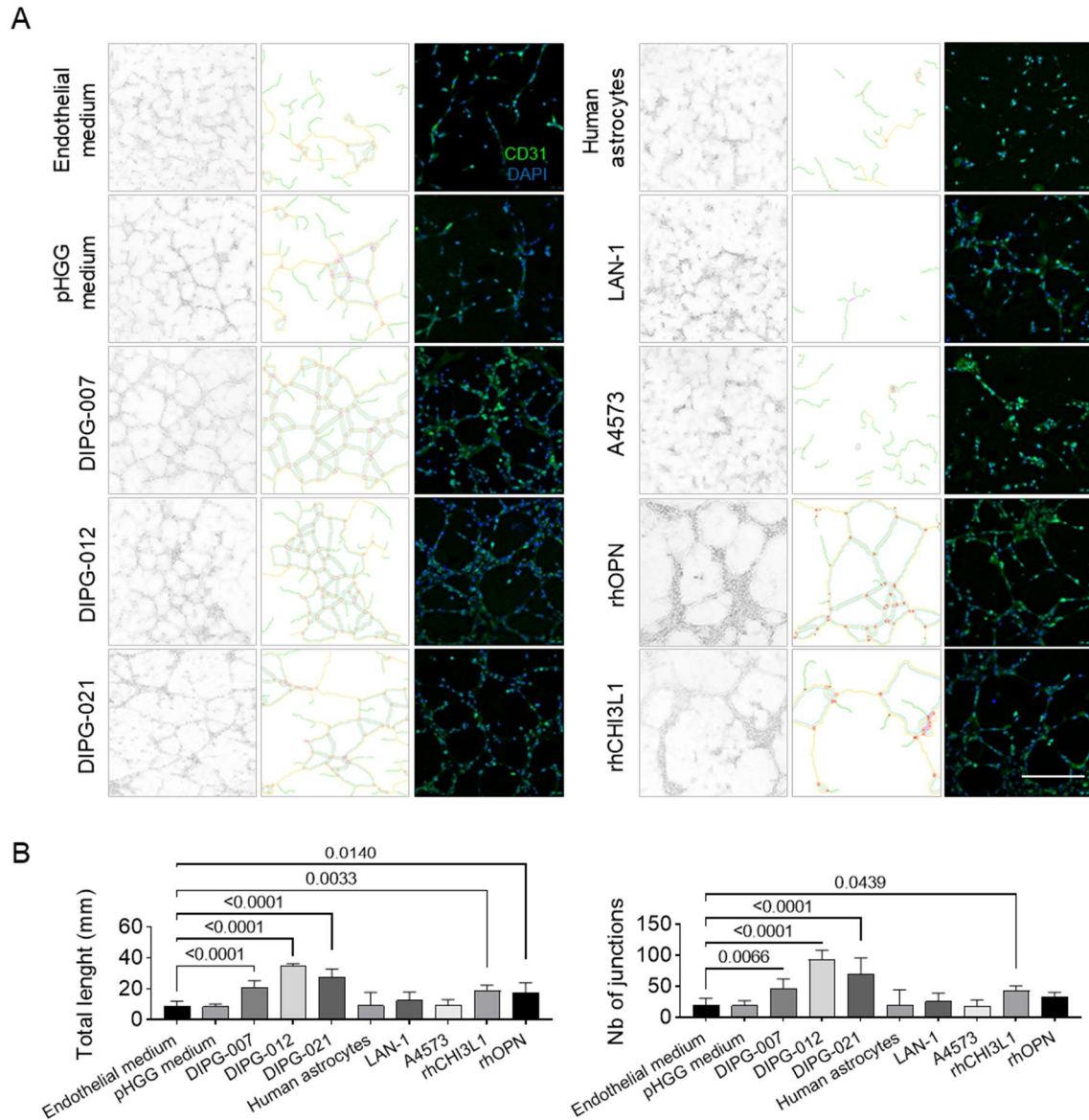
Figure 26. Effect of DIPG secretome on endothelial tube formation in vitro. (A) Representative images of tube formation assay of hCMEC/D3 cells exposed to fresh culture media, DIPG-conditioned media, human astrocytes conditioned media, LAN-1 conditioned media, A4573 conditioned media, rhOPN or rhCHI3L1 for 18 h; the scale bar is 400 µm. Immunofluorescences of CD31 with DAPI of the tube formation assay structures; the scale bar is 200 µm. (B) Tube formation assay quantification using total tubule length and number of junctions to determine net complexity.

Next, we observed that the expression of genes related to angiogenesis in hCMEC/D3 cells increased 100-1000 fold following supplementation of the endothelial cell culture medium with DIPG supernatants, recombinant osteopontin and CHI3L1 (**Figure 27A**). In contrast, cells supplemented with supernatants of tumor cell lines LAN-1 and A4573 and human astrocytes had only discretely increased levels of around 10-fold (**Figure 27A**). We confirmed by RT-qPCR the array results of genes fibronectin (*FN1*) and neuropilin 1 (*NRP1*) (**Figure 27B**). Expression of the blood-brain barrier marker *ABCG2* (BCRP) increased abruptly, around 100 times, in hCMEC/D3 exposed to DIPG supernatants, osteopontin and CHI3L1, while changes were not significant following exposure to HA, LAN-1 or A4573 cell lines (**Figure 27B**).

A

B
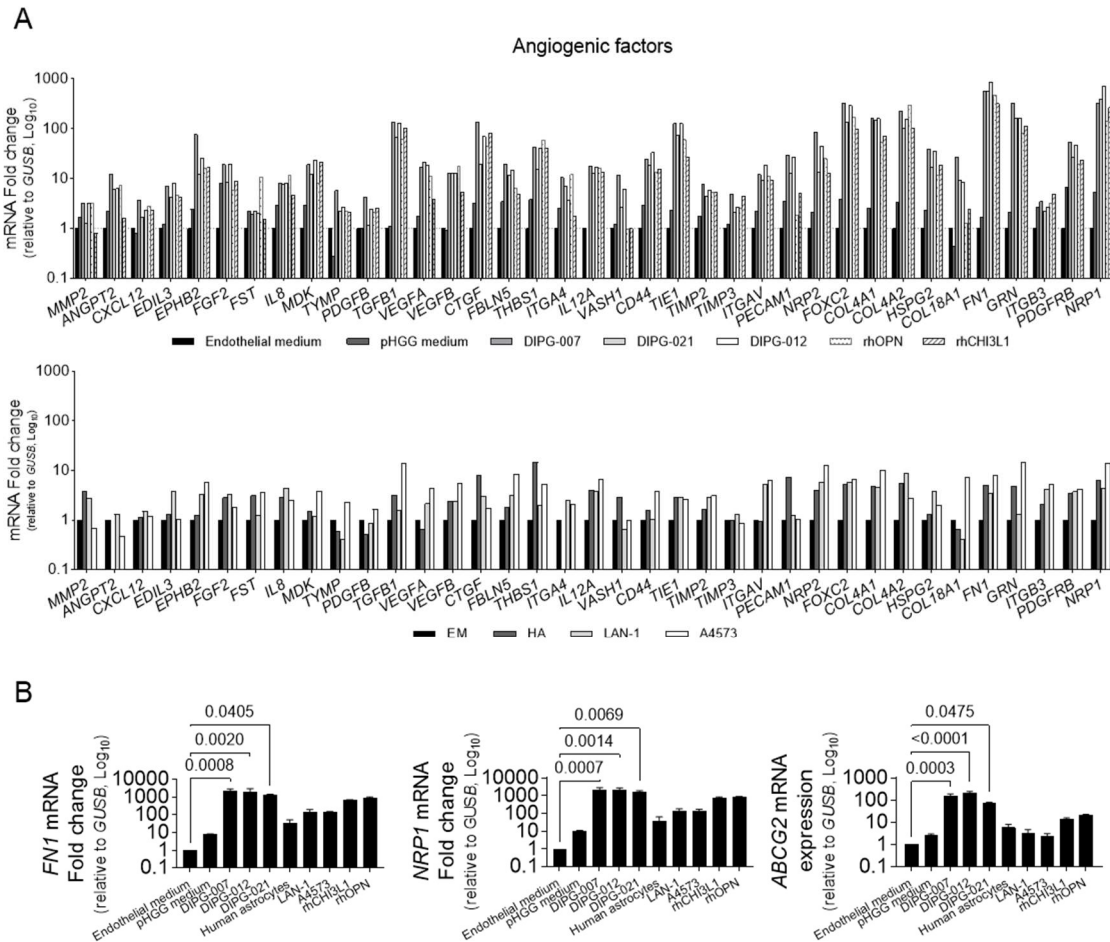
Figure 27. Effect of DIPG secretome on the expression of angiogenic factors. (A) Expression of angiogenic-related genes included in the TaqMan™ Human Angiogenesis Array in hCMEC/D3 cells exposed to fresh culture media, DIPG-conditioned media, rhOPN, rhCHI3L1, human astrocytes conditioned media, LAN-1 conditioned media and A4573 conditioned media for 48 h. Values are normalized to those obtained for hCMEC/D3 exposed to endothelial medium. (B) Validation of mRNA Fold changes detected in TaqMan™ Human Angiogenesis Array of *FN1* and *NRP1*, relative to *GUSB*. mRNA expression levels of *ABCG2*, relative to *GUSB*.

Co-culture of hCMEC/D3 cells and mesenchymal cells, in the presence of the conditioned media, resulted in complex BCRP-expressing endothelial networks surrounded by differentiated NG2-expressing pericyte-like mesenchymal cells, mimicking the primordial structure of blood vessels (¡Error! No se encuentra el origen de la referencia.). No structures were formed when the co-culture was with supernatants of human astrocytes, LAN-1 or A4573 (**Figure 28**).
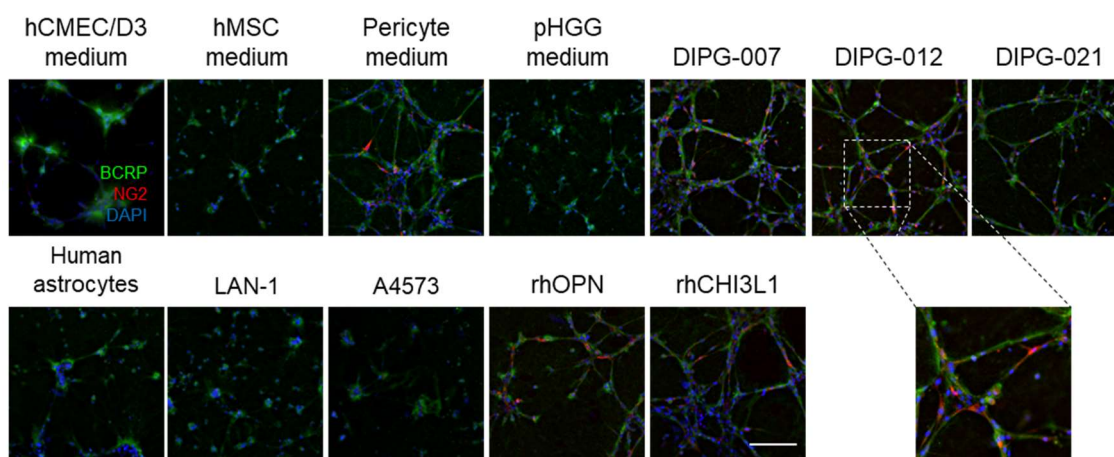
Figure 28. Effect of DIPG secretome on the formation of the basic vascular structure in vitro. Immunofluorescence of BCRP, NG2 and DAPI in co-cultures of hMSC-AT and hCMEC/D3 cells exposed to fresh culture media, DIPG-conditioned media, human astrocytes conditioned media, LAN-1 conditioned media, A4573 conditioned media, rhOPN or rhCHI3L1 for 18 h. The scale bar is 200 μm.

Then, we evaluated whether the intratumoral blood vessels of human xenografts implanted subcutaneously in mice expressed the blood-brain barrier marker BCRP. We found that CD31^{+} blood vessels expressed BCRP only in those subcutaneous xenografts established from pHGG cells, while they did not express BCRP in subcutaneous PDX established from non-CNS tumors such as Ewing sarcoma, neuroblastoma or Wilms tumor, suggesting that pHGG cells favor the formation of the blood-brain barrier in their microenvironment (**Figure 29**). To assure that the re-arranged endothelial cells were not reprogrammed cancer cells, we stained all human nuclei. We confirmed that the endothelial structures were not of human origin, as they were negative for the human-specific marker (**Figure 29**).
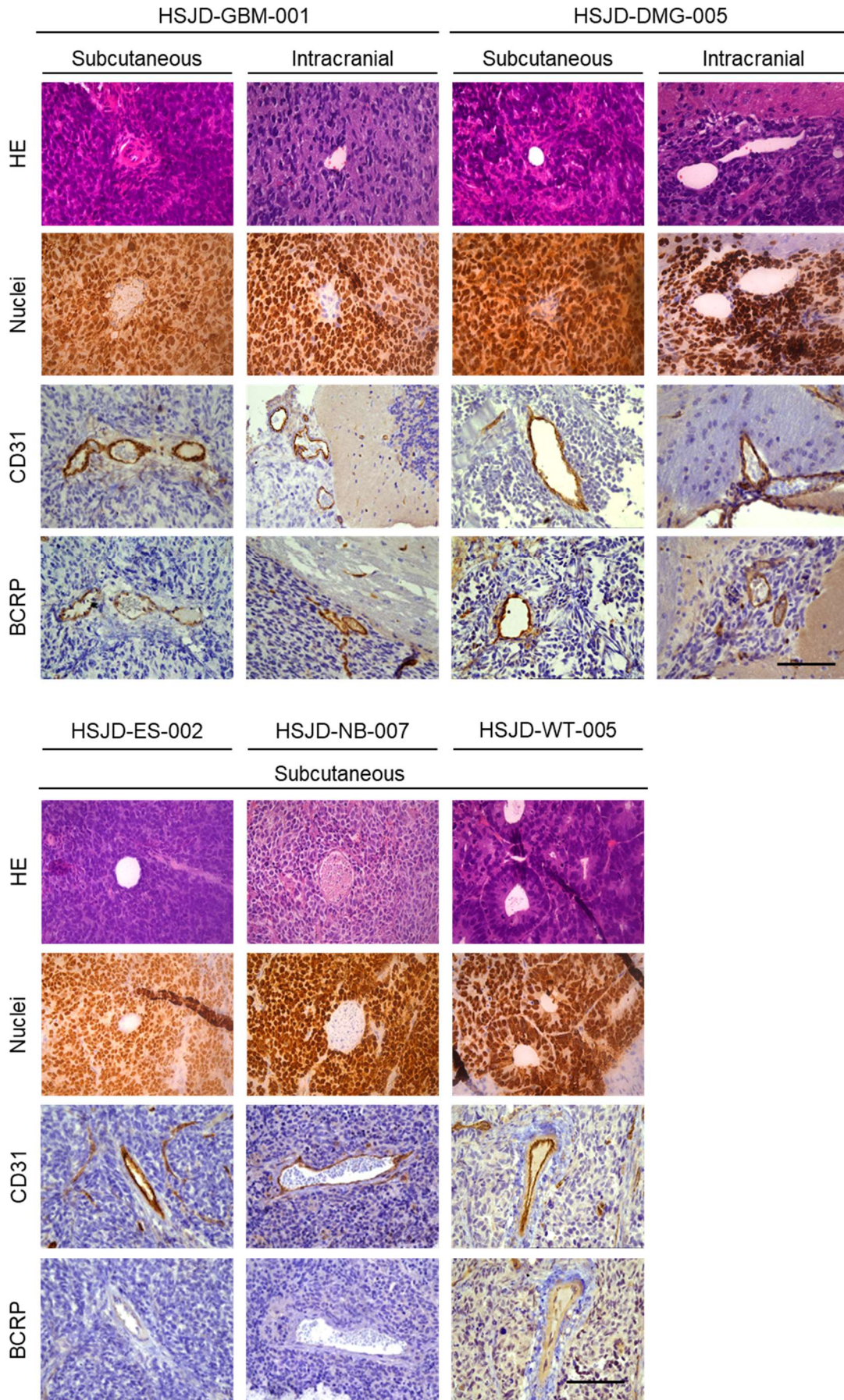
Figure 29. Study of the vasculature in subcutaneous and orthotopic xenografts. Immunostaining of human nuclei, CD31 and BCRP in intracranial and subcutaneous xenografts of pediatric cancers pHGG (models identified as HSJD-GBM-001 and HSJD-DMG-005), Ewing sarcoma (HSJD-ES-002), neuroblastoma (HSJD-NB-007) and Wilms tumor (HSJD-WT-005). Scale bar is 200 µm.

Modulation of the polarization and migration properties of macrophages by the DIPG secretome

PBMC-derived macrophages exposed to M1 and M2 cytokine cocktails expressed M1 and M2-associated genes accordingly in the expression array (**Figure 30A**). When the macrophages where incubated with DIPG supernatant or recombinant osteopontin, genes associated to the M1 phenotype, such as *CD80*, *HIF1A* and *IL1A*, were downregulated, and genes associated to the M2 immunosuppressive phenotype, such as *CD163*, *MMP-9* and *STAT3*, were increased, at levels similar to those obtained for the M2 cocktail (**Figure 30A**). In flow cytometry assays, macrophages exposed to DIPG supernatants had a significantly higher CD163$^+$/CD80$^+$ ratio, compared to macrophages exposed to the M1 cocktail. This phenomenon was characterized by the notable reduction of CD80$^+$ cells and a moderate increase of CD163$^+$ cells. Recombinant osteopontin induced similar effects (**Figure 30B** and **C**).

In the transwell assay, DIPG supernatant and recombinant osteopontin enhanced macrophage migration significantly, compared to the control condition (**Figure 30D** and **E**).
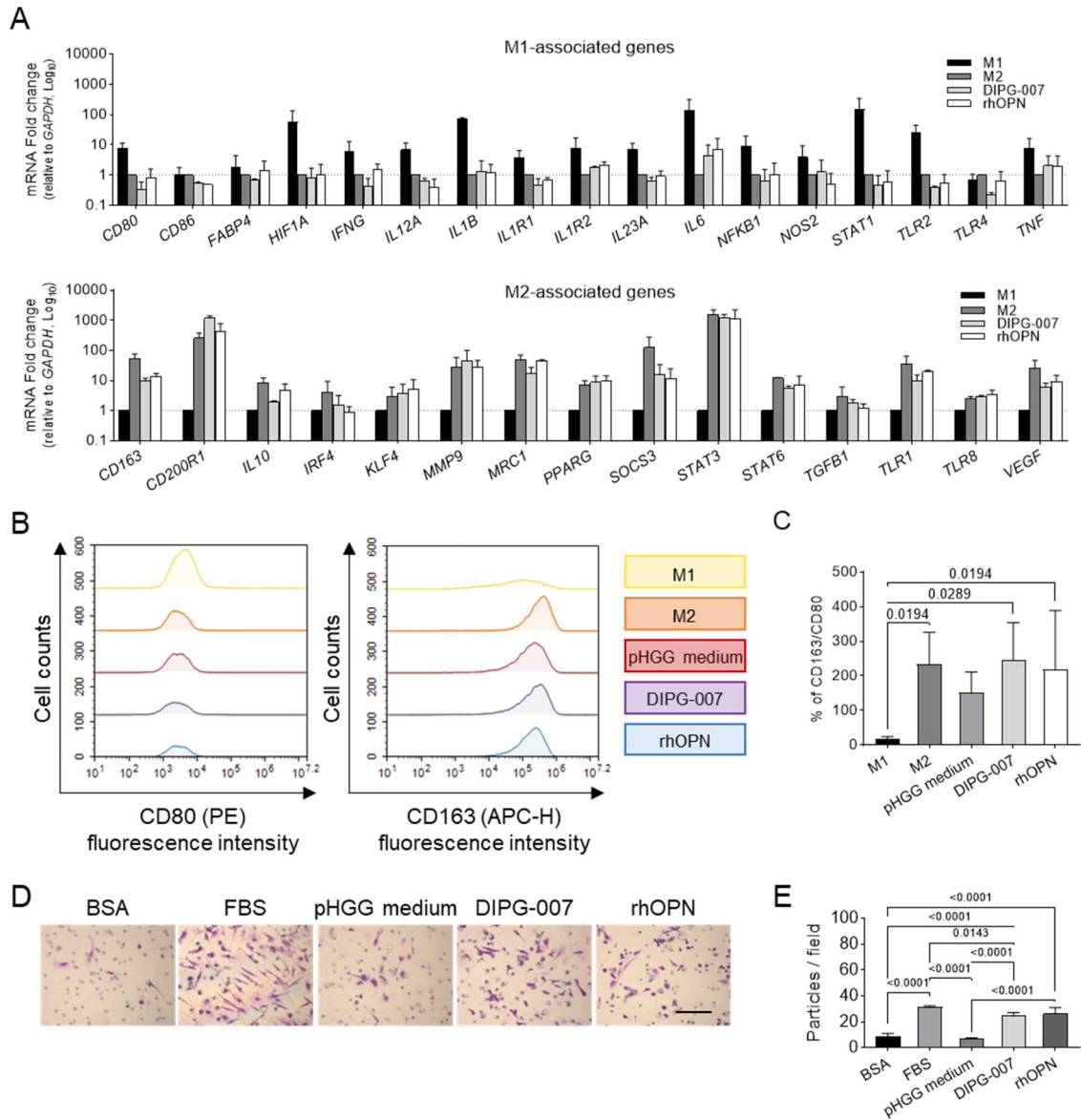
Figure 30. Effect of the DIPG secretome on the polarization and migration properties of PBMC-derived macrophages. (A) Expression of genes included in the GeneQuery™ Human Macrophage Polarization Markers qPCR Array Kit, in PBMC-derived macrophages exposed to fresh culture media, DIPG-conditioned medium, or recombinant osteopontin (rhOPN) for 24 h. Values of M1 and M2-associated genes are normalized to those obtained for macrophages exposed to M2 or M1-polarizing medium, respectively. Bars are means and SD of two independent experiments. (B) Representative flow-cytometry histograms of CD80+ (M1-like) and CD163+ (M2-like) macrophages exposed to fresh culture media, DIPG-conditioned medium, or recombinant osteopontin (rhOPN) for 24 h. (C) CD163+/CD80+ ratios of the experimental groups. Bars and error bars represent means and SD obtained from seven independent experiments, i.e., from seven different donors. (D) Representative images of macrophage invasion and migration in transwell assays. Cells were stained with crystal violet. The scale bar is 40 μm. (E) Quantification of migration of macrophages in each condition. Bars and error bars represent means and SD obtained from 4 independent experiments.

Expression of the CD44-xCT system in pHGG

Because osteopontin and CHI3L1 are highly expressed in pHGG, show potentially immunosuppressive roles, and one of their main receptors is the CD44 family, we next evaluated the presence of CD44 in pHGG. Using immunoblotting, we found CD44 standard form (CD44s) significantly overexpressed in DIPG necropsy samples, compared to control tissue samples (**Figure 31A**). We detected the variable form CD44v only in DIPG samples (**Figure 31A**). Using flow cytometry, we found that DIPG primary cell cultures expressed CD44 in at least 77% of cells, with the exception of one model (DIPG-011), which was below 5% (**Figure 31B**).

Because the variants of CD44 stabilize xCT (SLC7A1), which results in a higher antioxidant activity in the tumor cell, we next verified, through immunoblotting, that xCT protein was present in the primary pHGG cultures (**Figure 31C**). Using immunofluorescence, we stained xCT in the cancer cells in culture (**Figure 31D**).
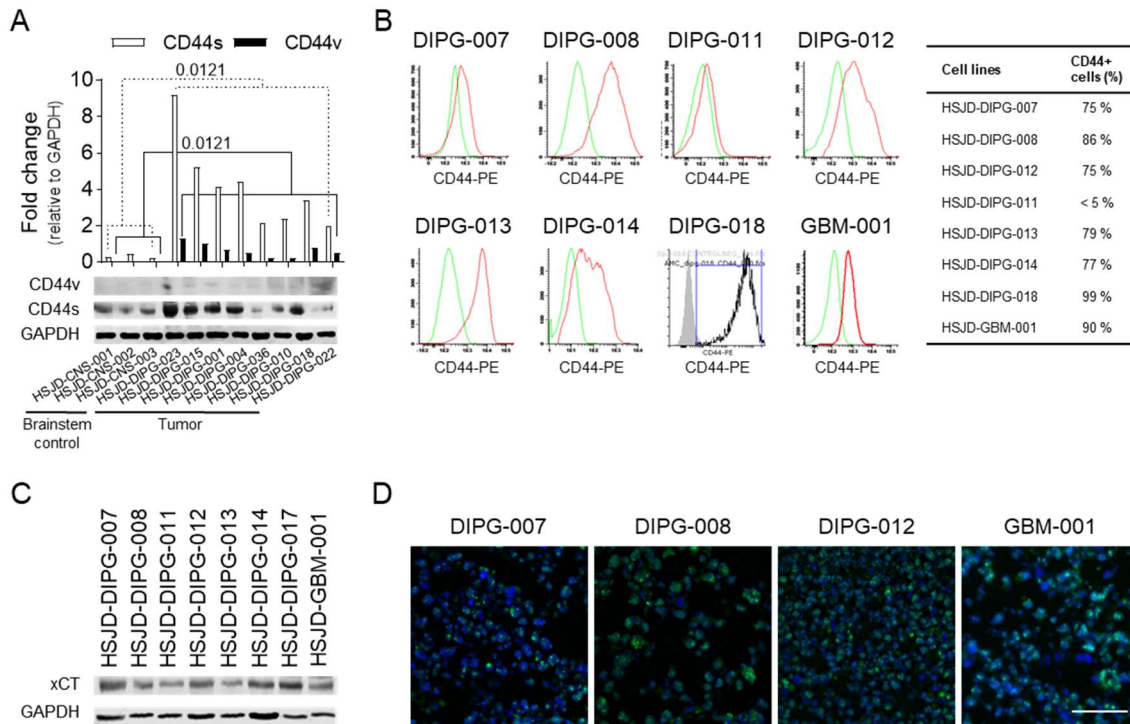
Figure 31. CD44 and xCT protein expression in pHGG. (A) Immunoblotting of CD44s (85 kDa) and CD44v protein (120kDa) in brainstem and pHGG necropsies. (B) Representative flow cytometry analysis of CD44 expression in primary pHGG cell cultures. (C) Immunoblotting of xCT in primary pHGG cultures. (D) Immunofluorescence images of xCT (green) in pHGG tumorspheres. DAPI is stained in blue. The scale bar is 50 µm.

To determine the relative expression of *CD44v* forms in pHGG, we used RT-qPCR with primer pairs for variants v2 to v10. For tumor tissue samples, the values were referenced to those obtained in samples of healthy brainstem. We observed an increased expression of *CD44s* mRNA confirming the western blot results, and *CD44v5* was the *CD44v* isoform with the highest median expression among the pHGG tumor samples (**Figure 32A**). In primary pHGG cultures (in vitro models) the results were similar (**Figure 32A**).

mRNA expression of *SLC7A11* was positive in all the primary pHGG cells, in comparison with HEK cells, used as a positive control (**Figure 32B**). pHGG

tissues obtained from autopsies had higher *SLC7A11* expression, than the normal control brainstem tissue (**Figure 32B**).
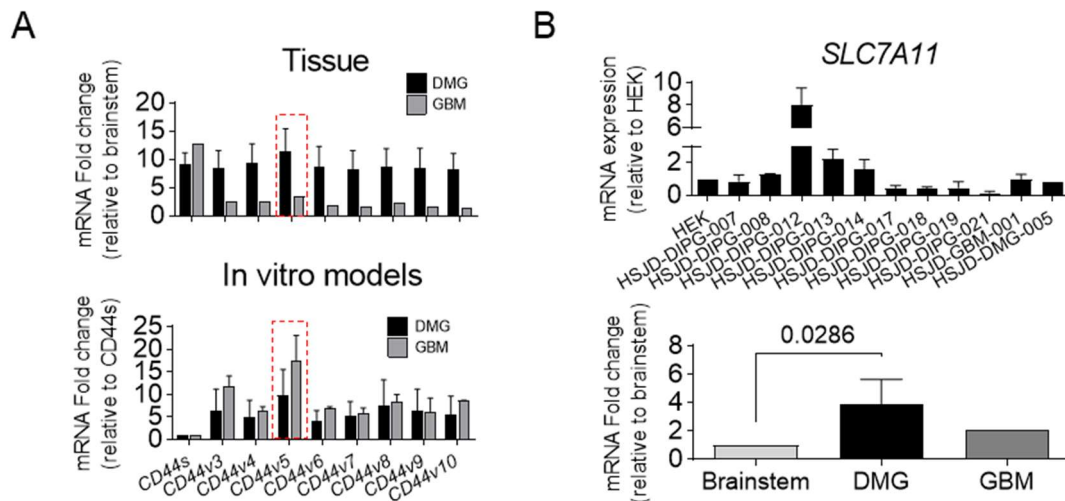
Figure 32. CD44 and xCT mRNA expression in pHGG. (A) mRNA expression of *CD44s* and *CD44v(2-10)* in pHGG tissue (8 DMG and 1 non-DMG, "GBM" in the legend) relative to healthy brainstem (n = 3), and pHGG primary cell cultures (6 DMG and 2 non-DMG, "GBM" in the legend), relative to paired expression levels of *CD44s* in the samples. (B) mRNA expression of *SLC7A11* in primary pHGG models (n = 11, referenced to the expression in HEK cells) and in pHGG necropsies (5 DMG and 1 non-DMD, "GBM") in comparison to brainstem control tissue (n = 4). All data are expressed as means and standard deviation (when possible).

Sorafenib induces antiproliferative effects and intracellular ROS accumulation

The interaction of osteopontin with the receptor CD44 is suitable to inhibition by anti-CD44 antibodies and other mechanisms (**Table 4**). However, we did not consider these CD44 inhibitors for our work, because some previous studies failed, due to their secondary effects, insufficient efficacy and their association to dysregulation of inflammatory processes[221,222]. Therefore, we aimed to select an inhibitor of xCT, preferably one already approved by the FDA and able to cross the BBB. Sorafenib was one of the few drugs that fulfilled these properties. To

assess the antiproliferative effect of sorafenib on pHGG in vitro, we plated DIPG-007, DMG-005 and GBM-001 cells in 96-well plates and analyzed their viability 48 h after adding sorafenib (**Figure 33A**). Cells were moderately sensitive to the drug, with concentrations inhibiting cell proliferation by half (i.e., IC50) in the low micromolar range (IC50$_{DIPG-007}$ = 3.6 μM, IC50$_{DMG-005}$ = 2.5 μM, IC50$_{GBM-001}$ = 1.5 μM). These values were comparable to those previously calculated for adult glioblastoma cell lines[198]. Because sorafenib is a well-known anti-angiogenic drug, we also studied the IC50 of hCMEC/D3 cells, which was 8.7 μM (**Figure 33A**).

To address the intracellular accumulation of ROS due to the inhibition of the xCT complex, we exposed pHGG cells to sorafenib 3 μM during a 6 h period. We observed that sorafenib treatment significantly increased cellular ROS generation in comparison with non-treated cells (**Figure 33B**).

Effect of sorafenib on the PI3K/Akt pathway, cell cycle and apoptosis markers in vitro

PI3K signaling can be activated by several receptors in the tumor cells, and one of them is CD44 (**Figure 16**)[223]. Thus, we assessed whether sorafenib altered the PI3K/Akt signaling cascade. We found that sorafenib did not induce clear effects on the expression of upper components of the pathway, such as PI3K (**Figure 33C**). Treatment clearly inhibited central components of the pathway, phospho-Akt and phospho-S6, in one of the three studied cell models, GBM-001, but no in the other two, DIPG-007 and DMG-005 (**Figure 33C**). At the highest drug concentration (12 µM), the cell cycle protein cyclin D1 decreased and cleaved caspase 3 increased in all cells, as signs of cell cycle arrest and apoptosis,

respectively (**Figure 33C**). Overall, these results suggest that sorafenib is effective promoting the activation of cell cycle arrest and apoptosis in all three models. However, the lack of inhibition of the PI3K pathway in the two DMG models, may result in drug resistance in the long-term.
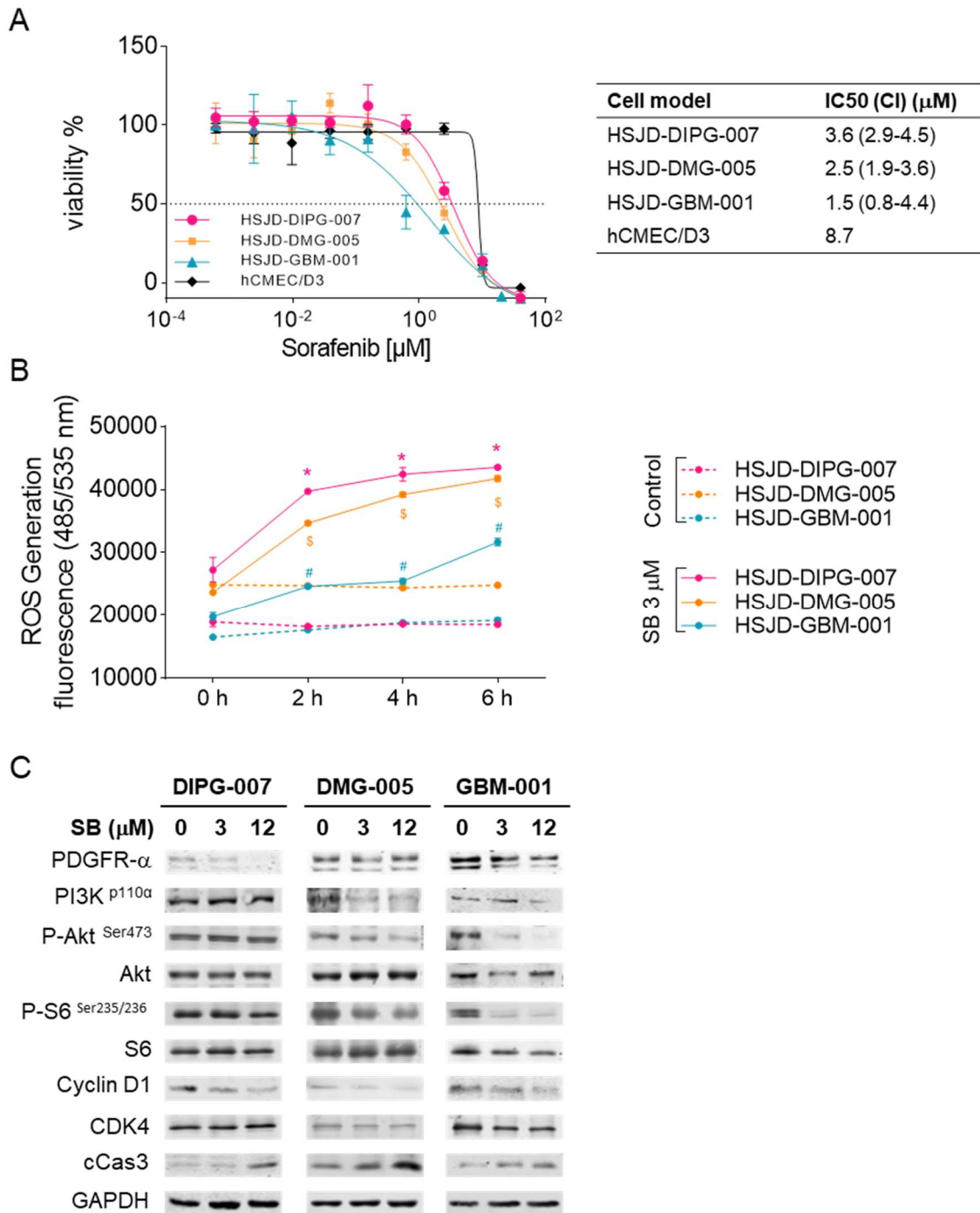
Figure 33. Effect of sorafenib on cell viability, intracellular ROS accumulation and the PI3K pathway in vitro. (A) Concentration-dependent cytotoxicity of sorafenib in DIPG-007, DMG-005, GBM-001 and hCMEC/D3. Dots are means of six replicates. (B) Intracellular ROS activity in DIPG-007, DMG-005 and GBM-001 treated with sorafenib 3 μM. (C) Immunoblotting of PI3K-related proteins, cell cycle regulator proteins (CDK4 and Cyclin D1) and apoptosis-related proteins (cCas3) of DIPG-007, DMG-005 and GBM-001 untreated and treated with sorafenib 3 and 12 μM.

Sorafenib inhibits cell migration in vitro

Through kinase inhibition, sorafenib may block essential processes in the tumor necessary for its expansion, such as tumor cell migration. To address this, first we studied whether treatment with sorafenib 3 µM changed the expression of metalloproteinases MMP-2 and MMP-9 in pHGG cells. We did not detect basal expression or changes for MMP-2, while we observed evident expression of MMP-9, with clear enzymatic activity in the zymogram, and both expression and activity decreased after sorafenib treatment (**Figure 34A** and **B**).

In the wound-healing assay we discovered that sorafenib 3 µM treatment for 24 h inhibited significantly the closure of the scratched area in all the studied pHGG models (**Figure 34C**).
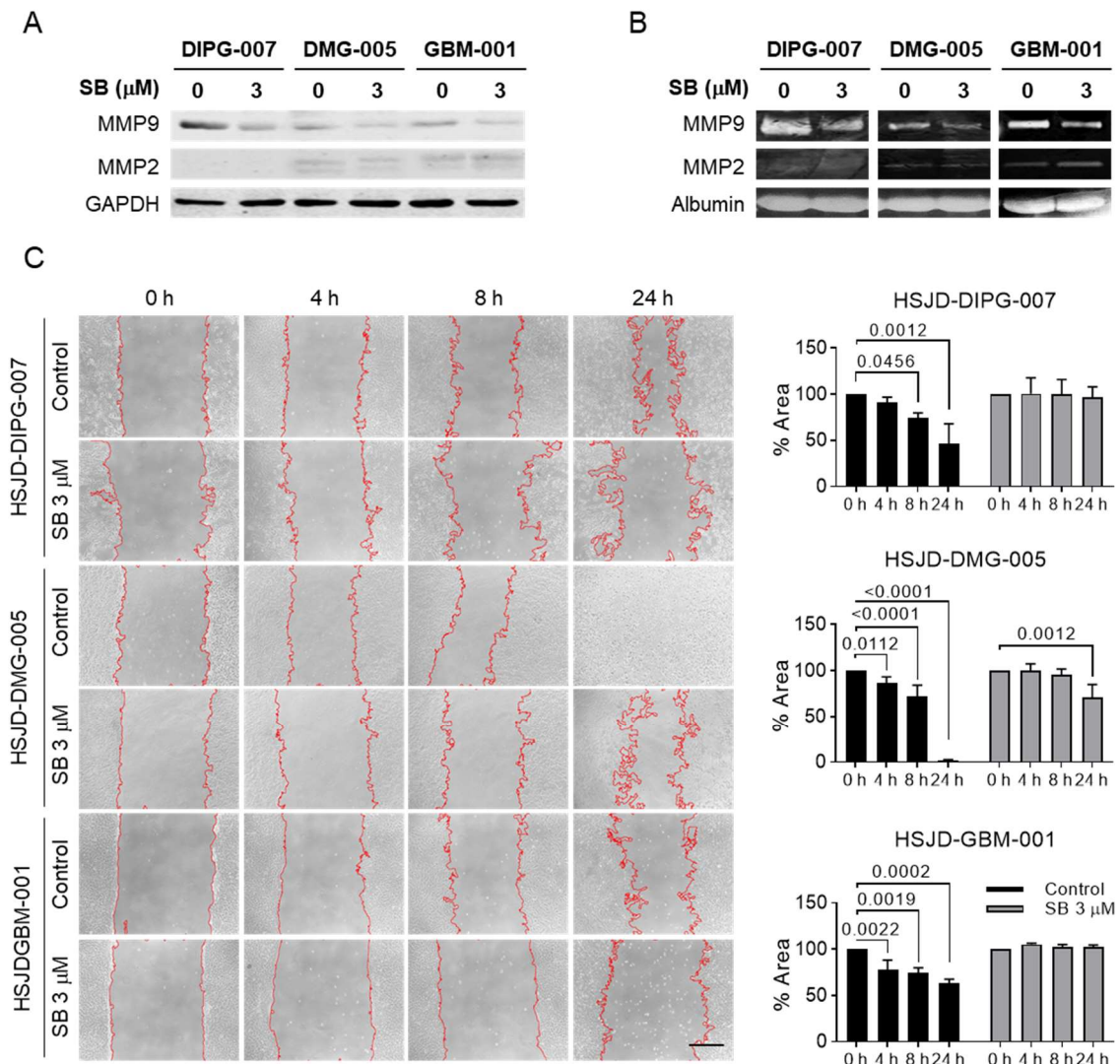
Figure 34. Effect of sorafenib on invasion and migration properties of pHGG. (A) Immunoblotting of MMP-9 and MMP-2 of DIPG-007, DMG-005 and GBM-001 untreated and treated with sorafenib 3 µM. (B) Activity of MMP-2 and MMP-9 by gelatin zymography of DIPG-007, DMG-005 and GBM-001 untreated and treated with sorafenib 3 µM. (C) Wound healing assay of DIPG-007, DMG-005 and GBM-001 untreated and treated with sorafenib 3 µM. Pictures were obtained at times 0, 4, 8 and 24 h. The scale is 200 µm.

Sorafenib inhibits vascular formation in vitro

Sorafenib has been associated to anti-angiogenic properties due to the inhibition of tyrosine-kinase receptors such as VEGFR or PDGFR, found in endothelial cells. The effect of sorafenib on the brain endothelial cells hCMEC/D3 has not been studied before. Because of our previous finding of DIPG secretomes

promoting vascular structures in hCMEC/D3 (**Figure 26**), we tested whether sorafenib reverted such effects. In the new assay we found that, as expected, hCMEC/D3 cells exposed to DIPG-007, DMG-005 and GBM-001 supernatants formed tube networks of higher complexity than those formed after culturing the cells in endothelial or pHGG culture media. However, this structures were not visible when cells were treated with sorafenib 3 µM (**Figure 35A** and **B**).
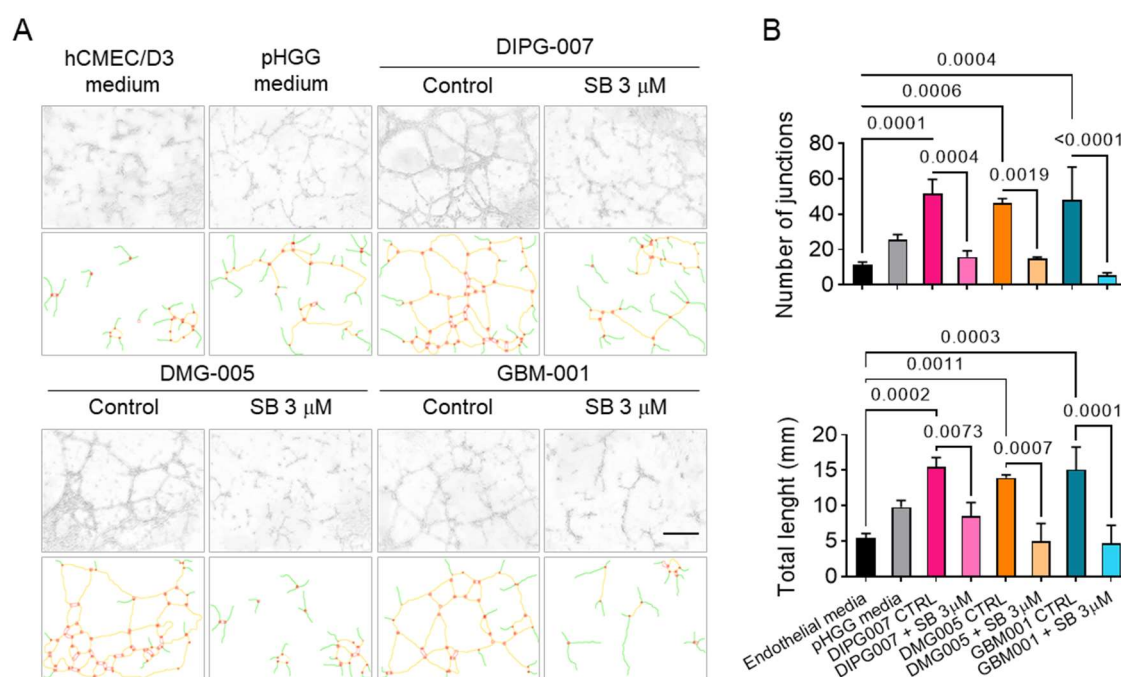
Figure 35. Effect of sorafenib on endothelial tube formation in vitro. (A) Representative images of tube formation assay of hCMEC/D3 cells exposed to fresh culture media, DIPG-conditioned media and DIPG-conditioned media supplemented with sorafenib 3 µM. (B) Tube formation assay quantification using total tubule length and number of junctions to determine net complexity.

Sorafenib exerts anti-tumor activity in pHGG

We treated with daily oral sorafenib mice with intracranial DIPG-007 and GBM-001 xenografts, following the scheme of **Figure 36A**. In DIPG-007, we started treatments at day 25 post-inoculation, and in GBM-001 (a very aggressive tumor

with a median survival of around 30 days), we started treatments at day 11 post-inoculation. In this model, we observed that sorafenib significantly increased median survival of the mice, from 33 days in controls, to 73 days in treated mice (**Figure 36B**). Such a difference in the survival of both groups was surprising, being this model very resistant to other treatments, such as irinotecan (data not shown). We harvested samples from three mice at day 29 and we found that non-treated animals had extensive tumor infiltration in the brain parenchyma, while the treated group conserved a healthy histology (**Figure 36B**). In contrast, in the animals with DIPG-007, we did not detect a therapeutic benefit in terms of animal survival following sorafenib treatment (**Figure 36**C). There were no differences in cancer cell infiltration in brains of DIPG-007 bearing mice at the end-of-treatment (day 43 post-inoculation) between control and treated mice (**Figure 36C**). We performed an immunostaining of CD31 in the harvested brains to study the anti-angiogenic capacity of sorafenib in vivo. In GBM-001 xenografts, we detected the expected pattern of CD31+ brain vasculature in the sorafenib-treated group, in which the infiltration of cancer cells was absent. In contrast, CD31+ staining was more intense in the areas of tumor infiltration in the brain of control animals, and stained vessels of aberrant morphology, characterized by an enlargement of the structures, with tortuous appearance and uneven vessel diameters (**Figure 36D**). The same study was performed in the tumor-infiltrated brains of the mice inoculated with DIPG-007 cells and, in both groups, we detected a similar extension of CD31+ blood vessels, although slightly sparser in the treated brains (**Figure 36D**).
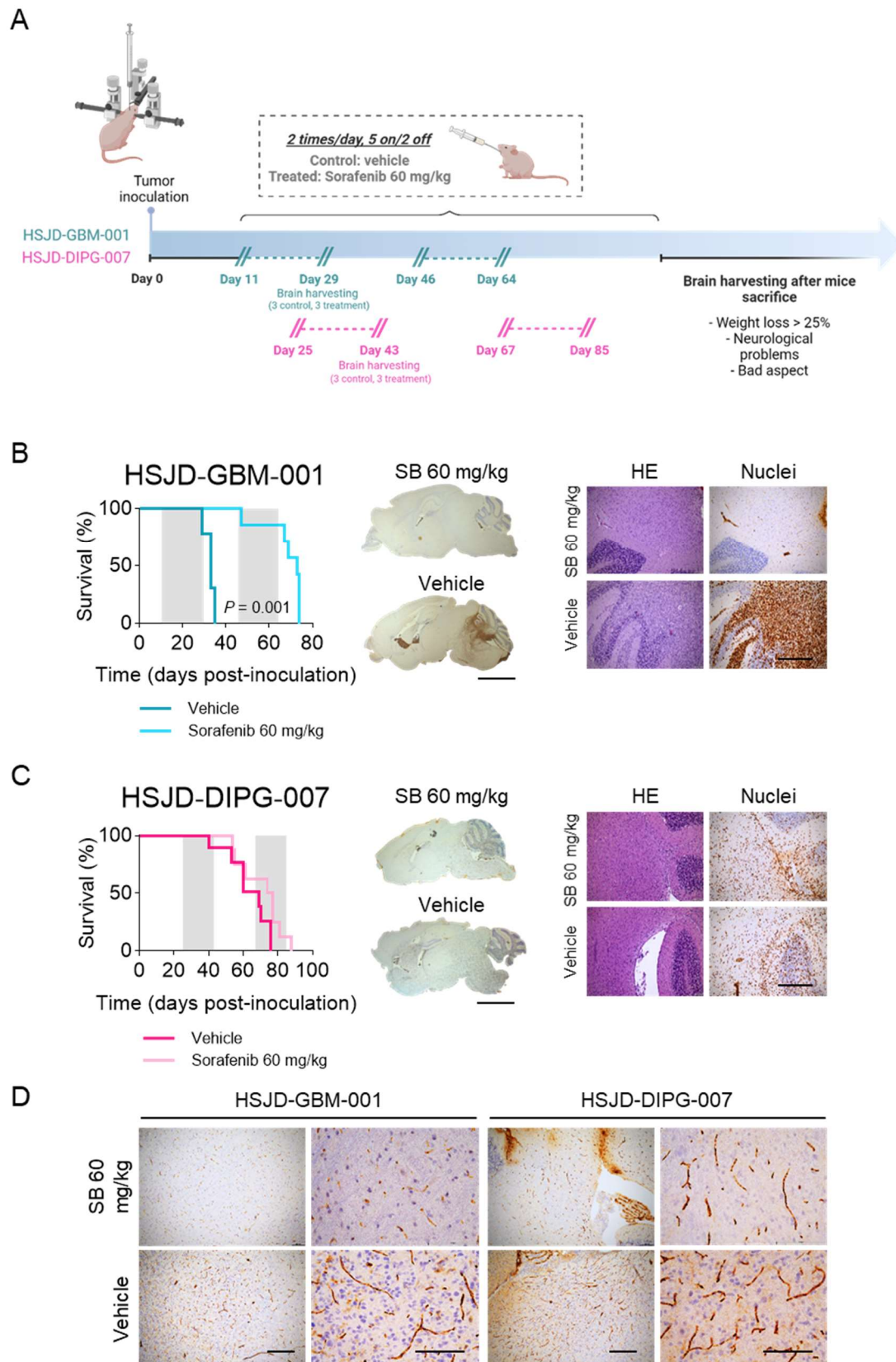
Figure 36. Effects of sorafenib in vivo. (A) Sorafenib treatment planning for DIPG-007 and GBM-001. (B) Survival of mice bearing intracranial GBM-001, untreated or treated with sorafenib 60 mg/kg. Anti-human nuclei IHC of whole brains harvested at the end of the first round of

treatment (day 29 post-inoculation). The scale is 50 μm. HE and anti-human nuclei IHC of brains harvested at day 29 post-inoculation. The scale is 400 μm. (C) Survival of mice bearing intracranial DIPG-007 untreated or treated with sorafenib 60 mg/kg. Anti-human nuclei IHC of whole brains harvested at the end of the first round of treatment (day 43 post-inoculation). The scale is 50 μm. HE and anti-human nuclei IHC of brains harvested at day 43 post-inoculation. The scale is 400 μm. (D) CD31 staining of GBM-001 and DIPG-007 brains harvested at days 29 and 43 post-inoculation, respectively. The scales are 200 μm and 150 μm.

DIPG-007 shows sorafenib resistance signs in vitro that can be reverted with a PI3K inhibitor

We observed that longer in vitro exposures (up to 7 days) of cells to sorafenib increased the antiproliferative activity against GBM-001 cells, but did not change the results on DIPG-007 cells (**Figure 37A**). Then, we addressed whether a known mutation (H1047R) in the gene *PIK3CA* in DIPG-007 may explain drug resistance to sorafenib, as observed in other cancers, which showed diminished response to anticancer drugs due to the overactivation of PI3K pathway[224-226]. Both GBM-001 and DIPG-007 cells were sensitive to the PIK3CA inhibitor inavolisib, in the low nanomolar range (**Figure 37B**). In DIPG-007 cells, inavolisib inhibited the phosphorylation of Akt and S6, showing the same results in combination with sorafenib (Figure 37**C**). The combination of both drugs clearly increased the apoptosis-related proteins cCas3 and Bax and reduced cyclin D1 in DIPG-007, suggesting inavolisib could help overcome the resistance of these cells to sorafenib (**Figure 37C**). In GBM-001 cells, we observed similar changes in protein expression following treatments with inavolisib, sorafenib, or the combination of both (**Figure 37D**), suggesting that the combination of both agents would not result in more-than-additive effects.

Inavolisib and sorafenib have a synergistic effect on DIPG-007 in vitro

We treated both cell models with selected concentrations of both drugs, separately or in combination, and we calculated the combination index (CI) score. The values of CI > 1, CI = 1, and CI < 1 were defined as antagonistic, additive, and synergistic, respectively. Concentrations in the low nanomolar range of sorafenib and inavolisib exhibited a slight synergistic effect, with CI < 1 (**Figure 37E**). In contrast, higher concentrations of both drugs, in the micromolar range, presented an antagonistic effect, especially in DIPG-007 cells (**Figure 37E**).
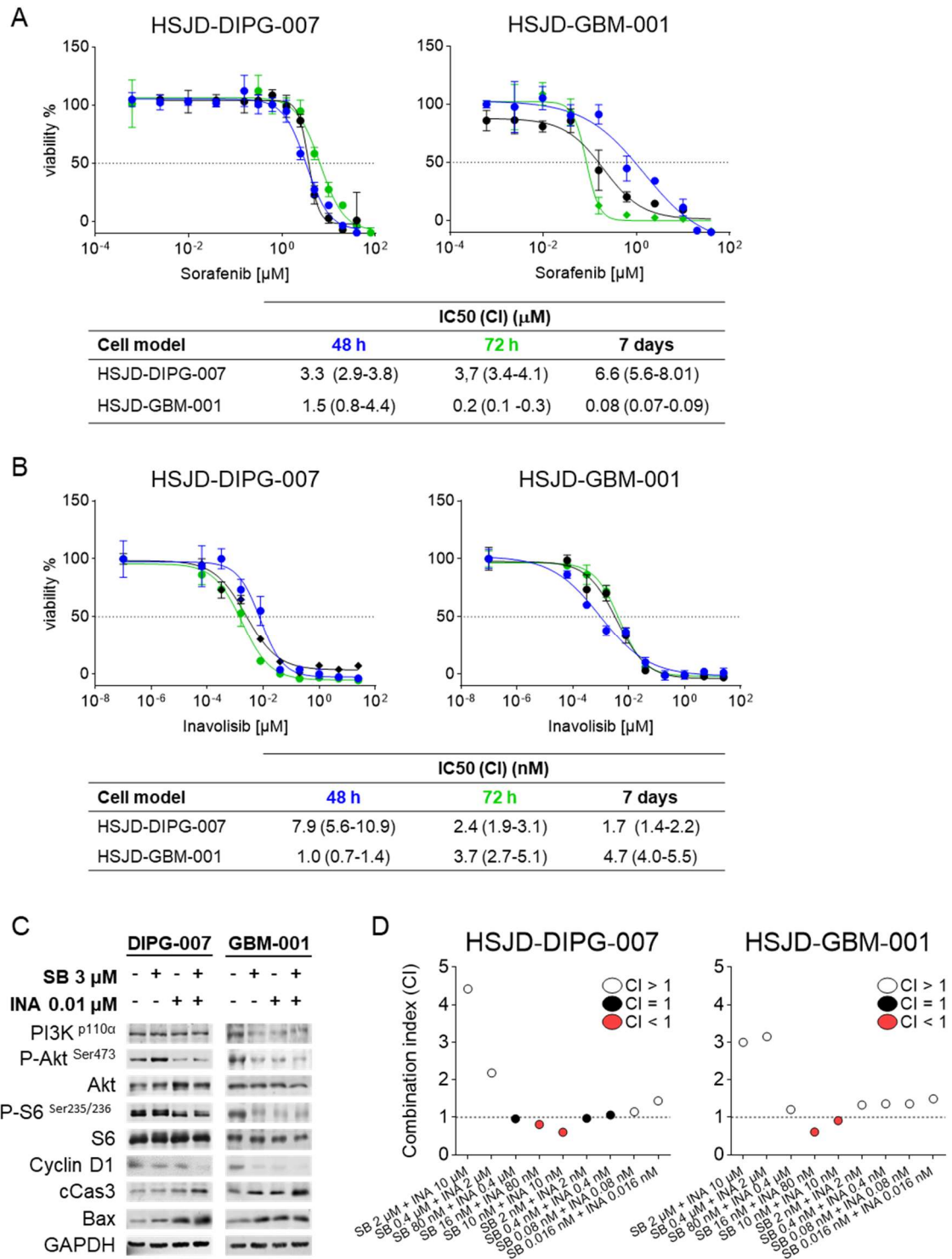
Figure 37. Effects of the combination of sorafenib and inavolisib in vitro. (A) Concentration-dependent cytotoxicity of sorafenib in DIPG-007, DMG-005, GBM-001 at 48 h, 72 h and 7 days. Dots are means of six replicates. (B) Concentration-dependent cytotoxicity of inavolisib in DIPG-007, DMG-005, GBM-001 at 48 h, 72 h and 7 days. Dots are means of six replicates. (C) Immunoblotting of PI3K-related proteins, cell cycle regulator proteins (CDK4 and Cyclin D1) and apoptosis-related proteins (cCas3) of DIPG-007, DMG-005 and GBM-001 untreated and treated

with sorafenib 3 and inavolisib 0.01 nM. (D) Combination index (CI) for sorafenib and inavolisib combination in DIPG-007 and GBM-001. CI > 1 is an antagonistic interaction, CI = 1 indicates additive drug interaction, and CI < 1 is considered a synergistic drug interaction.

DISCUSSION

Work included in this PhD thesis demonstrates that DIPG cells secrete soluble factors that induce changes in the surrounding stroma cells, leading to a favorable microenvironment for tumor expansion and growth (**Figure 38**). It is well known that cancers evade the immune response through the infiltration of anti-inflammatory cells[227], the disruption of the extracellular matrix and the promotion of aberrant neovascularization processes[67].
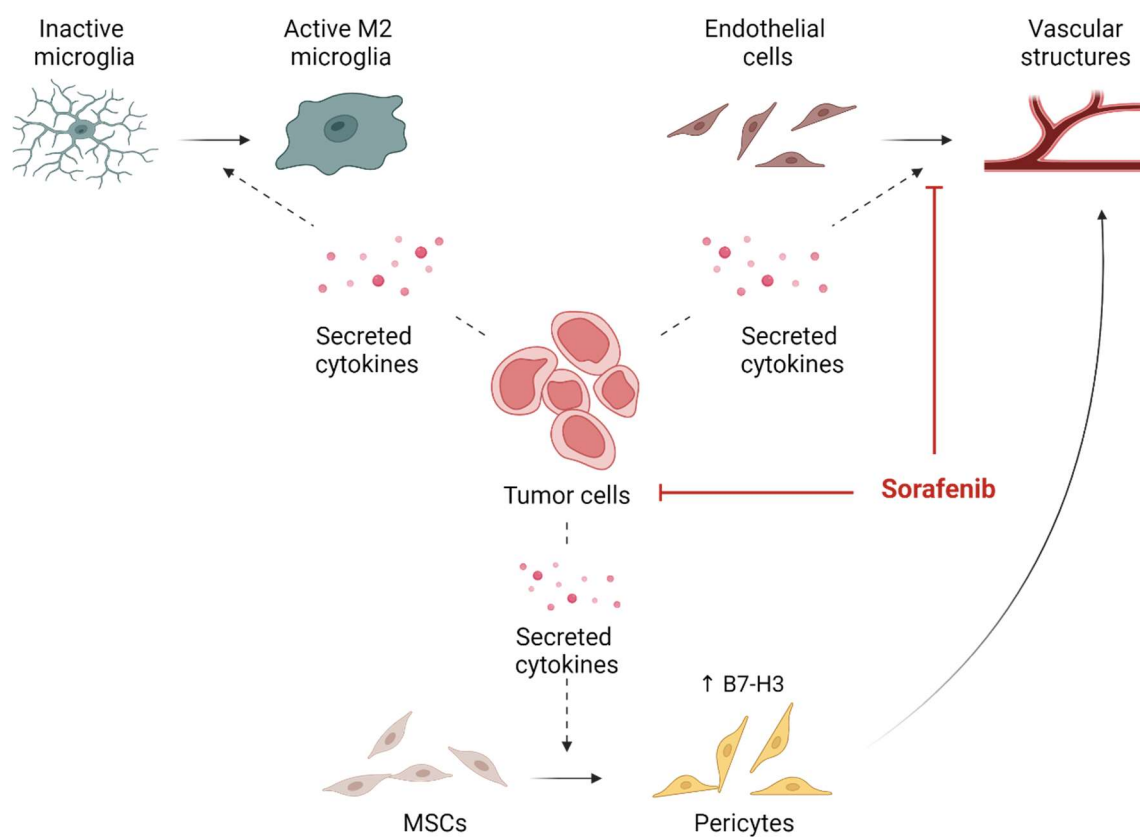
Figure 38. Graphical abstract. Through the secretion of immunosuppressive cytokines, tumor cells modify the nature of different microenvironment components. Sorafenib is able to revert some of these effects by reducing the angiogenic process in DIPG, and also directly killing the tumor cells.

Our study in human paraffin samples broadens previous knowledge, detecting a sparse presence and even absence of T and B cells infiltrating the tumor, in agreement with the previous classification of DIPG as a cold tumor[72,73]. Our finding of a very significant increase of M2-like activated microglia (CD163^{+}, Iba1^{+}) in DIPG is not in total agreement with previous reports in which CD163^{+} staining was considered not significantly higher than in control samples. In such studies, staining was compared between the tumor tissue and apparently normal adjacent tissue obtained from surgical resection[72]. We suggest that, even though the control sections were not infiltrated by tumor cells, they were probably indirectly affected by the surrounding tumor secretions. In our study, the inclusion of nontumor brainstem samples as controls allowed us to have a comparable sample obtained from the exact anatomical location in which DIPG arises, but without tumor activity or inflammation. Such control samples were almost totally devoid of CD163^{+} cells, in stark contrast to brainstem tumors.

The main contribution of our work is the functional characterization of the immunosuppressive secretome of DIPG cells and the identification of at least two proteins in such secretome. CHI3L1 is overexpressed in many cancers such as breast cancer[163], and related to worse prognosis, macrophage recruitment and angiogenesis[228]. Osteopontin has also been previously associated with cancer, metastatic processes[137,229] and immunosuppression, regulating the M2 polarization[128]. Both are secreted to the microenvironment, enabling tumor cells to interact with the surrounding components of the tumor. Our experiments confirm their powerful capacity to induce neovascularization and direct M2 macrophage polarization and migration, suggesting they intervene in a potential mechanism for the creation of an immunosuppressive niche in DIPG.

The fact that our study did not detect the main immune checkpoint molecules (PD-L1 and CTLA-4) in the patient samples (biopsies and autopsies), underscores that the niche of DIPG is highly immunosuppressive and cancer cells did not receive previous stimulation from T cells, as previous studies reported in patient samples[72]. Our experiments in vitro showed that, in the presence of an artificial inflammatory environment, such cells expressed high amounts of PD-L1 and CTLA-4, suggesting that the capacity of their machinery to induce checkpoint expression was intact, but the environment did not trigger such machinery. This has been previously observed for cultured cells of retinoblastoma[230] and non-small cell lung cancer[231]. Our finding that B7-H3 expression is high in DIPG was expected, as published by Zhou et al[232]. Our study contributes to describe different patterns of B7-H3 location in the cancer and stroma cells, which were not described before for pHGG[232]. B7-H3 is a molecule of the B7 family classified as an immune checkpoint molecule[99,233] and expressed in many cancers[234]. Although it was initially defined as pro-inflammatory, its inhibitory effect towards T cell proliferation has also been described, as B7-H3 inhibits the proliferation of $CD8^+$ and $CD4^+$ T cells[100] and the dendritic cell stimulatory capacity of T cell and production of IL-2 and IFN-γ[235]. B7-H3 has also been associated to macrophage recruitment[236] and M2 polarization[237]. Our findings are in agreement with studies describing the presence of B7-H3 in the tumor-associated vasculature, suggesting an important role in the neovascularization process[238], which is a very important mechanism used by tumors to expand and to recruit other cells to the niche[239]. Our results agree with previous studies, which determined the overexpression of B7-H3 in the membrane of DIPG cells and also expressed in the walls of the blood vessels in the tumor[232]. The fact that DIPG secretomes

increased the expression of B7-H3 and the early pericyte marker NG2 in MSCs in vitro suggests that this cancer contributes to the differentiation of MSCs to pericytes, necessary for the stabilization of vascular structures. This observation implies there is an active crosstalk between MSCs and DIPG microenvironment, involving the expression of B7-H3 for the creation of an immunosuppressed environment in the tumor. Moreover, we have been able to demonstrate the capacity of DIPG supernatants, osteopontin and CHI3L1 to induce not only the organization of endothelial cells into 2D tubular structures but also the positioning of pericyte–differentiated cells around them, basic for the establishment and stabilization of the basic histological capillary structure[240]. This finding, previously used to describe the implication of various molecules in the initial steps of the angiogenic process[241,242] suggests a critical role of the DIPG secretome in the creation of endothelial networks and in their stabilization by stimulating the differentiation of MSCs into pericytes.

Our finding of increased expression of BBB proteins in endothelial cells following exposure to the DIPG secretome is especially intriguing. Previous experimental attempts to address these questions used endothelial cells derived from CD34^{+} hematopoietic stem cells isolated from human umbilical cord blood, and reported minor changes in gene expression of *ABCG2* (BCRP) following exposure to the secretome of DIPG[243]. In contrast, our study found up to 250-fold increase in BCRP, and an increase in more than 40 angiogenic-related genes. The difference between our study and the previous one could be due to the use of different types of endothelial cells, because we used a brain microvascular cell line.

We expected that DMG and GBM xenografts grown in subcutaneous location in mice would not have vessels with BBB properties, because blood vessels would be recruited from the mouse. However, we demonstrated the expression of BCRP in pHGG xenografts engrafted subcutaneously in mice, which was not observed in subcutaneous tumors corresponding to non-brain cancers. To our knowledge, this finding is unique in the literature and suggests the capacity of the glioma cells to induce its own vasculature, creating an optimal microenvironment for tumor growth. This finding does not mean that the BBB is fully established in the DMG subcutaneous xenografts, because other factors such as the interstitial pressure, or the general anatomy of the vessels, might not have been reproduced in the subcutaneous setting.

The analysis of CHI3L1 or osteopontin in patient liquid biopsies (CSF and plasma) might be clinically useful to follow-up disease evolution and response to treatment. There are published studies on brain tumors[244], other cancers[245] and neurological pathologies[246] on the analysis of circulating DNA and RNA, cytokines, circulating tumor cells, extracellular vesicles or tumor-associated microparticles in the patient CSF and plasma. These analyses can be used for more precise diagnosis, prognosis, or follow-up of the disease, or even prediction of treatment responses. CHI3L1 and osteopontin have been previously described as potential inflammatory biomarkers in CSF and serum in other CNS-related diseases such as CNS lymphoma[149], histiocytosis[247] and multiple sclerosis[171,248]. In brain tumors and other cancers, the overexpression of these cytokines might represent a strategy used by the tumor to immunomodulate its environment and promote its own growth. The expression and secretion of the same cytokines in the CNS and bloodstream in other inflammatory and pathological entities seems

to be indicative of nervous tissue damage and related to the activity of resident cells in the CNS to control the inflammation produced by the disease itself and, consequently, an increased concentration could be related to disease progression[249]. It is thus coherent that tumor cells reproduce the same immunosuppressive situation that is physiologically used to maintain the immunoprivileged state of the CNS. Our study confirms a significant overexpression of osteopontin and CHI3L1 in CSF and serum of DIPG patients. Whether these proteins could be used as biomarkers for DIPG progression needs to be assessed in prospective work, which should be designed to determine the optimal cut-off points to discern positive and negative results.

Part of my work aimed to evaluate a new therapeutic approach targeting the interaction between the secreted cytokines and their suitable receptors (CD44) in the microenvironment of the disease. Overexpression of CD44s has been previously related to cancer signatures and tumor progression[177-180]. The variants of CD44, only expressed in cancer, receive the nomenclature CD44v1-v10 depending on the alternative splicing site by which they incorporate the genomic exons 6-15. Hyaluronic acid, one of the main components of the ECM, is the principal ligand of CD44, but this receptor also binds to other ECM-related and unrelated components[176], such as the DIPG-secreted proteins of interest osteopontin[183] and chitinase 3-like 1[168]. Thus, we focused our studies in a CD44v-related therapy. CD44v interacts with a protein named xCT, which is the light-chain subunit (*SLC7A11*) of the x_c^- cysteine/glutamate antiporter system, a transmembrane protein responsible for the exchange of intracellular glutamate and extracellular cysteine. This transporter regulates the accumulation of ROS inside the cells, usually as a result of the action of chemotherapeutic agents and

other anti-tumoral approaches, by the synthesis of intracellular glutathione (GSH). Expression of xCT has been widely associated to tumor growth, progression and chemoresistance. Inhibition of this antiporter has demonstrated antitumor activity in glioblastoma, melanoma and prostate cancer[191]. The variants of CD44 are responsible for x_c^- system stabilization, which entails a higher antioxidant activity in the tumor cell, making this molecule a candidate target for our studies. Because of the tumor-specific expression of xCT and its importance in the stabilization of CD44, we proposed that targeting this channel in DIPG could be a new therapeutic approach. To inhibit this antiporter, we aimed to test the efficacy of a previously-approved drug by the FDA which was also capable of crossing the BBB. Sorafenib is a bi-aryl urea and an oral multikinase inhibitor. It was first approved by the FDA and the EMA in 2007 for the treatment of hepatocellular carcinoma[131], and it is also indicated to treat renal carcinoma[231] and differentiated thyroid carcinoma[194]. It blocks the action of cell surface tyrosine kinase receptors and downstream intracellular kinases that are implicated in tumor cell proliferation, tumor angiogenesis and cell invasion[193], such as B-raf, RAF, VEGF 1/2/3, FLT3, PDGFR α/β and FGF. The administration of this drug, alone or in combination with other chemotherapeutics has shown promising effects in other malignancies[196,198,250-253], due to its capacity for blocking the x_c^- cysteine/glutamate antiporter system by which cancer cells reduce the accumulation of intracellular ROS and, consequently, become drug resistant. Because of these properties, we tested the effectivity of this drug in three pHGG cell models. All of them were responsive to the drug administration in vitro, with comparable IC50 between them, increased intracellular ROS

accumulation, increased apoptosis, and reduced cell cycle proteins, confirming cytotoxic efficiency in primary cell cultures.

Mechanistically, sorafenib has also been related to the reduction of VEGF and PDGF production by some tumors, and also to the inhibition their respective receptors (VEGFR and PDGFR, respectively), associated to pro-tumoral processes such as angiogenesis, and cell migration and invasion[201]. In previous microenvironment studies, we were able to demonstrate the capacity of pHGG supernatants, as well as osteopontin and CHI3L1, to induce angiogenesis in vitro. However, sorafenib reduced and even inhibited this effect in endothelial cells, supporting its previously-described antiangiogenic properties in other tumors.

Some of the pathways overactivated in DIPG lead to the expression and activation of metalloproteinases, which are responsible for the remodeling of the ECM, and the resultant tumor cells invasion of the surrounding healthy tissue[254]. MMP-9 is found at elevated levels in brain tumor tissues and indicates poor prognosis[255,256]. When we treated the pHGG cell models with this drug, we determined a reduction in the expression and activity of MMP-9, suggesting a role of sorafenib in hindering of the invasion capacity of tumor cells, which we validated by a wound-healing assay, where the treated tumoral cells were significantly unable to close the scratch in comparison with the non-treated malignant cells.

Importantly, it has been suggested the capacity of sorafenib to cross the blood-brain barrier, showing promising results in glioblastoma treatment in preclinical models[198]. In vivo, we observed striking differences in the anticancer efficacy of sorafenib in two pHGG models. Previous studies in hepatocellular carcinoma

reported acquired resistance to sorafenib due to PI3K activation[199,252,257]. Because the unresponsive xenograft (DIPG-007) presents a mutation in the gene *PIK3CA* (which encodes for PI3Kα) leading to an overstimulation of the PI3K pathway, we reasoned that targeting mutant PIK3CA could revert resistance to sorafenib. In the literature, combination of sorafenib with PI3K inhibitors LY294002[253,258] or copanlisib[252] reverted sorafenib resistance in *PIK3CA*-mutated models. Inavolisib (GDC-0077) is a potent, orally available, and selective PI3Kα inhibitor (by binding to the ATP binding site). Inavolisib is more selective for the mutant version of PI3Kα in breast cancer cells, and oral daily treatment of patient-derived *PIK3CA*-mutant breast cancer PDX induces tumor regressions[259]. Work of my laboratory mate Leire Balaguer shows that inavolisib crosses the blood-brain barrier in mice (unpublished data). Therefore, we studied the possibility to combine inavolisib and sorafenib for pHGG treatment, as it has also been described in preclinical studies[259], that led to Phase I clinical trials (NCT03006172). Our results are in agreement with studies that showed sorafenib increasing the efficacy of anti-tumoral treatments due to the inhibition of xCT and the consequent accumulation of intracellular ROS[260]. The fact that low concentrations of both drugs worked synergistically in pHGG cells suggests that they could be used as a therapeutic alternative in pHGG. The fact that there are two already commercialized and FDA-approved therapies endorses further developments, but in vivo preclinical studies should be completed to validate the in vitro results.

CONCLUSIONS

In this thesis, I analyzed a large cohort of samples obtained from patients with pHGG, most of them DIPG, including tissue samples, primary cell cultures, serum and CSF samples. I found that (i) DIPG tissues contain very few lymphocytes and abundant glial cells of the immunosuppressive type; (ii) DIPG cells secrete specific cytokines that interact with cellular components of the microenvironment promoting a pro-tumorigenic niche; (iii) DIPG cells express receptors for the secreted cytokines that are actionable with the clinically available anticancer molecule sorafenib.

Conclusions are grouped in the following three categories:

1. DIPG presents a cold immune microenvironment characterized by a low infiltrate of immune cells, high presence of protumoral microglia and low expression of immune checkpoints.

   a. The density of the T lymphocyte population (CD3+ cells) is low in the control brainstem samples and slightly higher in DIPG biopsies and necropsies.

   b. T helper (CD4+) cells are almost undetectable in control nontumor samples, while they are significantly more abundant in DIPG biopsies and necropsies.

   c. Tregs (FoxP3+) are not detectable in control brainstem samples, while they are significantly more abundant in the cancer biopsies.

   d. Microglia are the most abundant immune cells in DIPG, presented a more ramified shape in the control brainstem than in tumors and they are CD163+ in tumor samples, corresponding to a M2-like phenotype, anti-inflammatory.

e. Immune checkpoints PD-L1 and CTLA-4 are absent in all patient samples. Both increase significantly following the incubation of DIPG cells in pro-inflammatory conditions.

f. B7-H3 is expressed in all tumor samples, presenting three different expression patterns (perivascular, in cancer cells, or a mixed pattern), surrounded by CD163+ microglia and co-localizing with mesenchymal (CD90) and pericyte markers (PDGFRβ and NG2) in perivascular regions.

2. Osteopontin and chitinase-3-like 1 are two immunosuppressive cytokines found significantly increased in DIPG samples and contribute to create the immunosuppressed microenvironment in DIPG.

a. Osteopontin and chitinase 3-like 1 are homogenously overexpressed in DIPG tumor lysates, primary cultures, and serum and CSF from patients with DIPG.

b. Tumor secretomes, osteopontin and chitinase 3-like 1 induce the expression of B7-H3 in MSCs in vitro, as well as their differentiation to pericytes, characterized by an increase of NG2.

c. Tumor secretomes, osteopontin and chitinase 3-like 1 induce the angiogenic process in vitro by stimulating the expression of pro-angiogenic genes in endothelial cells, the formation of 2D networks and the wrapping of CD90+/NG2+ MSCs around them, mimicking vascular structures.

d. Tumor secretomes, osteopontin and chitinase 3-like 1 induce an increase in the expression of M2-associated growth factors and a down-regulation of the expression of M1-associated genes in

macrophages in vitro. They also increase their migratory capacity in vitro.

3. Targeting of the CD44-xCT system and other targets with sorafenib effectively inhibits tumor growth and angiogenesis in pHGG.

   a. DIPG and GBM significantly overexpress CD44s and exclusively express CD44v, being CD44v5 the most abundant isoform, both in cell models and tumor tissue.

   b. xCT expression, associated to CD44v, is significantly overexpressed in pHGG tissue samples in comparison to healthy brainstem, and it is expressed in all the analyzed pHGG cell models with variable levels.

   c. Sorafenib activity as inhibitor of the CD44-xCT system in pHGG was consistent with a significant sorafenib-induced intracellular ROS accumulation in pHGG cells in vitro. Other actions of sorafenib, such as the reduction of tumor cell migration, the induction of apoptosis and the reduction of cell cycle proteins could be the consequence of its action inhibiting several TKR in DIPG cells.

   d. Sorafenib does not induce endothelial cell death in vitro, but significantly reverts the neovascularization induced by culture media conditioned by pHGG cells in vitro.

   e. Sorafenib shows dissimilar in vivo activity in pHGG models, with very significant efficacy to increase survival of GBM-001 xenografts and no activity against DIPG-007 xenografts.

   f. The PIK3CA mutation in DIPG-007 may confer sorafenib-associated long-term resistance, due to the corresponding PI3K overactivation.

g. PI3K-induced resistance to sorafenib in vitro is at least partially reverted when administered in combination with the PI3K inhibitor inavolisib, with synergistic activity at low concentrations in PIK3CA-mutant cells.

REFERENCES

References

1.   Dean SJ, Farmer M. Pediatric cancer genetics. *Curr Opin Pediatr.* 2017; 29(6):629-633.

2.   Brodeur GM, Nichols KE, Plon SE, Schiffman JD, Malkin D. Pediatric Cancer Predisposition and Surveillance: An Overview, and a Tribute to Alfred G. Knudson Jr. *Clin Cancer Res.* 2017; 23(11):e1-e5.

3.   Mora J. What is a pediatric tumor? *Clinical Oncology in Adolescents and Young Adults.* 2012:7.

4.   Stoltze UK, Foss-Skiftesvik J, Hansen TVO, et al. The evolutionary impact of childhood cancer on the human gene pool. *Nat Commun.* 2024; 15(1):1881.

5.   Da-Veiga MA, Rogister B, Lombard A, Neirinckx V, Piette C. Glioma Stem Cells in Pediatric High-Grade Gliomas: From Current Knowledge to Future Perspectives. *Cancers (Basel).* 2022; 14(9).

6.   Steliarova-Foucher E, Colombet M, Ries LAG, et al. International incidence of childhood cancer, 2001-10: a population-based registry study. *Lancet Oncol.* 2017; 18(6):719-731.

7.   Aggarwal P, Luo W, Pehlivan KC, et al. Pediatric versus adult high grade glioma: Immunotherapeutic and genomic considerations. *Front Immunol.* 2022; 13:1038096.

8.   Louis DN, Perry A, Wesseling P, et al. The 2021 WHO Classification of Tumors of the Central Nervous System: a summary. *Neuro Oncol.* 2021; 23(8):1231-1251.

9.   Gianno F, Giovannoni I, Cafferata B, et al. Paediatric-type diffuse high-grade gliomas in the 5th CNS WHO Classification. *Pathologica.* 2022; 114(6):422-435.

10.   Warren KE. Diffuse intrinsic pontine glioma: poised for progress. *Front Oncol.* 2012; 2:205.

11.   Bailey S, Howman A, Wheatley K, et al. Diffuse intrinsic pontine glioma treated with prolonged temozolomide and radiotherapy--results of a United Kingdom phase II trial (CNS 2007 04). *Eur J Cancer.* 2013; 49(18):3856-3862.

12.   Srikanthan D, Taccone MS, Van Ommeren R, Ishida J, Krumholtz SL, Rutka JT. Diffuse intrinsic pontine glioma: current insights and future directions. *Chin Neurosurg J.* 2021; 7(1):6.

13.   Puget S, Beccaria K, Blauwblomme T, et al. Biopsy in a series of 130 pediatric diffuse intrinsic Pontine gliomas. *Childs Nerv Syst.* 2015; 31(10):1773-1780.

14.   Puget S, Blauwblomme T, Grill J. Is biopsy safe in children with newly diagnosed diffuse intrinsic pontine glioma? *Am Soc Clin Oncol Educ Book.* 2012:629-633.

15.   Jones C, Baker SJ. Unique genetic and epigenetic mechanisms driving paediatric diffuse high-grade glioma. *Nat Rev Cancer.* 2014; 14(10).

16.   Cantone I, Fisher AG. Epigenetic programming and reprogramming during development. *Nat Struct Mol Biol.* 2013; 20(3):282-289.

17.   Skene PJ, Henikoff S. Histone variants in pluripotency and disease. *Development.* 2013; 140(12):2513-2524.

18.   Wu G, Diaz AK, Paugh BS, et al. The genomic landscape of diffuse intrinsic pontine glioma and pediatric non-brainstem high-grade glioma. *Nat Genet.* 2014; 46(5):444-450.

19.   Castel D, Philippe C, Calmon R, et al. Histone H3F3A and HIST1H3B K27M mutations define two subgroups of diffuse intrinsic pontine gliomas with different prognosis and phenotypes. *Acta Neuropathol.* 2015; 130(6):815-827.

20.   Jones C, Karajannis MA, Jones DTW, et al. Pediatric high-grade glioma: biologically and clinically in need of new thinking. *Neuro Oncol.* 2017; 19(2):153-161.

21.   Mackay A, Burford A, Carvalho D, et al. Integrated Molecular Meta-Analysis of 1,000 Pediatric High-Grade and Diffuse Intrinsic Pontine Glioma. *Cancer Cell.* 2017; 32(4):520-537 e525.

22.   Hoeman CM, Cordero FJ, Hu G, et al. ACVR1 R206H cooperates with H3.1K27M in promoting diffuse intrinsic pontine glioma pathogenesis. *Nat Commun.* 2019; 10(1):1023.

23.   Taylor KR, Vinci M, Bullock AN, Jones C. ACVR1 mutations in DIPG: lessons learned from FOP. *Cancer Res.* 2014; 74(17):4565-4570.

24.   Becher OJ. CDK4/6 and diffuse intrinsic pontine glioma - Evaluate at diagnosis? *EBioMedicine.* 2019; 44:16-17.

25.   Hoeman C, Shen C, Becher OJ. CDK4/6 and PDGFRA Signaling as Therapeutic Targets in Diffuse Intrinsic Pontine Glioma. *Front Oncol.* 2018; 8:191.

26.   Ocasio JK, Budd KM, Roach JT, Andrews JM, Baker SJ. Oncohistones and disrupted development in pediatric-type diffuse high-grade glioma. *Cancer Metastasis Rev.* 2023; 42(2):367-388.

27.   Basinger H, Hogg JP. Neuroanatomy, Brainstem. *StatPearls*. Treasure Island (FL) ineligible companies. Disclosure: Jeffery Hogg declares no relevant financial relationships with ineligible companies.2023.

28.   Oliva I, Wanat MJ. Ventral Tegmental Area Afferents and Drug-Dependent Behaviors. *Front Psychiatry.* 2016; 7:30.

29.   Samineni VK, Premkumar LS, Faingold CL. Neuropathic pain-induced enhancement of spontaneous and pain-evoked neuronal activity in the periaqueductal gray that is attenuated by gabapentin. *Pain.* 2017; 158(7):1241-1253.

30.   Zelenin PV, Beloozerova IN, Sirota MG, Orlovsky GN, Deliagina TG. Activity of red nucleus neurons in the cat during postural corrections. *J Neurosci.* 2010; 30(43):14533-14542.

31.   Dutschmann M, Dick TE. Pontine mechanisms of respiratory control. *Compr Physiol.* 2012; 2(4):2443-2469.

32.   Valvi S, Gottardo NG. Diffuse Intrinsic Pontine Glioma. 2018.

33. Pan S, Ye D, Yue Y, et al. Leptomeningeal disease and tumor dissemination in a murine diffuse intrinsic pontine glioma model: implications for the study of the tumor-cerebrospinal fluid-ependymal microenvironment. *Neurooncol Adv.* 2022; 4(1):vdac059.

34. Kambhampati M, Perez JP, Yadavilli S, et al. A standardized autopsy procurement allows for the comprehensive study of DIPG biology. *Oncotarget.* 2015; 6(14):12740-12747.

35. Rutka JT. Biopsy of diffuse intrinsic pontine gliomas? *J Neurosurg Pediatr.* 2012; 10(2):79-80.

36. Poulet G, Massias J, Taly V. Liquid Biopsy: General Concepts. *Acta Cytol.* 2019; 63(6):449-455.

37. Miller AM, Karajannis MA. Current Role and Future Potential of CSF ctDNA for the Diagnosis and Clinical Management of Pediatric Central Nervous System Tumors. *J Natl Compr Canc Netw.* 2022; 20(12):1363-1369.

38. Mao X, Liu C, Tong H, Chen Y, Liu K. Principles of digital PCR and its applications in current obstetrical and gynecological diseases. *Am J Transl Res.* 2019; 11(12):7209-7222.

39. Azad TD, Jin MC, Bernhardt LJ, Bettegowda C. Liquid biopsy for pediatric diffuse midline glioma: a review of circulating tumor DNA and cerebrospinal fluid tumor DNA. *Neurosurg Focus.* 2020; 48(1):E9.

40. Li D, Bonner ER, Wierzbicki K, et al. Standardization of the liquid biopsy for pediatric diffuse midline glioma using ddPCR. *Sci Rep.* 2021; 11(1):5098.

41. Gallitto M, Lazarev S, Wasserman I, et al. Role of Radiation Therapy in the Management of Diffuse Intrinsic Pontine Glioma: A Systematic Review. *Adv Radiat Oncol.* 2019; 4(3):520-531.

42. Vanan MI, Eisenstat DD. DIPG in Children - What Can We Learn from the Past? *Front Oncol.* 2015; 5:237.

43. Pachocki CJ, Hol EM. Current perspectives on diffuse midline glioma and a different role for the immune microenvironment compared to glioblastoma. *J Neuroinflammation.* 2022; 19(1):276.

44. Pai Panandiker AS, Wong JK, Nedelka MA, Wu S, Gajjar A, Broniscer A. Effect of time from diagnosis to start of radiotherapy on children with diffuse intrinsic pontine glioma. *Pediatr Blood Cancer.* 2014; 61(7):1180-1183.

45. Frappaz D, Schell M, Thiesse P, et al. Preradiation chemotherapy may improve survival in pediatric diffuse intrinsic brainstem gliomas: final results of BSG 98 prospective trial. *Neuro Oncol.* 2008; 10(4):599-607.

46. Damato AR, Luo J, Katumba RGN, et al. Temozolomide chronotherapy in patients with glioblastoma: a retrospective single-institute study. *Neurooncol Adv.* 2021; 3(1):vdab041.

47. Pollack IF, Jakacki RI, Blaney SM, et al. Phase I trial of imatinib in children with newly diagnosed brainstem and recurrent malignant gliomas: a Pediatric Brain Tumor Consortium report. *Neuro Oncol.* 2007; 9(2):145-160.

48. Jansen MH, van Vuurden DG, Vandertop WP, Kaspers GJ. Diffuse intrinsic pontine gliomas: a systematic update on clinical trials and biology. *Cancer Treat Rev.* 2012; 38(1):27-35.

49. Broniscer A, Baker JN, Tagen M, et al. Phase I study of vandetanib during and after radiotherapy in children with diffuse intrinsic pontine glioma. *J Clin Oncol.* 2010; 28(31):4762-4768.

50. Hart E, Ode Z, Derieppe MPP, et al. Blood-brain barrier permeability following conventional photon radiotherapy - A systematic review and meta-analysis of clinical and preclinical studies. *Clin Transl Radiat Oncol.* 2022; 35:44-55.

51. Sharma HS, Ali SF. Alterations in blood-brain barrier function by morphine and methamphetamine. *Ann N Y Acad Sci.* 2006; 1074:198-224.

52. Hall WA, Doolittle ND, Daman M, et al. Osmotic blood-brain barrier disruption chemotherapy for diffuse pontine gliomas. *J Neurooncol.* 2006; 77(3):279-284.

53. Lonser RR, Warren KE, Butman JA, et al. Real-time image-guided direct convective perfusion of intrinsic brainstem lesions. Technical note. *Journal of neurosurgery.* 2007; 107(1):190-197.

54. Jenkinson MD, Smith TS, Haylock B, et al. Phase II trial of intratumoral BCNU injection and radiotherapy on untreated adult malignant glioma. *J Neurooncol.* 2010; 99(1):103-113.

55. Invernici G, Cristini S, Alessandri G, et al. Nanotechnology advances in brain tumors: the state of the art. *Recent Pat Anticancer Drug Discov.* 2011; 6(1):58-69.

56. Zhang Y, Zhang Z. The history and advances in cancer immunotherapy: understanding the characteristics of tumor-infiltrating immune cells and their therapeutic implications. *Cell Mol Immunol.* 2020; 17(8):807-821.

57. Mount CW, Majzner RG, Sundaresh S, et al. Potent antitumor efficacy of anti-GD2 CAR T cells in H3-K27M(+) diffuse midline gliomas. *Nat Med.* 2018; 24(5):572-579.

58. Majzner RG, Ramakrishna S, Yeom KW, et al. GD2-CAR T cell therapy for H3K27M-mutated diffuse midline gliomas. *Nature.* 2022; 603(7903):934-941.

59. Vitanza NA, Wilson AL, Huang W, et al. Intraventricular B7-H3 CAR T Cells for Diffuse Intrinsic Pontine Glioma: Preliminary First-in-Human Bioactivity and Safety. *Cancer Discov.* 2023; 13(1):114-131.

60. Tate MC, Lindquist RA, Nguyen T, et al. Postnatal growth of the human pons: a morphometric and immunohistochemical analysis. *J Comp Neurol.* 2015; 523(3):449-462.

61. Monje M, Mitra SS, Freret ME, et al. Hedgehog-responsive candidate cell of origin for diffuse intrinsic pontine glioma. *Proc Natl Acad Sci U S A.* 2011; 108(11):4453-4458.

62. Anderson JL, Muraleedharan R, Oatman N, et al. The transcription factor Olig2 is important for the biology of diffuse intrinsic pontine gliomas. *Neuro Oncol.* 2017; 19(8):1068-1078.

63.   Liu I, Jiang L, Samuelsson ER, et al. The landscape of tumor cell states and spatial organization in H3-K27M mutant diffuse midline glioma across age and location. *Nat Genet.* 2022; 54(12):1881-1894.

64.   Filbin MG, Tirosh I, Hovestadt V, et al. Developmental and oncogenic programs in H3K27M gliomas dissected by single-cell RNA-seq. *Science.* 2018; 360(6386):331-335.

65.   Neumann H. The immunological microenvironment in the CNS: implications on neuronal cell death and survival. *J Neural Transm Suppl.* 2000; 59:59-68.

66.   Yang HY, Wu CY, Powell JD, Lu KL. Manipulation of Metabolic Pathways and Its Consequences for Anti-Tumor Immunity: A Clinical Perspective. *Int J Mol Sci.* 2020; 21(11).

67.   Wang M, Zhao J, Zhang L, et al. Role of tumor microenvironment in tumorigenesis. *J Cancer.* 2017; 8(5):761-773.

68.   Ren X, Guo S, Guan X, Kang Y, Liu J, Yang X. Immunological Classification of Tumor Types and Advances in Precision Combination Immunotherapy. *Front Immunol.* 2022; 13:790113.

69.   Chen DS, Mellman I. Elements of cancer immunity and the cancer-immune set point. *Nature.* 2017; 541(7637):321-330.

70.   Zhang J, Huang D, Saw PE, Song E. Turning cold tumors hot: from molecular mechanisms to clinical applications. *Trends Immunol.* 2022; 43(7):523-545.

71.   Duan Q, Zhang H, Zheng J, Zhang L. Turning Cold into Hot: Firing up the Tumor Microenvironment. *Trends Cancer.* 2020; 6(7):605-618.

72.   Lieberman NAP, DeGolier K, Kovar HM, et al. Characterization of the immune microenvironment of diffuse intrinsic pontine glioma: implications for development of immunotherapy. *Neuro Oncol.* 2019; 21(1):83-94.

73.   Lin GL, Nagaraja S, Filbin MG, Suva ML, Vogel H, Monje M. Non-inflammatory tumor microenvironment of diffuse intrinsic pontine glioma. *Acta Neuropathol Commun.* 2018; 6(1):51.

74.   Zhang L, Yu H, Xue Y, Liu Y. Decreased natural killer cells in diffuse intrinsic pontine glioma patients. *Childs Nerv Syst.* 2020; 36(7):1345-1346.

75.   Lieberman NAP, Vitanza NA, Crane CA. Immunotherapy for brain tumors: understanding early successes and limitations. *Expert Rev Neurother.* 2018; 18(3):251-259.

76.   Oh DY, Fong L, Newell EW, et al. Toward a better understanding of T cells in cancer. *Cancer Cell.* 2021; 39(12):1549-1552.

77.   Qin Y, Lu F, Lyu K, Chang AE, Li Q. Emerging concepts regarding pro- and anti tumor properties of B cells in tumor immunity. *Front Immunol.* 2022; 13:881427.

78.   Kazemi MH, Sadri M, Najafi A, et al. Tumor-infiltrating lymphocytes for treatment of solid tumors: It takes two to tango? *Front Immunol.* 2022; 13:1018962.

79.   Lanca T, Silva-Santos B. The split nature of tumor-infiltrating leukocytes: Implications for cancer surveillance and immunotherapy. *Oncoimmunology.* 2012; 1(5):717-725.

80.   Whiteside TL. What are regulatory T cells (Treg) regulating in cancer and why? *Semin Cancer Biol.* 2012; 22(4):327-334.

81.   Bonavita E, Galdiero MR, Jaillon S, Mantovani A. Phagocytes as Corrupted Policemen in Cancer-Related Inflammation. *Adv Cancer Res.* 2015; 128:141-171.

82.   Ostuni R, Kratochvill F, Murray PJ, Natoli G. Macrophages and cancer: from mechanisms to therapeutic implications. *Trends Immunol.* 2015; 36(4):229-239.

83.   Barnes NG. Targeting TAMs. *Nat Rev Chem.* 2022; 6(10):678.

84.   Orecchioni M, Ghosheh Y, Pramod AB, Ley K. Macrophage Polarization: Different Gene Signatures in M1(LPS+) vs. Classically and M2(LPS-) vs. Alternatively Activated Macrophages. *Front Immunol.* 2019; 10:1084.

85.   Saqib U, Sarkar S, Suk K, Mohammad O, Baig MS, Savai R. Phytochemicals as modulators of M1-M2 macrophages in inflammation. *Oncotarget.* 2018; 9(25):17937-17950.

86.   He Z, Zhang S. Tumor-Associated Macrophages and Their Functional Transformation in the Hypoxic Tumor Microenvironment. *Front Immunol.* 2021; 12:741305.

87.   Pan Y, Yu Y, Wang X, Zhang T. Tumor-Associated Macrophages in Tumor Immunity. *Front Immunol.* 2020; 11:583084.

88.   Toor SM, Sasidharan Nair V, Decock J, Elkord E. Immune checkpoints in the tumor microenvironment. *Semin Cancer Biol.* 2020; 65:1-12.

89.   Bai R, Lv Z, Xu D, Cui J. Predictive biomarkers for cancer immunotherapy with immune checkpoint inhibitors. *Biomark Res.* 2020; 8:34.

90.   Collins M, Ling V, Carreno BM. The B7 family of immune-regulatory ligands. *Genome Biol.* 2005; 6(6):223.

91.   Sharpe AH, Wherry EJ, Ahmed R, Freeman GJ. The function of programmed cell death 1 and its ligands in regulating autoimmunity and infection. *Nat Immunol.* 2007; 8(3):239-245.

92.   Ahmadzadeh M, Johnson LA, Heemskerk B, et al. Tumor antigen-specific CD8 T cells infiltrating the tumor express high levels of PD-1 and are functionally impaired. *Blood.* 2009; 114(8):1537-1544.

93.   Zitvogel L, Kroemer G. Targeting PD-1/PD-L1 interactions for cancer immunotherapy. *Oncoimmunology.* 2012; 1(8):1223-1225.

94.   Latchman Y, Wood CR, Chernova T, et al. PD-L2 is a second ligand for PD-1 and inhibits T cell activation. *Nat Immunol.* 2001; 2(3):261-268.

References

95. Contardi E, Palmisano GL, Tazzari PL, et al. CTLA-4 is constitutively expressed on tumor cells and can trigger apoptosis upon ligand interaction. *Int J Cancer.* 2005; 117(4):538-550.

96. Krummel MF, Allison JP. Pillars article: CD28 and CTLA-4 have opposing effects on the response of T cells to stimulation. The journal of experimental medicine. 1995. 182: 459-465. *J Immunol.* 2011; 187(7):3459-3465.

97. Walunas TL, Lenschow DJ, Bakker CY, et al. CTLA-4 can function as a negative regulator of T cell activation. *Immunity.* 1994; 1(5):405-413.

98. Knieke K, Lingel H, Chamaon K, Brunner-Weinzierl MC. Migration of Th1 lymphocytes is regulated by CD152 (CTLA-4)-mediated signaling via PI3 kinase-dependent Akt activation. *PLoS One.* 2012; 7(3):e31391.

99. Yang S, Wei W, Zhao Q. B7-H3, a checkpoint molecule, as a target for cancer immunotherapy. *Int J Biol Sci.* 2020; 16(11):1767-1773.

100. Suh WK, Gajewska BU, Okada H, et al. The B7 family member B7-H3 preferentially down-regulates T helper type 1-mediated immune responses. *Nat Immunol.* 2003; 4(9):899-906.

101. Chen JT, Chen CH, Ku KL, et al. Glycoprotein B7-H3 overexpression and aberrant glycosylation in oral cancer and immune response. *Proc Natl Acad Sci U S A.* 2015; 112(42):13057-13062.

102. Jin Y, Zhang P, Li J, et al. B7-H3 in combination with regulatory T cell is associated with tumor progression in primary human non-small cell lung cancer. *Int J Clin Exp Pathol.* 2015; 8(11):13987-13995.

103. Liu C, Liu J, Wang J, et al. B7-H3 expression in ductal and lobular breast cancer and its association with IL-10. *Mol Med Rep.* 2013; 7(1):134-138.

104. Daneman R, Prat A. The blood-brain barrier. *Cold Spring Harb Perspect Biol.* 2015; 7(1):a020412.

105. Godwin L, Tariq MA, Crane JS. Histology, Capillary. *StatPearls.* Treasure Island (FL) ineligible companies. Disclosure: Muhammad Ali Tariq declares no relevant financial relationships with ineligible companies. Disclosure: Jonathan Crane declares no relevant financial relationships with ineligible companies.2023.

106. Zlokovic BV. The blood-brain barrier in health and chronic neurodegenerative disorders. *Neuron.* 2008; 57(2):178-201.

107. Reese TS, Karnovsky MJ. Fine structural localization of a blood-brain barrier to exogenous peroxidase. *J Cell Biol.* 1967; 34(1):207-217.

108. Coomber BL, Stewart PA. Morphometric analysis of CNS microvascular endothelium. *Microvasc Res.* 1985; 30(1):99-115.

109. Daneman R, Zhou L, Kebede AA, Barres BA. Pericytes are required for blood-brain barrier integrity during embryogenesis. *Nature.* 2010; 468(7323):562-566.

110. Rzucidlo EM, Martin KA, Powell RJ. Regulation of vascular smooth muscle cell differentiation. *J Vasc Surg.* 2007; 45 Suppl A:A25-32.

111. Armulik A, Genove G, Betsholtz C. Pericytes: developmental, physiological, and pathological perspectives, problems, and promises. *Dev Cell.* 2011; 21(2):193-215.

112. Attwell D, Buchan AM, Charpak S, Lauritzen M, Macvicar BA, Newman EA. Glial and neuronal control of brain blood flow. *Nature.* 2010; 468(7321):232-243.

113. Baluk P, Hashizume H, McDonald DM. Cellular abnormalities of blood vessels as targets in cancer. *Curr Opin Genet Dev.* 2005; 15(1):102-111.

114. Lugano R, Ramachandran M, Dimberg A. Tumor angiogenesis: causes, consequences, challenges and opportunities. *Cell Mol Life Sci.* 2020; 77(9):1745-1770.

115. Sarkaria JN, Hu LS, Parney IF, et al. Is the blood-brain barrier really disrupted in all glioblastomas? A critical assessment of existing clinical data. *Neuro Oncol.* 2018; 20(2):184-191.

116. Folkman J. Successful treatment of an angiogenic disease. *N Engl J Med.* 1989; 320(18):1211-1212.

117. Lopes-Coelho F, Martins F, Pereira SA, Serpa J. Anti-Angiogenic Therapy: Current Challenges and Future Perspectives. *Int J Mol Sci.* 2021; 22(7).

118. Lupo G, Caporarello N, Olivieri M, et al. Anti-angiogenic Therapy in Cancer: Downsides and New Pivots for Precision Medicine. *Front Pharmacol.* 2016; 7:519.

119. Zhang JM, An J. Cytokines, inflammation, and pain. *Int Anesthesiol Clin.* 2007; 45(2):27-37.

120. Dranoff G. Cytokines in cancer pathogenesis and cancer therapy. *Nat Rev Cancer.* 2004; 4(1):11-22.

121. Massague J. TGFbeta in Cancer. *Cell.* 2008; 134(2):215-230.

122. Lamort AS, Giopanou I, Psallidas I, Stathopoulos GT. Osteopontin as a Link between Inflammation and Cancer: The Thorax in the Spotlight. *Cells.* 2019; 8(8).

123. Maeda N, Maenaka K. The Roles of Matricellular Proteins in Oncogenic Virus-Induced Cancers and Their Potential Utilities as Therapeutic Targets. *Int J Mol Sci.* 2017; 18(10).

124. Rosmus DD, Lange C, Ludwig F, Ajami B, Wieghofer P. The Role of Osteopontin in Microglia Biology: Current Concepts and Future Perspectives. *Biomedicines.* 2022; 10(4).

125. Singh A, Gill G, Kaur H, Amhmed M, Jakhu H. Role of osteopontin in bone remodeling and orthodontic tooth movement: a review. *Prog Orthod.* 2018; 19(1):18.

126. Wang Y, Yan W, Lu X, et al. Overexpression of osteopontin induces angiogenesis of endothelial progenitor cells via the avbeta3/PI3K/AKT/eNOS/NO signaling pathway in glioma cells. *Eur J Cell Biol.* 2011; 90(8):642-648.

127. Kahles F, Findeisen HM, Bruemmer D. Osteopontin: A novel regulator at the cross roads of inflammation, obesity and diabetes. *Mol Metab.* 2014; 3(4):384-393.

128. Wei J, Marisetty A, Schrand B, et al. Osteopontin mediates glioblastoma-associated macrophage infiltration and is a potential therapeutic target. *J Clin Invest.* 2019; 129(1):137-149.

129. Moorman HR, Poschel D, Klement JD, Lu C, Redd PS, Liu K. Osteopontin: A Key Regulator of Tumor Progression and Immunomodulation. *Cancers (Basel).* 2020; 12(11).

130. Donati V, Boldrini L, Dell'Omodarme M, et al. Osteopontin expression and prognostic significance in non-small cell lung cancer. *Clin Cancer Res.* 2005; 11(18):6459-6465.

131. Pinter M, Jain RK, Duda DG. The Current Landscape of Immune Checkpoint Blockade in Hepatocellular Carcinoma: A Review. *JAMA Oncol.* 2021; 7(1):113-123.

132. Rudland PS, Platt-Higgins A, El-Tanani M, et al. Prognostic significance of the metastasis-associated protein osteopontin in human breast cancer. *Cancer Res.* 2002; 62(12):3417-3427.

133. Singhal H, Bautista DS, Tonkin KS, et al. Elevated plasma osteopontin in metastatic breast cancer associated with increased tumor burden and decreased survival. *Clin Cancer Res.* 1997; 3(4):605-611.

134. Wang H, Guo D, Li J, Wei B, Zheng H. Increased expression of osteopontin indicates poor prognosis in hepatocellular carcinoma. *Int J Clin Exp Pathol.* 2018; 11(12):5916-5922.

135. Rangel J, Nosrati M, Torabian S, et al. Osteopontin as a molecular prognostic marker for melanoma. *Cancer.* 2008; 112(1):144-150.

136. Sreekanthreddy P, Srinivasan H, Kumar DM, et al. Identification of potential serum biomarkers of glioblastoma: serum osteopontin levels correlate with poor prognosis. *Cancer Epidemiol Biomarkers Prev.* 2010; 19(6):1409-1422.

137. Lamort A-S, Giopanou I, Psallidas I, Stathopoulos GT. Osteopontin as a Link between Inflammation and Cancer: The Thorax in the Spotlight. *Cells.* 2019; 8(8):815.

138. Polat B, Wohlleben G, Kosmala R, et al. Differences in stem cell marker and osteopontin expression in primary and recurrent glioblastoma. *Cancer Cell Int.* 2022; 22(1):87.

139. Agnihotri R, Crawford HC, Haro H, Matrisian LM, Havrda MC, Liaw L. Osteopontin, a novel substrate for matrix metalloproteinase-3 (stromelysin-1) and matrix metalloproteinase-7 (matrilysin). *J Biol Chem.* 2001; 276(30):28261-28267.

140. Kariya Y, Kanno M, Matsumoto-Morita K, Konno M, Yamaguchi Y, Hashimoto Y. Osteopontin O-glycosylation contributes to its phosphorylation and cell-adhesion properties. *Biochem J.* 2014; 463(1):93-102.

141. Klement JD, Paschall AV, Redd PS, et al. An osteopontin/CD44 immune checkpoint controls CD8+ T cell activation and tumor immune evasion. *J Clin Invest.* 2018; 128(12):5549-5560.

142. Wu Q, Li L, Miao C, et al. Osteopontin promotes hepatocellular carcinoma progression through inducing JAK2/STAT3/NOX1-mediated ROS production. *Cell Death Dis.* 2022; 13(4):341.

143. Cao J, Li J, Sun L, et al. Hypoxia-driven paracrine osteopontin/integrin alphavbeta3 signaling promotes pancreatic cancer cell epithelial-mesenchymal transition and cancer stem cell-like properties by modulating forkhead box protein M1. *Mol Oncol.* 2019; 13(2):228-245.

144. Luo X, Ruhland MK, Pazolli E, Lind AC, Stewart SA. Osteopontin stimulates preneoplastic cellular proliferation through activation of the MAPK pathway. *Mol Cancer Res.* 2011; 9(8):1018-1029.

145. Qian J, LeSavage BL, Hubka KM, et al. Cancer-associated mesothelial cells promote ovarian cancer chemoresistance through paracrine osteopontin signaling. *J Clin Invest.* 2021; 131(16).

146. Cao L, Fan X, Jing W, et al. Osteopontin promotes a cancer stem cell-like phenotype in hepatocellular carcinoma cells via an integrin-NF-kappaB-HIF-1alpha pathway. *Oncotarget.* 2015; 6(9):6627-6640.

147. Rao G, Wang H, Li B, et al. Reciprocal interactions between tumor-associated macrophages and CD44-positive cancer cells via osteopontin/CD44 promote tumorigenicity in colorectal cancer. *Clin Cancer Res.* 2013; 19(4):785-797.

148. Huang RH, Quan YJ, Chen JH, et al. Osteopontin Promotes Cell Migration and Invasion, and Inhibits Apoptosis and Autophagy in Colorectal Cancer by activating the p38 MAPK Signaling Pathway. *Cell Physiol Biochem.* 2017; 41(5):1851-1864.

149. Strehlow F, Bauer S, Martus P, et al. Osteopontin in cerebrospinal fluid as diagnostic biomarker for central nervous system lymphoma. *J Neurooncol.* 2016; 129(1):165-171.

150. Anborgh PH, Caria LB, Chambers AF, Tuck AB, Stitt LW, Brackstone M. Role of plasma osteopontin as a biomarker in locally advanced breast cancer. *Am J Transl Res.* 2015; 7(4):723-732.

151. Wei R, Wong JPC, Kwok HF. Osteopontin -- a promising biomarker for cancer therapy. *J Cancer.* 2017; 8(12):2173-2183.

152. Kariya Y, Kariya Y. Osteopontin in Cancer: Mechanisms and Therapeutic Targets. *International Journal of Translational Medicine.* 2022; 2(3):419-447.

153. Bonneh-Barkay D, Bissel SJ, Wang G, et al. YKL-40, a marker of simian immunodeficiency virus encephalitis, modulates the biological activity of basic fibroblast growth factor. *Am J Pathol.* 2008; 173(1):130-143.

154. Junker N, Johansen JS, Andersen CB, Kristjansen PE. Expression of YKL-40 by peritumoral macrophages in human small cell lung cancer. *Lung Cancer.* 2005; 48(2):223-231.

155. Gorgens SW, Eckardt K, Elsen M, Tennagels N, Eckel J. Chitinase-3-like protein 1 protects skeletal muscle from TNFalpha-induced inflammation and insulin resistance. *Biochem J.* 2014; 459(3):479-488.

156. Rehli M, Krause SW, Andreesen R. Molecular characterization of the gene for human cartilage gp-39 (CHI3L1), a member of the chitinase protein family and marker for late stages of macrophage differentiation. *Genomics.* 1997; 43(2):221-225.

157. Yang PS, Yu MH, Hou YC, et al. Targeting protumor factor chitinase-3-like-1 secreted by Rab37 vesicles for cancer immunotherapy. *Theranostics.* 2022; 12(1):340-361.

158. Bonneh-Barkay D, Zagadailov P, Zou H, et al. YKL-40 expression in traumatic brain injury: an initial analysis. *J Neurotrauma.* 2010; 27(7):1215-1223.

159. Dela Cruz CS, Liu W, He CH, et al. Chitinase 3-like-1 promotes Streptococcus pneumoniae killing and augments host tolerance to lung antibacterial responses. *Cell Host Microbe.* 2012; 12(1):34-46.

160. Xu N, Bo Q, Shao R, et al. Chitinase-3-Like-1 Promotes M2 Macrophage Differentiation and Induces Choroidal Neovascularization in Neovascular Age-Related Macular Degeneration. *Invest Ophthalmol Vis Sci.* 2019; 60(14):4596-4605.

161. He CH, Lee CG, Dela Cruz CS, et al. Chitinase 3-like 1 regulates cellular and tissue responses via IL-13 receptor alpha2. *Cell Rep.* 2013; 4(4):830-841.

162. Schmidt IM, Hall IE, Kale S, et al. Chitinase-like protein Brp-39/YKL-40 modulates the renal response to ischemic injury and predicts delayed allograft function. *J Am Soc Nephrol.* 2013; 24(2):309-319.

163. Cohen N, Shani O, Raz Y, et al. Fibroblasts drive an immunosuppressive and growth-promoting microenvironment in breast cancer via secretion of Chitinase 3-like 1. *Oncogene.* 2017; 36(31):4457-4468.

164. Bergmann OJ, Johansen JS, Klausen TW, et al. High serum concentration of YKL-40 is associated with short survival in patients with acute myeloid leukemia. *Clin Cancer Res.* 2005; 11(24 Pt 1):8644-8652.

165. Hogdall EV, Johansen JS, Kjaer SK, et al. High plasma YKL-40 level in patients with ovarian cancer stage III is related to shorter survival. *Oncol Rep.* 2003; 10(5):1535-1538.

166. Johansen JS, Drivsholm L, Price PA, Christensen IJ. High serum YKL-40 level in patients with small cell lung cancer is related to early death. *Lung Cancer.* 2004; 46(3):333-340.

167. Li F, Qi B, Yang L, et al. CHI3L1 predicted in malignant entities is associated with glioblastoma immune microenvironment. *Clin Immunol.* 2022; 245:109158.

168. Geng B, Pan J, Zhao T, et al. Chitinase 3-like 1-CD44 interaction promotes metastasis and epithelial-to-mesenchymal transition through beta-catenin/Erk/Akt signaling in gastric cancer. *J Exp Clin Cancer Res.* 2018; 37(1):208.

169. Pinteac R, Montalban X, Comabella M. Chitinases and chitinase-like proteins as biomarkers in neurologic disorders. *Neurol Neuroimmunol Neuroinflamm.* 2021; 8(1).

170. Zhao T, Su Z, Li Y, Zhang X, You Q. Chitinase-3 like-protein-1 function and its role in diseases. *Signal Transduct Target Ther.* 2020; 5(1):201.

171. Comabella M, Fernandez M, Martin R, et al. Cerebrospinal fluid chitinase 3-like 1 levels are associated with conversion to multiple sclerosis. *Brain.* 2010; 133(Pt 4):1082-1093.

172. Conroy AL, Hawkes MT, Elphinstone R, et al. Chitinase-3-like 1 is a biomarker of acute kidney injury and mortality in paediatric severe malaria. *Malar J.* 2018; 17(1):82.

173. Hamilton G, Rath B, Burghuber O. Chitinase-3-like-1/YKL-40 as marker of circulating tumor cells. *Transl Lung Cancer Res.* 2015; 4(3):287-291.

174. Song Z, Chen E, Qian J, et al. Serum chitinase activity prognosticates metastasis of colorectal cancer. *BMC Cancer.* 2019; 19(1):629.

175. Xu H, Niu M, Yuan X, Wu K, Liu A. CD44 as a tumor biomarker and therapeutic target. *Exp Hematol Oncol.* 2020; 9(1):36.

176. Naor D, Sionov RV, Ish-Shalom D. CD44: Structure, Function and Association with the Malignant Process. 1997; 71:241-319.

177. Si D, Yin F, Peng J, Zhang G. High Expression of CD44 Predicts a Poor Prognosis in Glioblastomas. *Cancer Manag Res.* 2020; 12:769-775.

178. Xu H, Wu K, Tian Y, et al. CD44 correlates with clinicopathological characteristics and is upregulated by EGFR in breast cancer. *Int J Oncol.* 2016; 49(4):1343-1350.

179. Vega FM, Colmenero-Repiso A, Gomez-Munoz MA, et al. CD44-high neural crest stem-like cells are associated with tumour aggressiveness and poor survival in neuroblastoma tumours. *EBioMedicine.* 2019; 49:82-95.

180. Szczepanik A, Sierzega M, Drabik G, Pituch-Noworolska A, Kolodziejczyk P, Zembala M. CD44(+) cytokeratin-positive tumor cells in blood and bone marrow are associated with poor prognosis of patients with gastric cancer. *Gastric Cancer.* 2019; 22(2):264-272.

181. Chen C, Zhao S, Karnad A, Freeman JW. The biology and role of CD44 in cancer progression: therapeutic implications. *J Hematol Oncol.* 2018; 11(1):64.

182. Yan Y, Zuo X, Wei D. Concise Review: Emerging Role of CD44 in Cancer Stem Cells: A Promising Biomarker and Therapeutic Target. *Stem Cells Transl Med.* 2015; 4(9):1033-1043.

183. Pietras A, Katz AM, Ekstrom EJ, et al. Osteopontin-CD44 signaling in the glioma perivascular niche enhances cancer stem cell phenotypes and promotes aggressive tumor growth. *Cell Stem Cell.* 2014; 14(3):357-369.

184.   Nallasamy P, Nimmakayala RK, Karmakar S, et al. Pancreatic Tumor Microenvironment Factor Promotes Cancer Stemness via SPP1-CD44 Axis. *Gastroenterology.* 2021; 161(6):1998-2013 e1997.

185.   Bahnassy AA, Fawzy M, El-Wakil M, Zekri AR, Abdel-Sayed A, Sheta M. Aberrant expression of cancer stem cell markers (CD44, CD90, and CD133) contributes to disease progression and reduced survival in hepatoblastoma patients: 4-year survival data. *Transl Res.* 2015; 165(3):396-406.

186.   Herishanu Y, Gibellini F, Njuguna N, et al. Activation of CD44, a receptor for extracellular matrix components, protects chronic lymphocytic leukemia cells from spontaneous and drug induced apoptosis through MCL-1. *Leuk Lymphoma.* 2011; 52(9):1758-1769.

187.   Takahashi K, Eto H, Tanabe KK. Involvement of CD44 in matrix metalloproteinase-2 regulation in human melanoma cells. *Int J Cancer.* 1999; 80(3):387-395.

188.   Spessotto P, Rossi FM, Degan M, et al. Hyaluronan-CD44 interaction hampers migration of osteoclast-like cells by down-regulating MMP-9. *J Cell Biol.* 2002; 158(6):1133-1144.

189.   Liu S, Liu Z, Shang A, et al. CD44 is a potential immunotherapeutic target and affects macrophage infiltration leading to poor prognosis. *Sci Rep.* 2023; 13(1):9657.

190.   Dahlmanns M, Yakubov E, Chen D, et al. Chemotherapeutic xCT inhibitors sorafenib and erastin unraveled with the synaptic optogenetic function analysis tool. *Cell Death Discov.* 2017; 3:17030.

191.   Liu J, Xia X, Huang P. xCT: A Critical Molecule That Links Cancer Metabolism to Redox Signaling. *Mol Ther.* 2020; 28(11):2358-2366.

192.   Wada T, Ishimoto T, Seishima R, et al. Functional role of CD44v-xCT system in the development of spasmolytic polypeptide-expressing metaplasia. *Cancer Sci.* 2013; 104(10):1323-1329.

193.   Adnane L, Trail PA, Taylor I, Wilhelm SM. Sorafenib (BAY 43-9006, Nexavar), a dual-action inhibitor that targets RAF/MEK/ERK pathway in tumor cells and tyrosine kinases VEGFR/PDGFR in tumor vasculature. *Methods Enzymol.* 2006; 407:597-612.

194.   Fallahi P, Ferrari SM, Santini F, et al. Sorafenib and thyroid cancer. *BioDrugs.* 2013; 27(6):615-628.

195.   Abdelgalil AA, Alkahtani HM, Al-Jenoobi FI. Sorafenib. *Profiles Drug Subst Excip Relat Methodol.* 2019; 44:239-266.

196.   Kim JY, Jo Y, Oh HK, Kim EH. Sorafenib increases tumor treating fields-induced cell death in glioblastoma by inhibiting STAT3. *Am J Cancer Res.* 2020; 10(10):3475-3486.

197.   Carra E, Barbieri F, Marubbi D, et al. Sorafenib selectively depletes human glioblastoma tumor-initiating cells from primary cultures. *Cell Cycle.* 2013; 12(3):491-500.

198.   Siegelin MD, Raskett CM, Gilbert CA, Ross AH, Altieri DC. Sorafenib exerts anti-glioma activity in vitro and in vivo. *Neurosci Lett.* 2010; 478(3):165-170.

199.   Tang W, Chen Z, Zhang W, et al. The mechanisms of sorafenib resistance in hepatocellular carcinoma: theoretical basis and therapeutic aspects. *Signal Transduct Target Ther.* 2020; 5(1):87.

200.   Guo L, Hu C, Yao M, Han G. Mechanism of sorafenib resistance associated with ferroptosis in HCC. *Front Pharmacol.* 2023; 14:1207496.

201.   Zhu YJ, Zheng B, Wang HY, Chen L. New knowledge of the mechanisms of sorafenib resistance in liver cancer. *Acta Pharmacol Sin.* 2017; 38(5):614-622.

202.   Noorolyai S, Shajari N, Baghbani E, Sadreddini S, Baradaran B. The relation between PI3K/AKT signalling pathway and cancer. *Gene.* 2019; 698:120-128.

203.   Nicholson KM, Anderson NG. The protein kinase B/Akt signalling pathway in human malignancy. *Cell Signal.* 2002; 14(5):381-395.

204.   Mishra R, Patel H, Alanazi S, Kilroy MK, Garrett JT. PI3K Inhibitors in Cancer: Clinical Implications and Adverse Effects. *Int J Mol Sci.* 2021; 22(7).

205.   Mackall CL, Merchant MS, Fry TJ. Immune-based therapies for childhood cancer. *Nat Rev Clin Oncol.* 2014; 11(12):693-703.

206.   Daei Sorkhabi A, Mohamed Khosroshahi L, Sarkesh A, et al. The current landscape of CAR T-cell therapy for solid tumors: Mechanisms, research progress, challenges, and counterstrategies. *Front Immunol.* 2023; 14:1113882.

207.   Castillo-Ecija H, Pascual-Pasto G, Perez-Jaume S, et al. Prognostic value of patient-derived xenograft engraftment in pediatric sarcomas. *J Pathol Clin Res.* 2021; 7(4):338-349.

208.   Fernandez-Arjona MDM, Grondona JM, Granados-Duran P, Fernandez-Llebrez P, Lopez-Avalos MD. Microglia Morphological Categorization in a Rat Model of Neuroinflammation by Hierarchical Cluster and Principal Components Analysis. *Front Cell Neurosci.* 2017; 11:235.

209.   Du L, Xing Z, Tao B, et al. Correction: Both IDO1 and TDO contribute to the malignancy of gliomas via the Kyn-AhR-AQP4 signaling pathway. *Signal Transduct Target Ther.* 2021; 6(1):385.

210.   Jiang J, Qiu J, Li Q, Shi Z. Prostaglandin E2 Signaling: Alternative Target for Glioblastoma? *Trends Cancer.* 2017; 3(2):75-78.

211.   Burster T, Gartner F, Bulach C, Zhanapiya A, Gihring A, Knippschild U. Regulation of MHC I Molecules in Glioblastoma Cells and the Sensitizing of NK Cells. *Pharmaceuticals (Basel).* 2021; 14(3).

212.   Gong L, Ji L, Xu D, Wang J, Zou J. TGF-beta links glycolysis and immunosuppression in glioblastoma. *Histol Histopathol.* 2021; 36(11):1111-1124.

213.   Zininga T, Ramatsui L, Shonhai A. Heat Shock Proteins as Immunomodulants. *Molecules.* 2018; 23(11).

References

214. Iglesia RP, Fernandes CFL, Coelho BP, et al. Heat Shock Proteins in Glioblastoma Biology: Where Do We Stand? *Int J Mol Sci.* 2019; 20(22).

215. Piperi C, Papavassiliou KA, Papavassiliou AG. Pivotal Role of STAT3 in Shaping Glioblastoma Immune Microenvironment. *Cells.* 2019; 8(11).

216. Chen R, Zhang H, Wu W, et al. Corrigendum: Antigen Presentation Machinery Signature-Derived CALR Mediates Migration, Polarization of Macrophages in Glioma and Predicts Immunotherapy Response. *Front Immunol.* 2022; 13:931433.

217. Ye C, Li H, Li Y, et al. Hypoxia-induced HMGB1 promotes glioma stem cells self-renewal and tumorigenicity via RAGE. *iScience.* 2022; 25(9):104872.

218. Townsend MH, Tellez Freitas CM, Larsen D, et al. Hypoxanthine Guanine Phosphoribosyltransferase expression is negatively correlated with immune activity through its regulation of purine synthesis. *Immunobiology.* 2020; 225(3):151931.

219. Christensen B, Schack L, Klaning E, Sorensen ES. Osteopontin is cleaved at multiple sites close to its integrin-binding motifs in milk and is a novel substrate for plasmin and cathepsin D. *J Biol Chem.* 2010; 285(11):7929-7937.

220. Ozerdem U, Stallcup WB. Pathological angiogenesis is reduced by targeting pericytes via the NG2 proteoglycan. *Angiogenesis.* 2004; 7(3):269-276.

221. Cirillo N. The Hyaluronan/CD44 Axis: A Double-Edged Sword in Cancer. *Int J Mol Sci.* 2023; 24(21).

222. Man M, Elias PM, Man W, et al. The role of CD44 in cutaneous inflammation. *Exp Dermatol.* 2009; 18(11):962-968.

223. Peng Y, Wang Y, Zhou C, Mei W, Zeng C. PI3K/Akt/mTOR Pathway and Its Role in Cancer Therapeutics: Are We Making Headway? *Front Oncol.* 2022; 12:819128.

224. Wang Q, Shi YL, Zhou K, et al. PIK3CA mutations confer resistance to first-line chemotherapy in colorectal cancer. *Cell Death Dis.* 2018; 9(7):739.

225. Mosele F, Stefanovska B, Lusque A, et al. Outcome and molecular landscape of patients with PIK3CA-mutated metastatic breast cancer. *Ann Oncol.* 2020; 31(3):377-386.

226. Cho YA, Ko SY, Suh YJ, et al. PIK3CA Mutation as Potential Poor Prognostic Marker in Asian Female Breast Cancer Patients Who Received Adjuvant Chemotherapy. *Curr Oncol.* 2022; 29(5):2895-2908.

227. Balkwill F, Mantovani A. Inflammation and cancer: back to Virchow? *The Lancet.* 2001; 357(9255):539-545.

228. Kawada M, Seno H, Kanda K, et al. Chitinase 3-like 1 promotes macrophage recruitment and angiogenesis in colorectal cancer. *Oncogene.* 2012; 31(26):3111-3123.

229. Yan W, Qian C, Zhao P, et al. Expression pattern of osteopontin splice variants and its functions on cell apoptosis and invasion in glioma cells. *Neuro Oncol.* 2010; 12(8):765-775.

230. Cuadrado-Vilanova M, Liu J, Paco S, et al. Identification of immunosuppressive factors in retinoblastoma cell secretomes and aqueous humor from patients. *J Pathol.* 2022; 257(3):327-339.

231. Larsen TV, Daugaard TF, Gad HH, Hartmann R, Nielsen AL. PD-L1 and PD-L2 immune checkpoint protein induction by type III interferon in non-small cell lung cancer cells. *Immunobiology.* 2023; 228(3):152389.

232. Zhou Z, Luther N, Ibrahim GM, et al. B7-H3, a potential therapeutic target, is expressed in diffuse intrinsic pontine glioma. *J Neurooncol.* 2013; 111(3):257-264.

233. Wang L, Kang FB, Shan BE. B7-H3-mediated tumor immunology: Friend or foe? *Int J Cancer.* 2014; 134(12):2764-2771.

234. Picarda E, Ohaegbulam KC, Zang X. Molecular Pathways: Targeting B7-H3 (CD276) for Human Cancer Immunotherapy. *Clin Cancer Res.* 2016; 22(14):3425-3431.

235. Leitner J, Klauser C, Pickl WF, et al. B7-H3 is a potent inhibitor of human T-cell activation: No evidence for B7-H3 and TREML2 interaction. *Eur J Immunol.* 2009; 39(7):1754-1764.

236. Durlanik S, Fundel-Clemens K, Viollet C, et al. CD276 is an important player in macrophage recruitment into the tumor and an upstream regulator for PAI-1. *Sci Rep.* 2021; 11(1):14849.

237. Kang FB, Wang L, Li D, Zhang YG, Sun DX. Hepatocellular carcinomas promote tumor-associated macrophage M2-polarization via increased B7-H3 expression. *Oncol Rep.* 2015; 33(1):274-282.

238. Ingebrigtsen VA, Boye K, Tekle C, Nesland JM, Flatmark K, Fodstad O. B7-H3 expression in colorectal cancer: nuclear localization strongly predicts poor outcome in colon cancer. *Int J Cancer.* 2012; 131(11):2528-2536.

239. Katayama Y, Uchino J, Chihara Y, et al. Tumor Neovascularization and Developments in Therapeutics. *Cancers (Basel).* 2019; 11(3).

240. Mills SJ, Cowin AJ, Kaur P. Pericytes, mesenchymal stem cells and the wound healing process. *Cells.* 2013; 2(3):621-634.

241. Zhou Z, Pausch F, Schlotzer-Schrehardt U, Brachvogel B, Poschl E. Induction of initial steps of angiogenic differentiation and maturation of endothelial cells by pericytes in vitro and the role of collagen IV. *Histochem Cell Biol.* 2016; 145(5):511-525.

242. Schott NG, Stegemann JP. Coculture of Endothelial and Stromal Cells to Promote Concurrent Osteogenesis and Vasculogenesis. *Tissue Eng Part A.* 2021; 27(21-22):1376-1386.

References

243.   Deligne C, Hachani J, Duban-Deweer S, et al. Development of a human in vitro blood-brain tumor barrier model of diffuse intrinsic pontine glioma to better understand the chemoresistance. *Fluids Barriers CNS.* 2020; 17(1):37.

244.   Schmid D, Warnken U, Latzer P, et al. Diagnostic biomarkers from proteomic characterization of cerebrospinal fluid in patients with brain malignancies. *J Neurochem.* 2021; 158(2):522-538.

245.   Martins I, Ribeiro IP, Jorge J, et al. Liquid Biopsies: Applications for Cancer Diagnosis and Monitoring. *Genes (Basel).* 2021; 12(3).

246.   Mendioroz M, Martinez-Merino L, Blanco-Luquin I, Urdanoz A, Roldan M, Jerico I. Liquid biopsy: a new source of candidate biomarkers in amyotrophic lateral sclerosis. *Ann Clin Transl Neurol.* 2018; 5(6):763-768.

247.   Li N, Cui L, Ma H, et al. Osteopontin is highly secreted in the cerebrospinal fluid of patient with posterior pituitary involvement in Langerhans cell histiocytosis. *Int J Lab Hematol.* 2020; 42(6):788-795.

248.   Agah E, Zardoui A, Saghazadeh A, Ahmadi M, Tafakhori A, Rezaei N. Osteopontin (OPN) as a CSF and blood biomarker for multiple sclerosis: A systematic review and meta-analysis. *PLoS One.* 2018; 13(1):e0190252.

249.   Talaat F, Abdelatty S, Ragaie C, Dahshan A. Chitinase-3-like 1-protein in CSF: a novel biomarker for progression in patients with multiple sclerosis. *Neurol Sci.* 2023; 44(9):3243-3252.

250.   Roh JL, Kim EH, Jang H, Shin D. Aspirin plus sorafenib potentiates cisplatin cytotoxicity in resistant head and neck cancer cells through xCT inhibition. *Free Radic Biol Med.* 2017; 104:1-9.

251.   Li H, Xu K, Pian G, Sun S. Artesunate and sorafenib: Combinatorial inhibition of liver cancer cell growth. *Oncol Lett.* 2019; 18(5):4735-4743.

252.   Ye L, Mayerle J, Ziesch A, Reiter FP, Gerbes AL, De Toni EN. The PI3K inhibitor copanlisib synergizes with sorafenib to induce cell death in hepatocellular carcinoma. *Cell Death Discov.* 2019; 5:86.

253.   A Z, J SW, A M, et al. LY294002 and sorafenib as inhibitors of intracellular survival pathways in the elimination of human glioma cells by programmed cell death. *Cell Tissue Res.* 2021; 386(1):17-28.

254.   Gao X, Schottker B. Reduction-oxidation pathways involved in cancer development: a systematic review of literature reviews. *Oncotarget.* 2017; 8(31):51888-51906.

255.   Dobra G, Gyukity-Sebestyen E, Bukva M, et al. MMP-9 as Prognostic Marker for Brain Tumours: A Comparative Study on Serum-Derived Small Extracellular Vesicles. *Cancers (Basel).* 2023; 15(3).

256.   Xue Q, Cao L, Chen XY, et al. High expression of MMP9 in glioma affects cell proliferation and is associated with patient survival rates. *Oncol Lett.* 2017; 13(3):1325-1330.

257. Zhang H, Wang Q, Liu J, Cao H. Inhibition of the PI3K/Akt signaling pathway reverses sorafenib-derived chemo-resistance in hepatocellular carcinoma. *Oncol Lett.* 2018; 15(6):9377-9384.

258. Huang A, Zeng P, Li Y, Lu W, Lai Y. LY294002 Is a Promising Inhibitor to Overcome Sorafenib Resistance in FLT3-ITD Mutant AML Cells by Interfering With PI3K/Akt Signaling Pathway. *Front Oncol.* 2021; 11:782065.

259. Song KW, Edgar KA, Hanan EJ, et al. RTK-Dependent Inducible Degradation of Mutant PI3Kalpha Drives GDC-0077 (Inavolisib) Efficacy. *Cancer Discov.* 2022; 12(1):204-219.

260. Ishimoto T, Nagano O, Yae T, et al. CD44 variant regulates redox status in cancer cells by stabilizing the xCT subunit of system xc(-) and thereby promotes tumor growth. *Cancer Cell.* 2011; 19(3):387-400.